MODELING AND PERFORMANCE ANALYSIS OF LOW CONCENTRATION PHOTOVOLTAIC (LCPV) SYSTEM

BY

BILAL TANWEER

A Thesis Presented to the

DEANSHIP OF GRADUATE STUDIES

KING FAHD UNIVERSITY OF PETROLEUM & MINERALS

DHAHRAN, SAUDI ARABIA

In Partial Fulfillment of the

Requirements for the Degree of

MASTER OF SCIENCE

In

Mechanical Engineering

APRIL, 2014

KING FAHD UNIVERSITY OF PETROLEUM & MINERALS

DHAHRAN, SAUDI ARABIA

DEANSHIP OF GRADUATE STUDIES

This thesis, written by **Bilal Tanweer** under the direction of his thesis advisor and approved by his thesis committee, has been presented to and accepted by the Dean of Graduate Studies, in partial fulfillment of the requirements for the degree of **MASTER OF SCIENCE in MECHANICAL ENGINEERING**.

Thesis Committee

Thesis Advisor

Prof. Palanichamy Gandhidasan

Member

Dr. Haitham M. Bahaidarah

Department Chairman

Dr. Zuhair Mattoug Gasem

Anwar Khalil Sheikh

Member

Prof. Anwar Khalil Sheikh

Dean of Graduate Studies

Prof. Salam A. Zummo

5/4/15

Date

This Work is dedicated

to

My mother, mother, mother, father

for their constant support and prayers.

Also my wife, Umna, Abdullah and mys siters for their

dua, constant support and encouragement throughout my life

ACKNOWLEDGMENT

In the Name of Allah, the Most Beneficent, the Most Merciful.

> Praise belongs to Allah, the Lord of all the worlds (2) The All Merciful, the Very-Merciful. (3) The Master of the Day of Requital. (4) You alone do we worship, and from You alone do we seek help. (5) Take us on the straight path (6) The path of those on whom You have bestowed Your Grace, Not of those who have incurred Your wrath, nor of those who have gone astray. (7)
>
> Al-Fatiha

In the name of Allah, the most Merciful, the most Gracious. All praise is due to Allah; we praise Him, seek His help, and ask for forgiveness. Peace be upon the Prophet Mohammad, his family, his companions, and all those who followed him until the Day of Judgment.

I then would like to show my deepest gratitude and respect to my family, especially my mother and my father, the ones to whom I owe all the success in my life. No words can express my gratitude to them, but I pray Allah to bless them and reward them. Any success in my life so far is mostly charged to them and consequently any success in the future will have their signature as well.

Acknowledgements are due to King Fahd University of Petroleum and Minerals (KFUPM) which gave me the opportunity to pursue a graduate degree and also for all the support I received in carrying out this research. I would like to acknowledge the support provided by King Abdulaziz City for Science and Technology (KACST) through the Science & Technology Unit at (KFUPM) for funding this work through project No. 10-

ENE1376-04 (*PI-Dr. Haitham Bahaidarah*) as part of the National Science, Technology and Innovation Plan. I would also like to ***specially*** acknowledge the Project *R6-DMN-08-Design and Manufacturing of Solar Power Systems and Devices for Challenging Environments* Center for Clean Water and Clean Energy at KFUPM and MIT (*PI-Professor Anwar Khalil Sheikh*), which provided us the solar panels, with stand and manual tracker designed at KFUPM, along with all needed basic instrumentation for data acquisition of solar irradiance, along with the flat plate heat exchangers. This experimental system with some additional modifications was used throughout this entire study.

I would like to thank my research and academic supervisor Prof. Palanichamy Gandhidasan for his continuous supervision, advice, and guidance from the very beginning of this research. He taught me how to think, analyse, and solve problems independently in a professional and friendly manner. My appreciations are also extended to my committee members: Dr. Haitham Bahaidarah and Prof. Anwar Khalil Sheikh for their useful discussions.

I would also like to thank all my colleagues, friends and seniors at KFUPM for providing the moral support and a pleasant atmosphere. Special thanks to my best friends Waqas Khalid, Sheraz Khalid, Osama Hasan, Adnan Saeed, Khalid Naseem, Waqas Akram, Ibrar Hussain and Mudassar Imam for making my time in KFUPM memorable and unforgettable.

TABLE OF CONTENTS

LIST OF TABLES

LIST OF FIGURES

THESIS ABSTRACT (ENGLISH)

Name	Bilal Tanweer
Title	Modeling and Performance Analysis of Low Concentration Photovoltaic (LCPV) System
Degree	Master in Science
Major Field	Mechanical Engineering
Date of Degree	April 2014

Since the PV technology improves and maximizes the photoelectrical conversion rates, it has been extensively employed in the recent years. Due to the high initial capital cost of PV systems, their wide-ranging applications are restricted. This issue of cost reduction can be resolved either by increasing the efficiency of the solar cells or using the technology of concentration photovoltaics. The objective of this thesis is to reduce the cost of the direct conversion of solar radiation to electricity and present higher efficiency than the typical flat-type photovoltaic (PV) modules using low concentration technology. For this purpose two configurations of LCPV are employed: V-trough PV system and compound parabolic concentrator (CPC) integrated with PV. In the present study optical and thermal modeling for both of these configurations are developed. These models are coupled with the electrical model to estimate the overall performance of these respective LCPV systems. This analytical tool can be very useful to check the liability of these systems at various geographical environment conditions. By integrating uncooled simple flat PV string with unglazed CPC, the amount of power was increased by 45.2%. If water

cooling was provided along with the unglazed CPC reflectors and compared with uncooled simple flat PV string, the increase in the electrical power was about 73.6%. Effect of glazing was also studied in PV-CPC system. Glazing protects the reflectors and PV-panel from dust and moisture, but on the other hand it also raises the temperature of the PV panel. From electrical point of view glazing reduces the power output and from thermal point of view it is beneficial as it increases the thermal gain of the PV-CPC system. Therefore, unglazed PV-CPC is recommended for greater electric power output but with a little compensation to the advantages of glazing. Similarly for V-trough PV system, the power was increased by 37% with the integration of V-trough to simple PV panel. Maximum power output of the actively cooled module changes sharply under concentration and non-concentration conditions. The maximum power increases from 207.4(non-concentration) to 298.8 W (concentration) with a percentage increase of 44%.

Furthermore, the experimental setup for V-trough PV system and PV-CPC system has been designed, fabricated and tested for various ambient conditions in Dhahran. Six different configurations were tested simultaneously for PV-CPC system analysis. Experimental data extracted from these laboratory scale bench-top systems showed a good agreement with the numerical model results.

THESIS ABSTRACT (ARABIC)

ملخص الرسالة

الاسم ال : بلال تنوير

عنوان الرسالة : تحليل عددي و تجريبي لنظام الخلايا الضوئية الجهدية منخفضة التركيز

التخصص : الهندسة الميكانيكية

تاريخ الدرجة العلمية : ابريل ٢٠١٤

منذ تحسين تكنولوجيا الخلايا الكهروضوئية لمعدلات التحويل الكهروضوئية، فقد استخدمت على نطاق واسع في السنوات الأخيرة, إلا أن تطبيقات هذه الأنظمة الكهروضوئية الكثيرة قد إنحصرت بسبب إرتفاع رأس المال ، ويمكن حل مشكلة إرتفاع التكاليف إما عن طريق زيادة كفاءة الخلايا الشمسية أو باستخدام تكنولوجيا تركيز الخلايا الكهروضوئية. الهدف من هذه الرسالة هو خفض تكلفة التحويل المباشر للإشعاعات الشمسية إلى كهرباء، وتقديم كفاءة أعلى من نموذج الخلايا الضوئية مسطحة الشكل باستخدام تكنولوجيا تركيز منخفض. لهذا الغرض يتم توظيف اثنين من تكوينات LCPV: نظام PV-V الحوض ومركزات مكافئ مركب (CPC) متكاملة مع PV. في هذه الدراسة تم تطوير نمذجة ضوئية وحرارية لكلا هذه التكوينات. تم دمج هذه النماذج مع النموذج الكهربائي لتقدير الأداء العام لنظم LCPV. هذه الأداة التحليلية يمكن أن تكون مفيدة للغاية للتأكد من إعتمادية هذه الأنظمة في مختلف ظروف البيئة الجغرافية. من خلال دمج سلسلة PV المسطحة والغير مبردة مع مركزات مكافئ مركب (CPC) غير المغطى ، تم زيادة كمية الطاقة بنسبة 45.2٪. إذا تم توفير مياه التبريد مع عاكسات مركزات مكافئ مركب غير المغطى وغير مبرد مقارنة مع سلسلة PV المسطحة ، وكانت الزيادة في الطاقة الكهربائية حوالي 73.6٪. تمت دراسة تأثير الزجاج أيضا في نظام CPC-PV . الزجاج يحمي عاكسات لوحة PV من الغبار والرطوبة، ولكن من ناحية أخرى فإنه يزيد أيضا درجة حرارة لوحة الخلية الكهروضوئية. من وجهة نظر كهربائية فإن الزجاج يقلل من

انتاج الطاقة ومن وجهة نظر حرارية فإنه المفيد كما أنه يزيد من الكسب الحراري للنظام CPC-PV . لذا، يوصى CPC-PV الغير مغطى لزيادة انتاج الطاقة الكهربائية ولكن مع تعويض قليل من مزايا الزجاج. على نحو مماثل لنظام PV-V الحوض ، تمت زيادة الطاقة بنسبة 37٪ مع دمج V-الحوض للوحة كهروضوئية بسيطة. انتاج الطاقة القصوى في وحدة تبريد فعال تتغير بشكل حاد في ظل ظروف التركيز وعدم التركيز. زيادة الطاقة القصوى من 207.4 (غير تركيز) إلى 298.8 واط (تركيز) مع زيادة نسبة 44٪.

إضافة لذلك، فقد تم تصميم الإعدادات التجريبية لنظام PV-V الحوض ونظام CPC-PV ، واختبارها لمختلف الظروف المحيطة في الظهران. تم اختبار ستة تكوينات مختلفة في نفس الوقت لتحليل نظام CPC-PV . وأظهرت البيانات التجريبية المستخلصة من أنظمة المختبر اتفاق جيد مع نتائج النموذج العددي.

CHAPTER 1 INTRODUCTION

Energy is currently an important issue all over the world. The demand for fossil fuel has grown steadily due to increased industrial activities in developing and developed countries. It is estimated that the world energy demand will increase by 45% between 2006 and 2030, and the rate of increase will be 1.6% per year. Figure 1.1 shows the estimated world primary energy consumption from 1990 to 2040 [1].

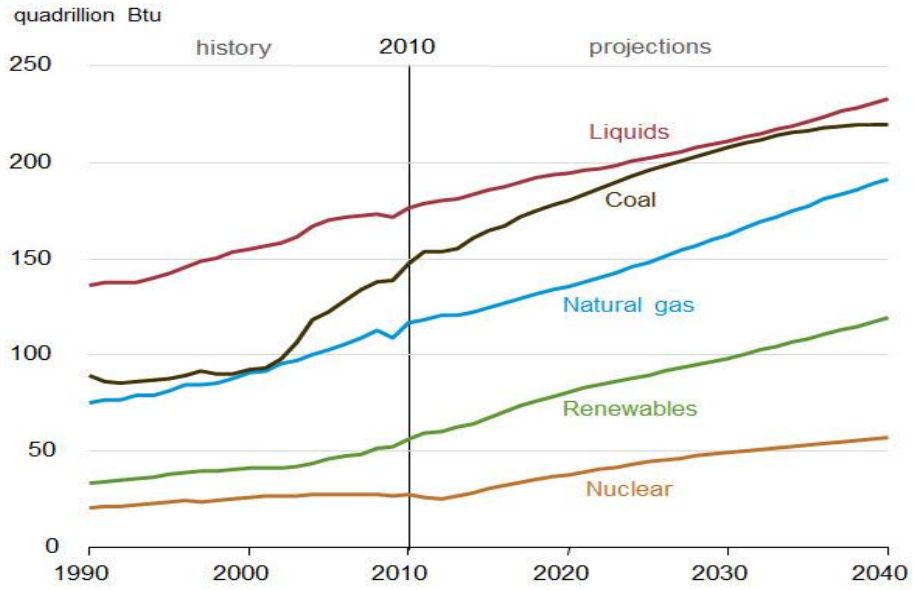

Figure 1.1: World's energy consumption by fuel type

Transportation energy consumption in the Middle East grows by an average of 1.5 percent per year in the International Energy Outlook (IEO) 2013 Reference case, to 9.5 quadrillion Btu in 2040 as shown in Figure 1.2. Although the Middle East has a relatively small population, population growth and continued urbanization are expected to result in increased demand for transportation. High world oil prices have increased revenues in many of the oil-exporting countries of the Middle East, and as a result several transportation infrastructure projects, including mass transit projects, have been launched. In the GCC countries, railways have been identified as a preferred mode of transportation for the future, capable of meeting the challenges of rapid urbanization and growth in freight transport. Some $106 billion has been allocated for railway and metro construction projects in GCC countries through 2014 [1].

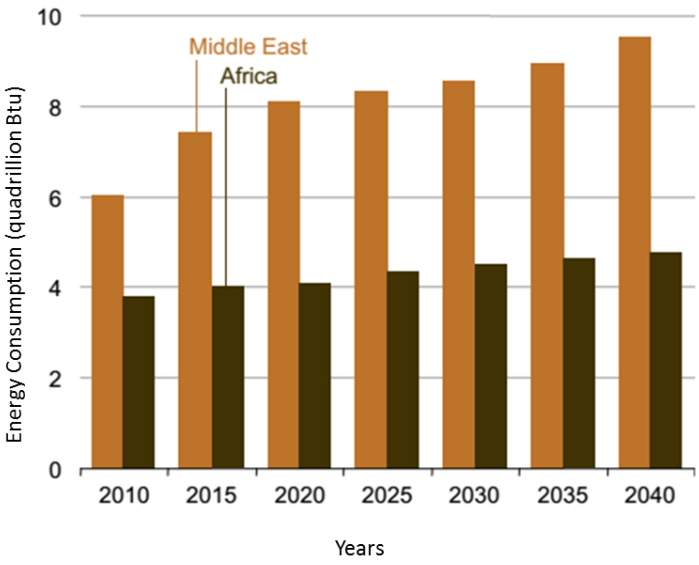

Figure 1.2: Non-OECD Middle East and Africa transportation sector delivered energy consumption by region, 2010-2040 (quadrillion Btu)

In general, fossil fuels such as oil, natural gas and coal can be considered as primary sources of energy, especially, oil is the dominant fuel of the world. The increase of the energy demand may be met by utilizing fossil fuel resources but the amount of greenhouse gas emissions in the atmosphere will reach a dangerous level. According to the fourth assessment report from 2007 Inter-governmental Panel on Climate Change, the increases of sea level are consistent with global warming. But China is not alone; energy consumption in India and the Middle East has also grown rapidly in the last five years. Between 2007 and 2011, China's energy consumption grew 34%, while India's increased by 35% and the Middle East by 22% [2]. Looking ahead to the next five years, energy usage in these markets is not expected to slow down, with double-digit growth rates forecast across all three of these areas as shown in Figure 1.3 below.

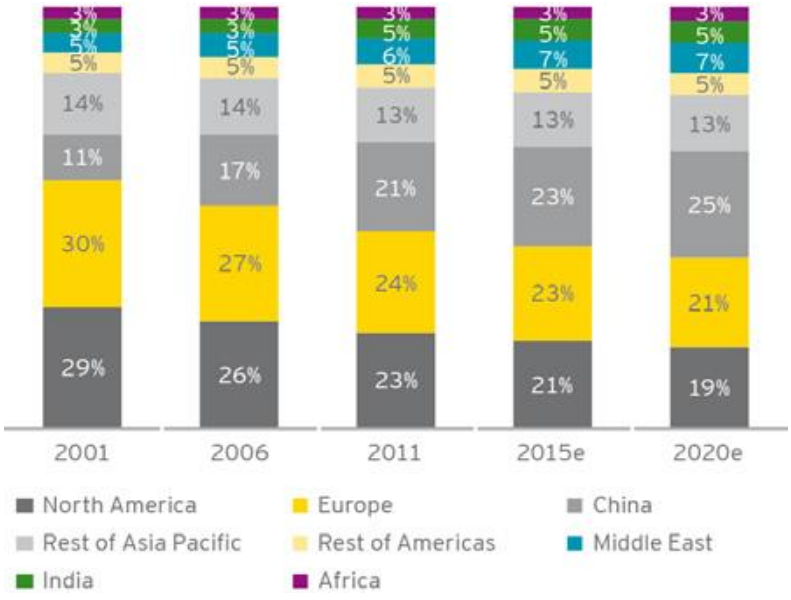

Figure 1.3: Global energy consumption by different regions (Million Tons of Oil Equivalent)

1.1 RENEWABLE ENERGY

Renewable energies including solar energy, wind power, hydropower, biofuel, geothermal energy are suggested to provide a solution to resolve the global warming problem and alleviate the potential of energy crisis. The demand of fossil fuels will be reduced when the renewable energies become popular in the energy market. Furthermore, potential climate change will be mitigated when the renewable energies replace fossil fuels in the future. One of the renewable energy sources that can be used for this purpose is the light received from the sun. Solar energy is one of the most promising energy sources with solar radiation reaching the earth's surface at a rate approximately 80,000 TW and this figure is more than 10,000 times the present consumption of energy in the world. Solar energy has the capability to meet the current energy demand compared to the other form of renewable energy sources shown in Table 1-1 [3]. Liu et al [4] estimates from theoretical calculations that by harnessing the solar energy from eight different solar power plant sites throughout the world, the energy produced will have the capacity to satisfy the present global energy utilization. Suitable sites for these solar power plants are located in the deserts of Saudi Arabia and southwest Asia, Mexico, United States, Australia, China and Southern South America.

Table 1-1: Power available from renewable resources

Energy Source	Max Power (TW)
Total surface solar	85000
Desert solar	7650
Ocean thermal	100
Wind	72
Geothermal	44
River hydroelectric	7
Biomass	7
Open ocean wave	7
Tidal wave	4
Coastal wave	3

Renewable energy can be included as the source in the energy mix to overcome the problems related to the production of electricity from fossil fuels. Amongst the renewable energies present, light as a form of energy from the sun can be used for this purpose. Electricity from the sun can be produced in two different ways. One of them is by using solar concentrator thermal system and the other is by photovoltaic (PV) technology. In the first method the sun rays are focused to produce steam, which in returns drives the generator to produce electricity. PV technology converts the sunlight directly into electricity and has wider range of applications in residential sector and remote places. PV process can convert the sunlight to clean electricity without adding detrimental components to the environment. Usage of PV system for electricity production began in 20^{th} century and is presently developing quickly in the world. A rapid growth in the PV industry can be seen even in the times of economic crisis. The global solar electricity market is currently more than $10 billion/year and the industry is rising at a rate of greater than 30% per annum [5].

1.2 PHOTOVOLTAIC CELLS

A PV cell normally consists of two types of semiconductors namely P-type and N-type. These semiconductors are made of different materials like, cadmium telluride (CdTe), cadmium sulfide (CdS), mono and polycrystalline silicon (Si), and amorphous silicon (a-Si). Availability of electron-hole pair (+) is present in P-type semiconductor and free electrons (-) are present in N-type semiconductors. A potential difference is generated in the region known as P-N junction when the two semiconductors are placed next to each other. As the solar radiation strikes the PV cell, the photons with high energy moves the electrons and generates the electron-hole pair. In case of N-on-P silicon cell, these electron-hole pairs tend to move to the back contact electrode whereas the free electrons accumulate at the front contact electrode as explained in the Figure 1.4. Current is generated when the load is attached to the front and back electrodes and the electrons follow the newly created oath to return back to the P-type contact grid.

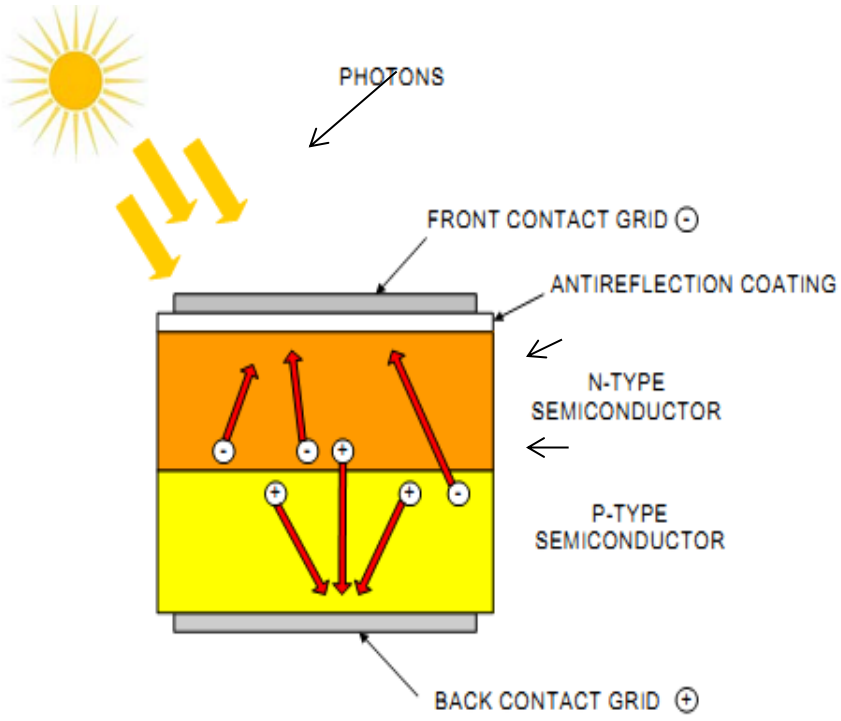

Figure 1.4: Schematic diagram of the principle of PV cells

A PV cell is generally characterized by a current-voltage (*I-V)* curve. A typical *I-V* curve is shown in Figure 1.5. In this figure, the value of current where the voltage is zero is termed as the short-circuit current, I_{sc}, and the value of voltage where the current is zero is termed as open-circuit voltage, V_{oc}. Generally PV cells always operate somewhere on their *I-V* curve depending upon the resistive load attached to the cell. In ideal scenario, it should operate at the locus on the *I-V* curve called maximum power point, where the voltage (V_{mp}) and current (I_{mp}) generated are such that they produce maximum amount of power possible.

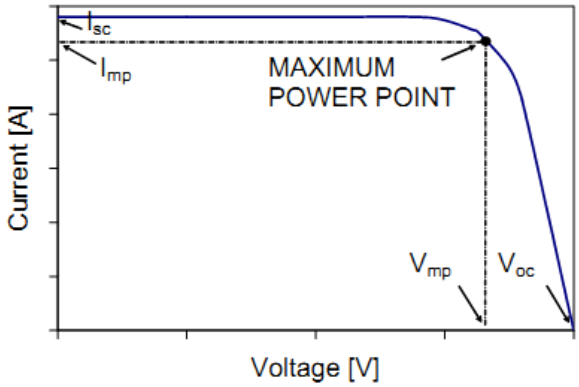

Figure 1.5: Typical I-V curve of a PV module

Generally PV cells only convert a little portion of absorbed solar energy into electricity. Their efficiency usually ranges from 6-28%, depending on the kind of PV cells used. One of the reasons for this poor efficiency is that only those photons are able to generate the electron-hole pairs, which have certain amount of energy. The photons with insufficient amount of energy are unable to generate the electron-hole pairs and hence cannot produce electricity. Instead their energy is converted into heat energy which plays a role in increasing the cell temperature. This unwanted heat energy is unfavorable for PV cells as it decreases the electrical conversion efficiency of the PV system.

1.3 PHOTOVOLTAIC CONCENTRATOR TECHNOLOGY

The most expensive component of a PV system is the solar cell and its area can be reduced by the use of concentrator to produce the same amount of electrical energy. In photovoltaic concentrator technology, concentrators are the optic devices that concentrate

sunlight on to solar cells using lenses or mirrors. The main purpose of the concentrator is to cut down the cost of electricity produced by replacing costly PV cell area with optical materials (plastic refractors or metal reflectors) which are comparatively less expensive. Types of concentrators, the solar cell used and the reflector materials of the concentrator are the main factors which decide the performance of a photovoltaic concentrator system. In this study we will only deal with concentrator with reflector surfaces. Mostly the concentrating system requires direct sunlight rather than diffuse light, which require clear and sunny locations. In such cases tracking might also be needed.

The concentrating solar systems are characterized by their concentration ratio (CR). It is the parameter which is defined by the ratio of available aperture area to the receiver (absorber) area. Concentrating systems having concentration ratio greater than 2.5X need to track the sun, while systems having concentration ratio less than 2.5X can be used as stationary concentrating devices. Low concentration systems (CR<10X) are of main interest for photovoltaic as their geometry is linear and only one axis tracking is sufficient for their effective performance. Various types of solar concentrators used in PV concentrator technology are categorized according to their optical properties. They can be grouped into four categories, which are shown in Table 1-2 [6] below.

Table 1-2: Types of solar concentrators.

Type	Description
Reflector	Upon hitting the concentrator, the sun rays will be reflected to the PV cell Example: *Parabolic Trough, Parabolic Dish, CPC Trough, Hyperboloid Concentrator.*
Refractor	Upon hitting the concentrator, the sun rays will be refracted to the PV cell. Example: *Fresnel Lens Concentrator*
Hybrid	Upon hitting the concentrator, the sun rays can experience both reflection and refraction before hitting to the PV cell. Example: *Dielectric Totally Internally Reflecting Concentrator (DTIRC), Flat High Concentration Devices*
Luminescent	The photons will experience total internal reflection and guided to the PV cell. Example: *Quantum Dot Concentrator*(*QDC)*

There are several advantages of concentrator PV-systems over flat-plate (non-concentrating) PV systems. The cell efficiency is enhanced and the power output is increased while reducing the area of the cell needed. Increase in efficiency is mainly dependent on the cell material and the design of the solar cell.

Advantages of concentrator PV-system [6,7]:

1. Reliance on the silicon cell is minimized

2. Cell efficiency is enhanced by increasing the intensity of solar irradiance

3. System Cost is reduced by using cheap reflectors

Disadvantages of concentrator PV-system[8-13] :

1. Lifespan of the PV cell is degraded due to intense conditions

2. Mechanical tracking is necessary in systems with high concentration ratio

3. To ensure the optimum performance of PV cells, cooling is required.

For concentrating PV systems monocrystalline silicon PV cells are the mostly used but their electrical output is reduced by the non-uniform distribution of solar flux and increase in temperature. Error in the mirror shape is the main cause of non-uniform illumination of the photovoltaic cells, which has a significant effect on the flux profile even if it is very small. Gallium arsenide (GaAs) cells have a better performance at higher temperatures and their conversion efficiency is also greater than monocrystalline silicon cells but have considerable higher cost. To encounter the problem of non-uniform flux distribution, thin film PV are used because they are less sensitive to uneven flux distribution. But thin film PV has lower efficiency than crystalline silicon cells. The efficiency of concentrating PV module is usually in the range of 15-30%. To increase the amount of solar flux on the focal point or on the focal line, plane and curved reflectors are normally used. The material of the concentrator should be durable for a long period in order to bear with the life of the PV cell, which is approximately more than 20 years. Concentrator material should also be inexpensive compared to the cells, as it covers a larger aperture area than of the cell.

1.4 CONCENTRATOR PV/T HYBRID SYSTEM

The electrical output of the PV cell is affected by the temperature rise of the module and distribution of the solar radiation. Applying a suitable cooling mode and uniform distribution of the concentrated solar radiation on cell surface can enhance the electrical output and the maximum power can be extracted out of the system. To maintain the module temperature at normal operating range, passive or active cooling techniques are applied. A concentrator device, PV cells and a thermal receiver make up a concentrator photovoltaic/Thermal (PV/T) hybrid system. The solar energy received at the solar cell after being concentrated is partly converted into electricity and rest is the thermal energy which is extracted by cooling mechanisms for some useful purpose. The performance of the photovoltaic hybrid system depends upon many factors, such as the geographic location, climatic conditions, orientation of the PV/T system, type of the solar cell, mass flow rate of the fluid medium (water/air), etc. To analyse the effectiveness of concentrator PV/T hybrid system the following aspects should be taken into consideration:

I. Reflectors used should be capable of concentrating sun accurately over the area of solar cell and should be cheap.
II. The flux profile of the concentrated solar intensity should be uniform in order to obtain the maximum output from the PV/T system.

III. The cooling mechanism should be able to extract the maximum possible thermal energy and maintain the operating temperature of the PV/T system to the optimal range in order to maintain the maximum power output.

IV. The thermal energy extracted should be utilized efficiently in order to increase the overall efficiency of the concentrator PV/T system.

1.5 OBJECTIVES

The aim of this research is to analyse the different low concentration photovoltaic systems used to generate the cost effective PV electricity. This thesis deals with the performance of two low concentration systems, namely V-trough and compound parabolic concentrator (CPC) and their performances are predicted through numerical modelling. Experimental setup is developed to investigate and evaluate the performance of V-trough and PV-CPC systems. Experimental results are compared to the results predicted by numerical modelling.

Following are the main objectives of this research work:

1. To investigate the performance analysis of various configurations of the low concentration photovoltaic (LCPV) system which are :
    - V-trough PV/T system
    - Glazed PV-CPC system
    - Unglazed PV-CPC system
    - Flat plate PV system

2. To develop comprehensive optical models which would predict the amount of energy absorbed by the different concentrating geometries.
3. To develop thermal models by using energy balance equations to estimate the module and fluid temperatures.
4. To develop the electrical model for estimation of the maximum power output from the LCPV systems.
5. To couple all these models and obtain I-V characteristic curves for the above LCPV systems.
6. Fabrication and testing of the above LCPV systems and comparing the experimental results with the numerical results.

CHAPTER 2 LITERATURE SURVEY

In this review different configuration for low concentrated photovoltaic (LCPV) is discussed. Advancements and progress of work on V-trough and CPC configuration is presented. To obtain the power output from the PV panel different models are used which include radiation model, thermal model and electrical model. A comprehensive review on all of these models is presented.

2.1 LOW CONCENTRATION PHOTOVOTAICS (LCPV)

Among LCPV, curved and flat reflectors, dielectric lens and Fresnel lenses are the type of concentrators being studied. Fresnel lens function is similar to the conventional lens, by refracting the rays and focusing them at one focal point. The advantage of the Fresnel lens over a conventional lens is that its thinner and requires a lesser amount of material to fabricate [13]. The application of this concentrator can be seen in the Sacramento Municipal Utility District, where they are employed in the 30kW utility grid-connected plant [6]. It also has the capability to separate the direct and diffuse light, making it suitable to control the illumination and temperature of a building [14]. Regarding the V-trough reflectors, many studies are referred to one or two tracking axis using flat mirrors. The flat mirrors are used to increase solar radiation on PV module

surface resulting in a uniform distribution of solar radiation on it. They are simple devices, achieving concentration ratios up to about two with east-west or north-south orientated reflectors.

CPC type concentrators are another category of devices that are coupled with PV modules. Most of them are static concentrators (no movements to track the sun), but the non-uniform distribution of solar radiation on the surface of cells decreases their electrical efficiency. Bifacial cells are used in order to concentrating system geometry, reducing cell material.

Finally, among the studies on dielectric lens-type concentrators, optical results for 3D static acrylic lens concentrators were presented, achieving a reduction of 62% in cell surface [15]. Comparison results give an idea about the benefits of low concentrating photovoltaics. Results from a study of several types of PV modules (concentrating and flat type) showed that concentrators can reduce the environmental impact of PV [16].

In the present study V-trough PV and PV-CPC system are selected amongst the different categories of LCPV. The reason for selecting these systems is that by integrating simple low cost reflectors with the PV cell, the efficiency is considerably increased and the cost per watt is reduced considerably.

2.2 REVIEW OF V-TROUGH PV SYSTEM

Considerable research has been carried out on the V-trough collectors for achieving the high thermal efficiency as compared to simple flat plate collectors. Other than that V-trough collectors are also found suitable for PV concentrator cells because of their uniform illumination. By comparing V-trough and CPC collectors it was found that reflector-to-aperture ratio of the V-trough is less than that of the CPC for the same concentration ratio. Because of its simplicity and uniform output radiation it might be well suited for the PV applications [17].

Geometrical configuration of the V-trough is one of the main factors which affect the collectible radiation on the panel. Geometrical optimization of the V-trough was performed in order to produce uniform monthly flux enhancement with minimum adjustment of the concentrator. This optimization was carried out by using performance curves which were generated from single reflector-receiver system [18]. Comparing symmetric and asymmetric trough it was found that symmetrical trough is best suited for uniform year round flux-augmentation.

The performance of the low concentration systems like V-trough depends on many parameters like global irradiance, module temperature, collector tilt, etc. A sensitivity analysis was performed on the theoretical model which was developed to study the response of V-trough system in terms of module temperature, power output and energy

yield, and it was found that global irradiance is the crucial parameter that effects the system performance [19]. In this model solar tracking was incorporated and the model was validated with DoubleSun concentration technology. System performance can be enhanced by increasing the concentration ratio but, if it reaches beyond a critical value, cooling of the panel needs to be carried out.

To increase the performance of the solar cell, a V-trough concentrator with a two-axis tracking system was designed and fabricated [20]. It was concluded that v-trough concentrator system is the best suited method to increase the power output from the solar cell considering its cost and the simplicity of its materials. In the experimental setup two types of solar cells namely amorphous Si and polycrystalline Si solar cells were tested simultaneously. Results showed that amorphous Si cell gave 40% more output than the cell without reflector and the reason was that for amorphous Si solar cells the effective wavelength is mainly in the visible band. On the other side polycrystalline Si cell did not enhance the power output as expected because commercially available mirrors coated with aluminum have their lowest reflectivity around 900 nm, which is the center of the effective wavelength required for polycrystalline Si cells.

In order to design the V-trough PV system, the mirrors and PV modules should be characterized from an optical point of view. Optical performance is characterized by the spectral response of the module, together with the angular reflectance inside the cavity. It was observed that optical losses depend on cavity angle, angular reflectance, the mirrors spectral and surface dirtiness. Angular losses were estimated theoretically to about 2.5%

having an ideal 100% reflectance mirror, and it increased significantly with presence of dust to about 12% if surface is moderately dirty and around 24% if the dust quantity is very high [21].

To estimate the amount of collectible radiation on the base of the V-trough PV system, a mathematical model was developed [22]. Optical modeling and design optimization was performed based on this model. Two cases were compared, one in which the V-trough was aligned on the east-west axis (EW-V trough) fixed all the year around and the other one in which tilt adjustment was done four times at three fixed tilt-angle (3T-EW-V troughs) yearly. Results showed that annual solar gain captured by 3T-EW-V troughs was more than the fixed EW-V trough provided with the same geometrical parameters.

Output characteristics of V-trough PV system with super cell array and polysilicon cell array was assembled and tested. It was found that polysilicon cell array produced 1.2 times more power output as compared to the one without concentration, and the super cell made 81.5% more power output as compared to the one without concentration [23]. Furthermore the power out in both the cell arrays was affected by the increase in the temperature, and by using a cooling mechanism power output was further increased with concentration.

Standard PV modules are designed to operate under one sun condition. Their main concern is that when they are exposed to concentrated radiation or integrated with concentration photovoltaic (CPV) systems, their performance remains the constant or it

changes. This issue was dealt and possible accelerated modules degradation rates were analyzed [24]. Results showed that standard silicon modules undergo 1.7% of power degradation when coupled with V-trough system with concentration ratio of 1.9. It was suggested that standard silicon cells may be eligible for concentration, after the successful results for the range of concentration factors tested according to International Electrotechnical Commission (IEC) 62108 standards.

V-trough systems enhance the solar radiation and at the same time the temperature of the module also increases which reduces the electrical efficiency and life of the panel. To counter this issue, a study was presented which took the advantage of enhanced insolation by V-trough reflectors and at the same time the temperature of the module was maintained to the limit where standard PV module operates without concentration [25]. Paraffin wax was employed as the phase change material (PCM) having 56-58 $^{\circ}$C melting range and was integrated at the rear side of the module to absorb the excess heat. The output power over the day could be enhanced 1.55 times with this technique of self-regulation of temperature. Through V-trough PV-PCM system safe operation of module could be carried out even in the presence of low wind velocity and without sacrificing the operational simplicity.

Many techniques have been implemented in order to regulate the increased module temperature due to concentration. In 2008, a V-trough PV system was designed to effectively dissipate the enhanced heat of the PV module for better performance [26]. In this design the concept was using a single aluminum metal sheet frame that incorporated

6 rows of mono-crystalline Si cells mounted on 6 V-trough channels, to achieve a better heat dissipation from the cell under concentration. In this way the V-trough walls were used for increasing the light intensity as well for dissipating the heat from the cells which provided 4 times greater heat dissipation area as compared to the case where V-trough walls were not connected as a single metal sheet. As a result of this design, the current density and open circuit voltage of the module increased due to the lower temperature of the module.

Photovoltaic/Thermal (PVT) solar energy systems that generate both thermal and electrical energy have been under great interest in the recent times. Amongst them one particular area is building integrated PVT (BIPVT) systems. A BIPVT concentrator system was developed that incorporated a V-trough concentrator [27]. In this study optical, thermal and electrical performance of the collector was theoretically modeled but it needed improved heat transfer correlations to ensure a better validation to the experimental performance of the collector.

Amount of absorbed radiation depends upon the type of reflectors being used in the V-trough PV system. The effect of reflectance of aluminum sheet and aluminum foil on the V-trough PV system was studied [28]. Total reflectance for both reflectors was the same but the specular reflectance which is greater in the aluminum foil reflectors, resulted in increasing the solar radiation intensity concentration factor and hence, increase in the total daily thermal and electrical energy generated by PV/Thermal system. By calculating the optimal position of planar reflectors, thermal and electrical efficiency

of PV/Thermal system was determined. It was concluded that aluminum foil reflector system produced higher energy in optimal position than with aluminum sheet reflector system. Total daily thermal energy generated by aluminum foil reflector system produced 55% more energy and aluminum sheet reflector system produced 39% higher energy as compared to PV/Thermal system without reflectors.

V-troughs are particularly suitable for PV applications as they generate a perfectly uniform illumination at the module surface, provided with certain combinations of concentration ratio and vertex angle. A drip irrigation system was simulated and maximum surface that can be irrigated by a V-trough PV pumping system was estimated by performing the water balance on a monthly basis [29]. Results showed that maximum irrigated area was increased up to 76% by the use of V-trough concentration cavity for PV pumping system, when compared with a fixed system of the same PV array.

A design procedure and experimental facility was built to assess the technical viability of a V-trough tracking PV system [30]. Collected radiation at the cavities aperture and absorber region was presented. A simple and basic theoretical tool was used to analyze the performance of the system which can be reliably used for design and evaluation purposes. Simulations were performed and the results indicated 26% increase in electric energy due to tracking, and the electric energy output for V-trough system was increased up to 72%, compared with horizontal fixed collector.

To design an efficient V-trough PV system, the optical and geometrical modeling should be done precisely. In order to obtain the maximum solar radiation and at the same

time keeping the size of the system compact, geometrical modeling was carried out [31]. Numerical simulations were conducted to find the parameters that can maximize the received global radiation of the PV cell and at the same time keeping an overall geometric size of the system as small as possible. Results indicated that concentration ratio increases with the increase in incidence angle and the tracking step duration does not affect the reflected radiation. However, in this study basic correlations were adopted which could be improved.

2.3 REVIEW OF PV-COMPOUND PARABOLIC CONCENTRATOR (CPC) SYSTEM

In the past, several novel designs of optical concentrating device for solar energy collection have been developed in order to reach high collecting temperatures with high efficiency. The compound parabolic concentrator (CPC) is the most promising low-concentration device which produces elevated operating temperature and represents the optimum optical properties. The performance of the solar collectors based on the CPC principles was evaluated by calculating the convective and radiative heat transfer through CPC [32]. To determine the optical losses, analytical technique was developed to calculate the average number of reflections for radiation passing through CPC. The effect of truncation was also considered which reduced the unwanted reflector area by compromising very little in the system performance.

Garg and Adhikari [33] have made optical design calculations of a CPC suitable for its coupling with a hybrid PV/T system. Results have been presented for a full and truncated 3X CPC. A theoretical analysis was presented for the modeling of thermal process of a hybrid PV/T collector coupled with CPC [34]. Parametric study showed that the thermal performance increased with the increase in collector length, cell density and mass flow rate, and decreased by the increasing the duct depth.

A PV system consisting of CPC with flat plate absorber integrated with Organic Rankine Cycle (ORC) was proposed [35]. Heat transfer and energy conversion processes were studied by developing mathematical formulations. Results concluded that PV-CPC module can produce much more electricity per unit surface area than side by side flat PV panels and CPC collectors for thermal electric generation. It was observed that when the evaporation temperature was 118 $^{\circ}$C, the system electricity efficiency was 13.1%, which is nearly twice as much as the PV efficiency at room temperature.

The concept of lens-walled CPC was presented and comparison was made with the common mirror and dielectric solid CPC's in terms of solar energy collection per annum [36]. This novel lens-walled CPC had a thin lens-shape wall with mirror coating on its back surface, and it had a larger acceptance angle due to refraction of lens. Optical analysis was carried out on PHOTOPIA, the results showed that lens walled-CPC can achieve about 80% of the solid CPC performance and 20-30 % greater than the mirror CPC in terms of monthly accumulative solar energy collection.

An interesting performance comparison between common flat and the solar concentrating PV/T systems using CPC was presented [37]. In this system they used a U-type pipe as a thermal collector as it avoids the temperature gradient on the whole absorber and on every block cell. A steady state model was developed to predict the thermal and electrical performances of PV/T-CPC. Simulations showed that PV/T-CPC significantly increased the overall thermal as well as electrical efficiencies compared to the common flat plate PV panel and required less number of PV cells.

A prototype double-pass PV/T solar air collector with CPC was designed with fins and fabricated [38]. The performance of this system over a range of operating conditions was studied. Energy balance equations were applied at various nodes of the system and the thermal performance was estimated. The results showed that electricity production decreased with the increase in temperature of air flow. Significant amount of increase in power production and decrease in cost of photovoltaic electricity can be obtained by this system.

Optical analysis of water-cooled PV/T hybrid system with low concentrating aluminum CPC was performed by Brogren et al [39]. Cost per energy produced was reduced by using concentrating hybrid systems due to simultaneous electricity and heat production. Optical efficiency of the PV-CPC system was determined to be 71%, which is in agreement with the optical efficiency estimated by the thermal and electrical measurements. It was concluded that optimized antireflection-treated glazing and reflectors could further increase the electric power yield.

A PV/T system with CPC was presented and three different reflector materials were analyzed for fill factor improvements in low concentrating system [40]. Effective specular reflectance was predicted for each reflecting material by short-circuit current measurements, flux distribution profile measurements and ray tracing method within 10^{o} from normal incidence. The fill factors gave a percentage decrease of 10% under concentration, due to result of high and non-uniform irradiance that increased the resistive losses during concentration. As the cost of aluminum is two to three times less than that of anodized aluminum and six times less than the cost of the micro reflector per square meter, it has the potential to be used as a PV-CPC reflector for cost reduction.

To estimate the annual collectible radiation captured by fixed CPC, a mathematical procedure was developed [41]. Theoretical analysis showed that the acceptance half-angle is the key parameter affecting the amount of collectible radiation around the year. It was found that CPC's were more favorable to be used in areas with higher latitude and abundant solar resources. The yearly optimal tilt-angle was equal to the latitude of the location in which CPC's were installed.

Many researches and development programs have been carried out in order to improve the applications of PV-CPC systems. Solar air heater with solar cells located at the absorber and CPC used for increasing the solar intensity was investigated experimentally [42]. Performance of the photovoltaic cells coupled with CPC showed that electrical performance decreased as the temperature of the air increased. On the other hand for thermal efficiency the system should deliver hot air for other purposes.

Therefore a compromise has to be made between maximizing electricity production and producing hot air for other domestic purposes.

2.4 REVIEW OF PV/T SYSTEM

Water and air are the most efficient medium of cooling the PV panels utilized rather than refrigerants because of the high maintenance and capital cost. Due to high thermal conductivity and high heat capacity, water is mostly used to remove the heat from the PV panels. There are different flow configurations of the water through the micro-channel heat exchanger. Through numerical analysis different flow configurations can be analyzed and after doing the preliminary studies an optimal model can be selected for manufacturing.

The thermal yield of a combined PV/T collector was simulated by a 3D dynamical model and three steady state models (1D,2D and 3D) [43] . It was found that the simple 1D steady state model performed equally better than time consuming 3D dynamical model. To perform optimization of the collector 2D and 3D models were easily adaptable to different configurations and also provided more detailed information. For an accurate prediction of the collector yield a transient model was required due to difference in measurement of starting temperature and temperature at the end. Numerical and experimental results were in a good agreement within 5% accuracy.

Performance of a PV/T collector is not accurately predicted by utilizing a steady state model. The issue is that heat removal fluid is under fluctuating irradiance and is in the

state of intermittent flow at times. Therefore, an explicit dynamic model was presented to study the operating characteristics of PV/T collector [44]. Estimation of the experimental parameters can be more accurately carried out by a transient case. Control-volume finite difference approach was applied to solve the transient model as it provided the detailed analysis of the transient energy flow through different types of collector components. This transient model also enables the instantaneous energy output to be examined. Electrical and thermal efficiencies were also reported to increase when flow rate in tube increases from 0.002 to 0.016 kg/s.

Harjit Singh and Eames [45] analyzed the correlations developed for heat transfer in the regular shaped cavities, like those of rectangular, square cross-section, or cylindrical annuli. It was concluded that employment of these correlations to describe natural convection in CPC solar collector cavities can be misleading.

Performance of hybrid PV-Thermal systems in which panels were made from different materials like crystalline silicon, amorphous silicon and $CuInSe_2$ was investigated [46]. For better extraction of heat from the panel, the thermal contact between the absorber surface and the panel substrate should be efficient. By using a metallic substrate covered with thin insulating layer, the prototype panel showed 10% increase of the power produced due to its efficient thermal contact with the collector.

A hybrid PV/T water-heating system with natural circulation was fabricated and experimental results showed that daily primary energy saving reached up to 65% for the

proposed system [47]. It was concluded from the results that overall system performance would be better if the packing factor and glazing transmissivity is higher.

An integrated photovoltaic and thermal solar system (IPVTS) was compared to a conventional solar water heater [48]. IPVTS was designed and the idea was demonstrated by using a commercial polycrystalline PV module for making a PV/T collector. Primary-energy saving efficiency for the evaluation of a PV/T system was introduced by the above study and it exceeded 60% for the present IPVTS system, which was higher than a pure solar hot water heater or pure PV system. The performance of the PV/T collector could be improved by packing heat-collecting plate, the PV cells and the glass cover together to form a glazed collector.

Relation between the geometric parameter W/D and the performance of the PV/T system was investigated [49]. An algorithm was developed to simulate the performance of a hybrid PV/T system. The thermal efficiency is approximately halved when the fin width to tube diameter ratio is increased from 1 to 10. The relative increase in solar cell efficiency as the result of cooling was in the order of 10-30%. It was reported that as the water flow rate was increased from 0.001 to 0.0075 kg/s, the thermal efficiency increased by a factor of 0.1.

A polymer solar thermal collector was developed with combining the single-crystal silicon PV cells in a hybrid energy-generating unit [50]. A comparison made with a PV/T absorber to a pure thermal absorber showed reduced thermal efficiency for the PV/T system. On the other hand the PV/T system can reduce the heat loss from the collector as

the solar act as selective surface. An analytical model for the PV/T system was developed which simulated the temperature development and the performance of both the thermal and photovoltaic units. The model was the modified version of Hottel and Willier model made for flat plate thermal collectors. About 10% energy reduction was observed after attaching the PV cells onto an absorbing surface because the absorptivity of the PV cell is lower than that of a black absorber.

Electrical and thermal efficiency can be increased through good thermal-contact between the thermal absorber and the PV module. Fin performance of the heat exchanger is also one of the important factors in achieving a high overall energy yield. By reviewing the design developments of the PV/T collectors, an aluminum-alloy flat-box type hybrid solar collector functioning as a thermo syphon system was constructed [51]. Results indicated that the daily thermal efficiency could reach about 40% provided the initial water temperature in the system is equivalent to daily mean ambient temperature.

Numerical simulation was carried out by Kalogirou [52] to study the output characteristics of a hybrid PV/T system using TRNSYS. The whole setup consisted of series of PV panels, a battery bank, a hot water storage tank, a pump, a differential thermostat and an inverter. Meteorological data of Cyprus was used and optimized flow rate was calculated.

A PV/T hybrid collector was designed and constructed by Fujisawa and Tani [53]. The collector comprised of a liquid heating flat-plate solar collector with monocrystalline silicon PV cells on absorber plate made of aluminum. As exergy can be used to

qualitatively compare the electrical and thermal energy based standard, exergy analysis was carried out to evaluate the experimental performance of the designed PV/T system.

Garg and Agarwal [54] utilized the finite difference method to investigate PV/T system with different solar cell areas and flow rates. The system comprised of a storage tank, pump, differential controller and PV modules. The optimum flow rate of this experimental setup was 0.03 kg/s, for maximum thermal efficiency. It was shown that the electrical efficiency decreased at this flow rate and was lowest when the insolation was highest (as the temperature of absorber is maximum).

2.5 ELECTRICAL MODELING

For the simulation study of the power system the system designers require an efficient and regimented PV array electrical model that is capable of generating electrical characteristics, i.e I-V and P-V relationship of PV panel under different radiation and cell operating temperature conditions. The output characteristic of PV devices (panels or arrays) is extremely nonlinear and it is not suitable to represent them with constant or controlled voltage/current source. Several PV electrical models have been proposed and developed by the researchers including the models that use experimental correlations, are based on the analytical information of PV cell working and combination of both the methods. Some of these models are described vaguely and some of them are much complex for the simple power system studies.

The proposed simplest model is temperature and radiation scaling of maximum power point [55]. It requires the temperature and irradiation coefficient of the maximum power point and predicts the performance of the PV device only at one point. A method of translation of I-V curve from one environmental condition to other is adopted [56]–[58]. A bilinear interpolation method is presented by Marion et. al [57] that requires four practically determined I-V curves, two at different insolation and two at different cell temperatures. Behavior of the PV panel at any ambient condition is determined by interpolating the four I-V curves with short circuit current and open circuit voltage to check for solar irradiance and temperature respectively. These models are quite complex and require a large amount of data that is not usually provided from the manufacturer. The most efficient and practical model for PV array simulation is King et. al model [58]. This model takes three inputs, namely ambient temperature, solar radiation and wind speed and computes the voltage and current of PV array at five main points on the I-V. This model requires thirty practically determined constants to simulate the behavior of any PV panel. The values of these coefficients are available for a large number of commercial PV modules [59]. Due to the complexity of these models power system studies like load flow, maximum power point tracking, load frequency match become difficult and requires large computational time. Electrical characteristics of the PV panel can be modeled by representing it with equivalent electrical circuit [60].

This model has the advantage over the other models due to its electrical circuit nature and the behavior of the PV array can easily be understood in the circuit connected. This

model is best suited for the dynamic and transient study of the power electronics converters.

The electric circuit based model of the PV device is further classified as an ideal diode model (three parameters model), four parameters model (R_s model), five parameters model (R_p model) and double diode model (seven parameters model) as shown in Figure 2.1.

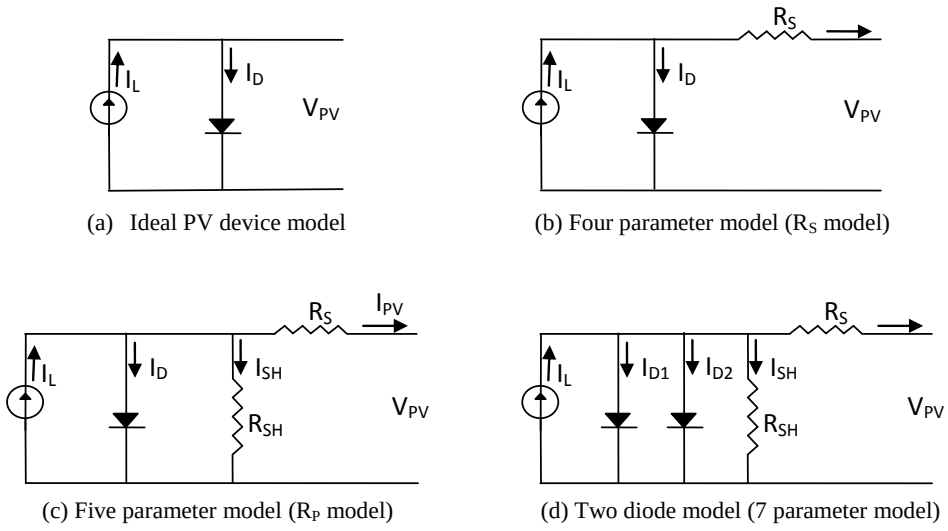

(a) Ideal PV device model

(b) Four parameter model (R_S model)

(c) Five parameter model (R_P model)

(d) Two diode model (7 parameter model)

Figure 2.1: Equivalent electric circuit model of PV device.

The simplest among these models is the ideal diode model it consist of a single diode and irradiation dependent current source [61]–[63] as shown in Figure 2.1(a). This model needs three parameters, i.e. I_L light current, I_o saturation current of diode and a ideality factor of diode to generate the complete output characteristics of a PV device.

Performance of this ideal model is enhanced by adding a resistance in series and it is generally known as four parameter model (R_s-model) [60], [64]–[68] as shown in Figure 2.1(b). This model requires one additional parameter (R_s series resistance) to be known to characterize the I-V curve. A model is implemented in MATLAB programming and examines the modeling process and illustrates the PV panel's output characteristics with the varying ambient conditions [68]. This model is easy in implementation and provides acceptable results but its performance deteriorates at high temperatures and low irradiation and also for thin film technology based PV panels [58-59]. Considering this issue, an improved circuit based model is developed widely known as five parameters model (R_p model) as shown in Figure 2.1(c) [70]–[73]. An additional parameter, shunt resistance, is considered which was neglected in four parameter model. Comparison of four and five parameter model is done for the mono crystalline PV panel and showed that the five parameters model is more efficient in estimating the operating current and power at different atmospheric conditions [66]. To further improve the efficiency of the circuit based model some authors used the two diode model (seven parameters model) [69], [74]–[76] as shown in Figure 2.1(d). The number of parameters to be computed during simulation is increased by inclusion of an extra diode that will make the model computationally inefficient. The competency of the two diode model over R_s-model and R_p-model is shown in [69]. To make the model computational efficient values of some parameters are assumed to be constant which deteriorates its performance under the partial shading condition. Carrero et al. [71] suggested that the five parameters model is a good compromise between accuracy and simplicity and it is the most widely used model

in the literature. Behavior of the PV device under the partial shaded condition has been studies by various researchers [77]–[80]. This situation may happen due to the passing clouds, dust or snow covering the PV panel, shadows of trees or birds litters. In partial shading state the un-shaded cells of the PV panel become more forward biased and the shaded cells become reverse bias. When the reverse voltage increases beyond the breakdown voltage of the cell the "hot-spot" phenomenon take place and causes the irreparable damage to the cell. This problem is solved by using the by-pass diodes [77]. Due to by-pass diodes multiple peaks occur in the P-V characteristics which add additional complexity in modeling the PV array. The impact on the I-V curve and output of the PV panel due to the partial shading condition is studied [78]. Experimental work on panel shading was performed in [79] . A comprehensive MATLAB based modeling of the shaded PV array is carried out in [80].

The most challenging part in the implementation of equivalent circuit based models is to identify the values of these parameters as their values are not provided in the solar panel catalogues. The performance and competence of these models are entirely dependent on these parameters and their values should be estimated using accurate and efficient algorithms. Two approaches are widely used for the estimation, one approach approximate the original I-V and P-V characteristics using the selected key points, i.e. the short circuit point, open circuit point and maximum power point [81], [82]while the other approach works on the curve fitting principle [83]–[85].Both methods have their own pros and cons. The latter have the advantage that it considers all the experimental data. However, it has the difficulty of artificial solutions [81] and requires large number of

experimental data which is not usually provided by the manufacturer. The preceding method is simple and fast as compare to the curve fitting method and utilized in this study. However, it optimizes the values of parameters only at the selected key points [84]. Several algorithms have been utilized by the researchers for the identifications of these parameters. The simplest method is to assume the value of one parameter and calculate other parameters using analytical equations and iterative methods [64], [68], [73], [86]–[88]. Villalva et al. [86] supposed the value of *a* and found the values of R_s and R_{sh} concurrently by numerical technique and values of I_o and I_L analytically. An iterative technique is utilized in [58,54] to find the valued of R_S and *a* by neglecting the effect of R_{sh}. R_{sh} is ignored by considering it to be infinite and value of *a* is taken constant and compute other parameters by solving the analytical equations [87]. The efficiency of these methods is tainted because of the assumption considered and their scope is limited. In [60,78] authors used the nonlinear equation solver software for the solution of non-linear equations to find the model parameters. These softwares have limitation and cannot be able to provide result for all the PV panels. To estimate the values of these parameters accurate and efficient algorithms should be used for the optimization process. Ishaque and Salam [89] presented a novel scheme for determination of the five parameters. Their method works on the principle of adjusting the I-V and P-V curve at three key point short circuit point, open circuit point and maximum power point and find out the best values of model parameters that result in the slightest error at these three key points. An iterative method is implemented for the estimation of parameters [90]. This method uses simplified I-V equation and results in fast convergence.

Five parameter model is used in the current study. Engineering Equation Solver is used to solve the highly non-linear equations of the five parameter model. The details of the five-parameter model are presented in Chapter 3.

CHAPTER 3 PROPOSED MODELING

Low concentration PV (LCPV) systems have a concentration ratio of less than 10X. These systems include various configurations like compound parabolic concentrator (CPC), prism-based concentrators and V-troughs. These configurations often utilize single junction silicon cell and have simple design. The concentrating optics or reflectors used in such systems are easier and cheaper to manufacture than high concentrating systems as they do not normally require tracking. In addition to direct component of solar radiation, LCPV systems have the capability to capture the large amount of diffuse solar radiation, making them suitable for stand-alone application and building integration. Different configurations of PV-CPC system and V-trough PV system are considered in this study. The details of the modeling for these configurations are given in this section.

3.1 PV-CPC SYSTEM

The CPC contains two parabolic reflectors which funnel the incident solar radiation on to the absorber/PV cell. Absorber/PV cell is located between the distances of focuses of two parabolas. CPC troughs are usually mounted in east–west direction with the aperture inclined from the horizon. Thus, for a fixed east–west aligned CPC, the acceptance half angle is a crucial parameter to determine its performance in term of annual solar gain. For such fixed CPC's, the smaller the acceptance half-angle, the

greater the geometrical concentration factor, but the time for accepting direct radiation in a day is shorter, and less beam radiation will be accepted. Many researchers have carried out the optical and thermal modeling of the PV-CPC separately, but the efficient comparison and prediction of their performance require coupling of all these models. In this work detailed optical modeling has been presented which estimates the amount of absorbed radiation by PV-CPC system. This absorbed energy partially gets converted to electrical energy and the remaining is used to heat up the PV cell. In order to estimate the PV cell temperature, energy balance equations are applied at each component of the PV-CPC system. Finally the absorbed radiation and the cell temperature are used as input parameters from optical and thermal model into electrical model to estimate the maximum power output from the PV-CPC system.

3.1.1 Geometrical Modeling

Three cases are considered for the present study:

Case1: Glazed PV-CPC system

Case2: Unglazed PV-CPC system

Case3: Flat PV string

The CPC contains two parabolic reflectors and the absorber/solar cell is located between the distances of two focuses of parabolas. CPC has the advantage that it can achieve some concentration without continuous tracking. But to get the maximum output from the collector, CPC should be properly oriented along east-west axis and tilted

towards due south with slope equal to latitude of the location. The width of the PV strings used in the present case is 125 mm and the CPC is modeled for 134 mm including the width of the back sheet and tolerances. The surfaces become parallel to central plane of symmetry at the upper end points of CPC, thus contributing little to the radiation reaching the absorber. Therefore 38% truncation was applied to save the reflector area and along with a little compensation in the performance. In order to model the CPC for the current PV strings, following equations [32] are simultaneously solved in the EES software.

$$\bar{l} = 2\bar{x}\cos\theta - \frac{\bar{x}^2 \sin\theta}{s(1+\sin\theta)} + s(\sin\theta - \cos^2\theta) \tag{3.1}$$

$$\bar{x} = \frac{s(1+\sin\theta)}{\cos\theta}\left(\left(1+\frac{\bar{h}\cos^2\theta}{h\sin^2\theta}\right)^{0.5} - \sin\theta\right) \tag{3.2}$$

$$\bar{h} = \bar{x}\sin\theta + \frac{\bar{x}^2\cos\theta}{2s(1+\sin\theta)} - \frac{s\cos\theta(1+\sin\theta)}{2} \tag{3.3}$$

$$h = \frac{s}{2}\left(1+\frac{1}{\sin\theta}\right)\frac{\cos\theta}{\sin\theta} \tag{3.4}$$

In the above equations barred quantities are used for representing the truncated dimensions as $\bar{l}$ for the opening aperture, $\bar{h}$ is the height, s is the width of the absorber and Θ is the half acceptance angle of CPC as shown in Figure 3.1.

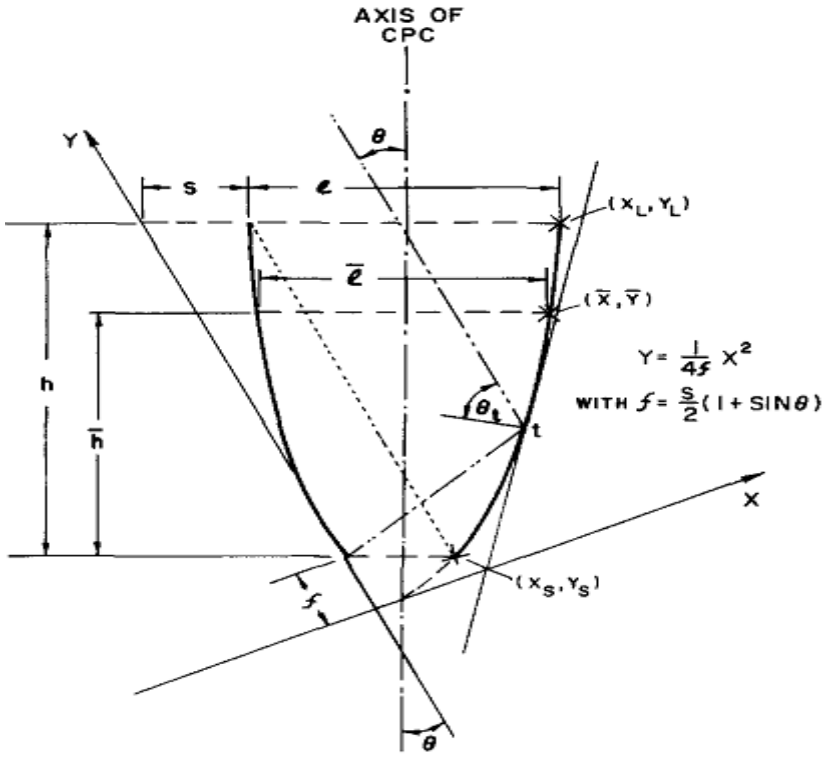

Figure 3.1: Coordinate system used for describing CPC.

After solving the above equations simultaneously, the half acceptance angle for this geometry was 41.75°. The geometrical concentration ratio for truncated CPC was calculated to be 2.3X. Stainless Steel (mirror type) was used as reflecting material for the walls of CPC which has good reflectivity and provides better resistance to corrosion. Schematic diagram of glazed and unglazed PV-CPC system is shown in Figure 3.2.

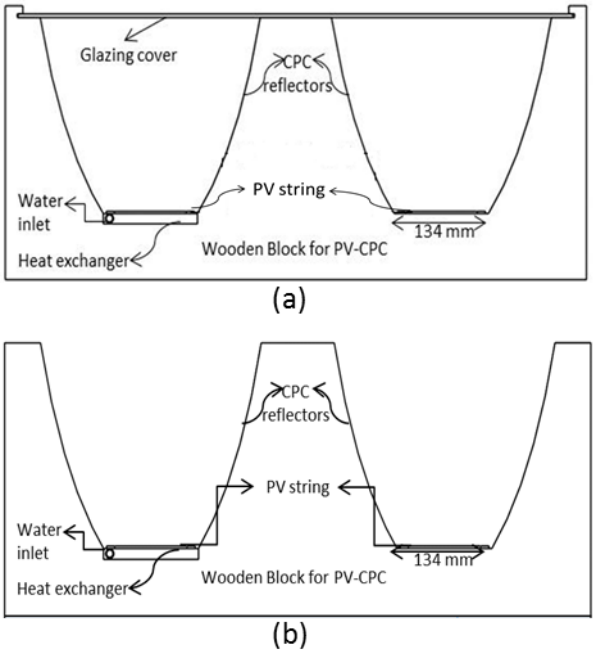

Figure 3.2: Schematic diagram of (a) glazed and (b) unglazed PV-CPC with and without cooling

3.1.2 Optical Modeling

The amount of solar radiation incident on the tilted surface I_T is estimated by using Isotropic model [91].

$$I_T = I_b R_b + I_d \left(\frac{1+\cos\beta}{2} \right) + I\rho g \left(\frac{1-\cos\beta}{2} \right) \tag{3.5}$$

In the above equation I_b and I_d are the beam and diffuse component respectively, β is the slope which is mostly equal to the latitude of the location, ρ_g is the ground reflectivity. Now to estimate the amount of energy absorbed, we need to determine the contribution of diffuse, ground reflected and beam component in the total absorbed

radiation. ($\boldsymbol{\tau\alpha}$) is the product of transmittance absorbance product of solar cell which is calculated separately for beam, diffuse and ground reflected radiation from Equation (3.6) and (3.7), where θ_r is the angle of refraction. While determining the ($\boldsymbol{\tau\alpha}$)product, internal reflection losses are also incorporated which occur in the different layers of the solar cell.

$$\tau\alpha\left(\theta_i\right) = e^{-(KL/\cos\theta_r)}\left[1-\frac{1}{2}\left(\frac{\sin^2(\theta_r-\theta_i)}{\sin^2(\theta_r+\theta_i)}+\frac{\tan^2(\theta_r-\theta_i)}{\tan^2(\theta_r+\theta_i)}\right)\right] \tag{3.6}$$

Since there is little refraction at the back of the glass, i.e., there is no glass-air interface; the angle of incidence of the radiation on the cells will be the angle of refraction for the air-glass interface which is given by Snell's law. The angular dependence of the absorptance α, is given by [91]

$$\frac{\alpha}{\alpha_n} = 1 + 2.0345\times10^{-3}\theta_i - 1.990\times10^{-4}\theta_i^2 + 5.324\times10^{-6}\theta_i^3 - 4.799\times10^{-8}\theta_i^4 \tag{3.7}$$

In order to estimate the amount of radiation absorbed by the CPC absorber/solar cell, it is important to determine that whether the incidence angle of beam radiation is within the acceptance angle of CPC 2θ or not. Absorbed radiation for CPC is given by

$$S_{CPC} = G_{b,CPC}\tau_{CPC,b}\left(\tau\alpha\right)_b + G_{d,CPC}\tau_{CPC,d}\left(\tau\alpha\right)_d + G_{g,CPC}\tau_{CPC,g}\left(\tau\alpha\right)_g \tag{3.8}$$

In the above equation $\boldsymbol{G_{b,CPC}}$is the beam component of the radiation that is within the acceptance angle,$\boldsymbol{\tau_{CPC,b}}$ is the transmittance of the CPC which incorporates the reflection losses and is dependent on the average number of reflections of incident radiations.

Similarly the terms for diffuse and ground reflected are analogous to those for beam radiation which can be found by the following equations given in [91]

$$G_{b,CPC} = FG_{bn}\cos\theta_i \tag{3.9}$$

$$G_{d,CPC} = \begin{cases} \dfrac{G_d}{C} & \text{if } (\beta+\theta_i)<90^o \\ \dfrac{G_d}{2\left(\dfrac{1}{C}+\cos\beta\right)} & \text{if } (\beta+\theta_i)>90^o \end{cases} \tag{3.10}$$

$$G_{g,CPC} = \begin{cases} 0 & \text{if } (\beta+\theta_i) < 90^o \\ \dfrac{G_g}{2\left(\dfrac{1}{C}-\cos\beta\right)} & \text{if } (\beta+\theta_i) > 90^o \end{cases} \tag{3.11}$$

$$(\beta-\theta_i) \le \tan^{-1}\left(\tan\theta_z\cos\gamma_s\right) \le (\beta+\theta_i) \tag{3.12}$$

In Equation (3.9) F is the control function introduced which is 1 if the criterion of Equation(3.12) satisfies otherwise it is zero.

3.2 V-TROUGH PV SYSTEM

To analyze the performance of V-trough PV system, a sequential modeling is required which involves the integration of radiation model, thermal model and electrical model. The radiation model used to estimate the amount of available radiation is Isotropic model as discussed earlier in section 3.1.2.

3.2.1 Optical Modeling of V-trough PV System

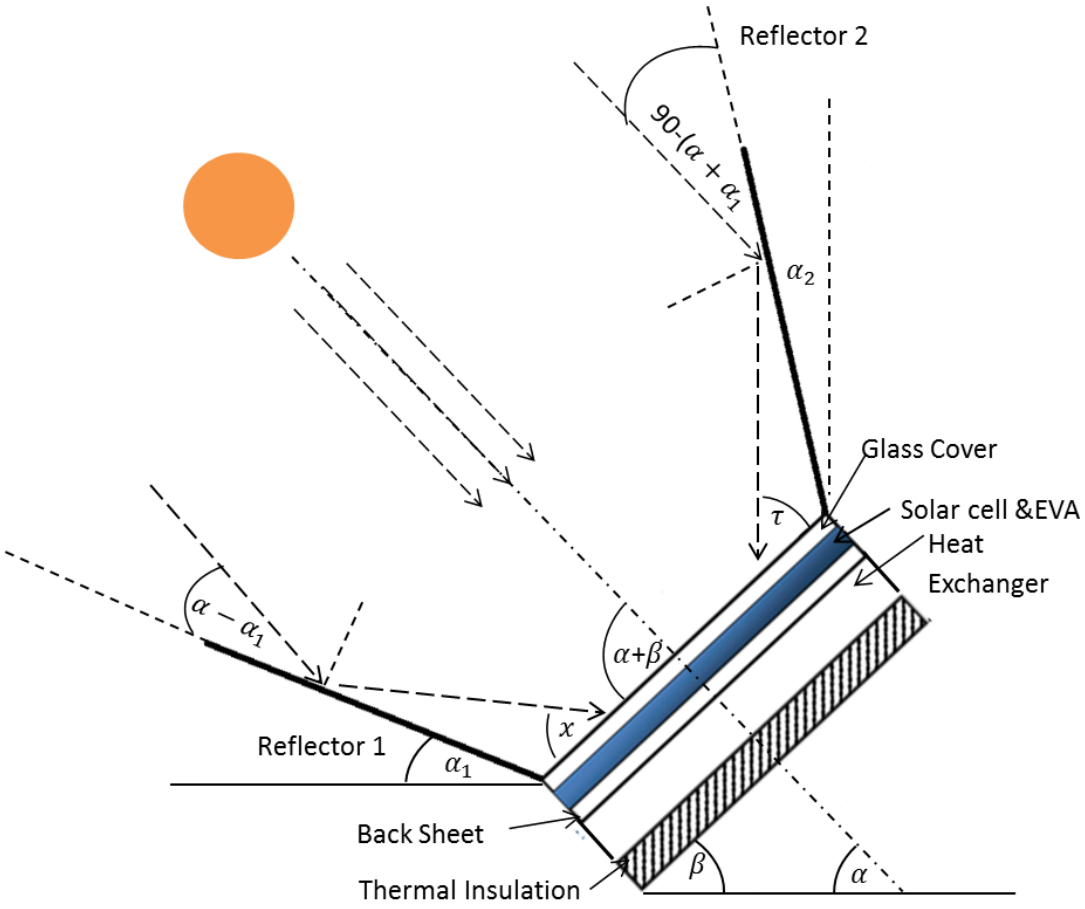

Figure 3.3: Schematic diagram of V-trough PV system

The total solar radiation absorbed by the V-trough PV system is equal to the sum of direct radiation S_b on the PV surface, the sky-diffuse radiation S_d, the ground reflected radiation S_g, the radiation reflected from the bottom reflector to the PV panel with tilted

plane angle α_1 and the reflected radiation from upper reflector to the surface of PV panel with tilted plane angle α_2, i.e.[92]

$$S_{tot} = S_b + S_d + S_g + S_{ref,r1} + S_{ref,r2} \tag{3.13}$$

where

$$S_b = \left(I_T \cdot sin\left(\alpha + \beta\right)\right)(\tau\alpha)_b \tag{3.14}$$

$$S_d = I_d \left(\frac{1+Cos\beta}{2}\right) \cdot (\tau\alpha)_d \tag{3.15}$$

$$S_g = \rho_g I_0 \left(\frac{1-Cos\beta}{2}\right)(\tau\alpha)_g \tag{3.16}$$

$$S_{ref,r1} = \rho_{Al} \cdot I_T \cdot sin(x) \cdot sin\left(\alpha - \alpha_1\right) \cdot \left(\tau\alpha\right)_b ; x = \beta + 2\alpha_1 - \alpha \tag{3.17}$$

$$S_{ref,r2} = \rho_{Al} \cdot I_T \cdot sin\left(\tau\right) \cdot sin\left(\alpha + \alpha_2\right) \cdot \left(\tau\alpha\right)_b ; \tau = \alpha + 2\alpha_2 - \beta \tag{3.18}$$

In the above equations, α is the solar altitude angle which is given by

$$\sin\alpha = \cos\phi.\cos\delta.\cos\omega + \sin\phi.\sin\delta \tag{3.19}$$

The optical model presented by the Equations (3.13) to (3.19) has been used to calculate the amount of absorbed energy in the V-trough PV system. The transmittance absorptance product for different components is calculated by the same procedure as discussed earlier in section 3.1.2.

3.3 THERMAL MODELING

Absorbed radiation estimated from the optical models of the PV-CPC system and V-trough PV system is employed to evaluate the thermal model for the temperature distribution in different components.

Following assumptions are made while modeling the thermal network.

1. Energy transfer in the problem is one-dimensional and steady state of energy transfer is achieved.
2. Convection and radiation losses from the front cover and insulation are same to the ambient. The temperature gradient of the glass cover and solar cell is neglected.
3. Temperature variation along the thickness and width of the solar cell is negligible.
4. There is no dust and dirt effect on the collector.
5. The water flow in the rectangular channel is uniform and fully developed.
6. Contact resistance between the reflectors and the solar cell is neglected.

Based on the above assumptions the energy balance equations on the different components of the PV-CPC system and V-trough PV system are written as follows:

3.3.1 PV-CPC system

In case of PV-CPC system there are two cases; (a) glazed PV-CPC system with and without cooling, (b) unglazed PV-CPC system with and without cooling. Energy balance equations for the case of glazed PV-CPC system are written as follows:

(1) PV cell

$$S = U_t(T_c - T_a) + h_T(T_c - T_{bs}) \tag{3.20}$$

In this equation the amount of energy absorbed is calculated by a detailed optical model described above. U_t is the overall top loss coefficient from the cell to the ambient. h_T is the overall heat transfer coefficient from the cell to the back sheet.

(2) Cell Glass cover

$$U_{cg}\left(T_c - T_g\right) = U_{gcpc}\left(T_g - T_{cpc}\right) \tag{3.21}$$

where U_{cg} is the overall heat transfer coefficient from solar cell to the glass cover and U_{gcpc} is the overall heat transfer from coefficient from the cell glass cover to the above glazed cover.

(3) Glazing Cover

$$U_{gcpc}\left(T_g - T_{cpc}\right) = U_{cpca}\left(T_{cpc} - T_a\right) \tag{3.22}$$

where U_{cpca} is the overall heat transfer coefficient from the top of the CPC glazing cover to ambient through radiation and wind convection.

(4) Back Sheet

$$U_{cbs}\left(T_c - T_{bs}\right) = U_{bsf}\left(T_{bs} - \bar{T}_f\right) \tag{3.23}$$

where U_{cbc} is the heat transfer coefficient from cell to back sheet and U_{bsf} is the heat transfer coefficient from back sheet to the flowing fluid.

(5) Fluid flowing in the heat exchanger

$$U_{bsf}(T_{bs} - \bar{T}_f) = \dot{m}C_p \frac{dT_f}{dx}dx + U_{fa}(T_f - T_a) \tag{3.24}$$

where $\dot{m}$ the mass flow rate of fluid flowing and C_p is the specific heat of fluid flowing in the rectangular heat exchanger. U_{fa} is the overall heat transfer coefficient from the flowing fluid to the ambient.

Useful energy gain from the system is calculated by

$$Q_u = \dot{m}C_p(T_{fo} - T_{fi}) \tag{3.25}$$

where T_{fo} and T_{fi} are fluid inlet and outlet temperatures respectively.

In above equations, related heat transfer coefficients are defined for PV-CPC system with cover as follows

$$U_t = (R_1 + R_2 + R_3)^{-1} \tag{3.26}$$

$$U_{cbs} = 1/R_4 \tag{3.27}$$

$$U_{cg} = 1/R_3 \tag{3.28}$$

$$U_{gcpc} = 1/R_2 \tag{3.29}$$

$$U_{acpc} = 1/R_1 \tag{3.30}$$

$$U_{cbs} = 1/R_4 \tag{3.31}$$

$$U_{bsf} = 1/R_5 \tag{3.32}$$

$$U_{fa} = 1/\left(R_6 + R_7\right) \tag{3.33}$$

The resistances of the thermal network shown in Figure 3.4 are calculated by the mode of heat transfer between the nodes. Mode of heat transfer between glass and cover of CPC includes convective and radiative heat transfer as given in the equation below

$$R_2 = 1/(h_{g-cpc} + h_{r,g-cpc}) \tag{3.34}$$

Similarly other resistances can also be determined by adding the respective heat transfer coefficients. Convective heat transfer coefficient $h_{g\text{-}cpc}$ is calculated by assuming convective heat transfer between two flat parallel plates [32].

In case of uncooled glazed PV-CPC, there is no heat exchanger present and hence the energy balance equation of the flowing fluid is omitted in the thermal network as shown in Figure 3.5. The resistances from the thermal network shown in Figure 3.5 are solved to evaluate the temperature distribution in different components of the glazed PV-CPC system.

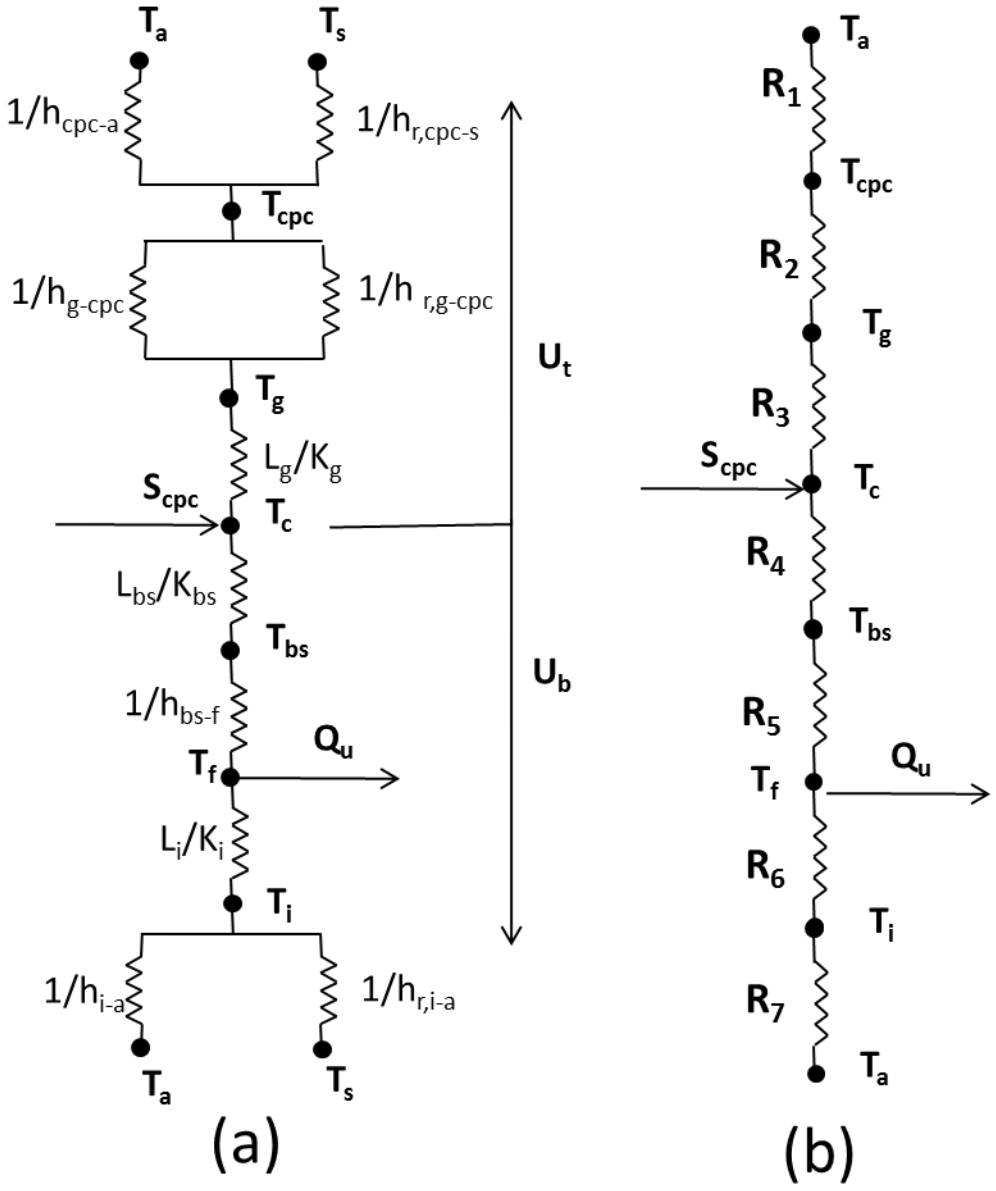

Figure 3.4: Thermal network for glazed PV-CPC with cooling (a) in terms of conduction, convection and radiation resistances; (b) in terms of resistances between plates.

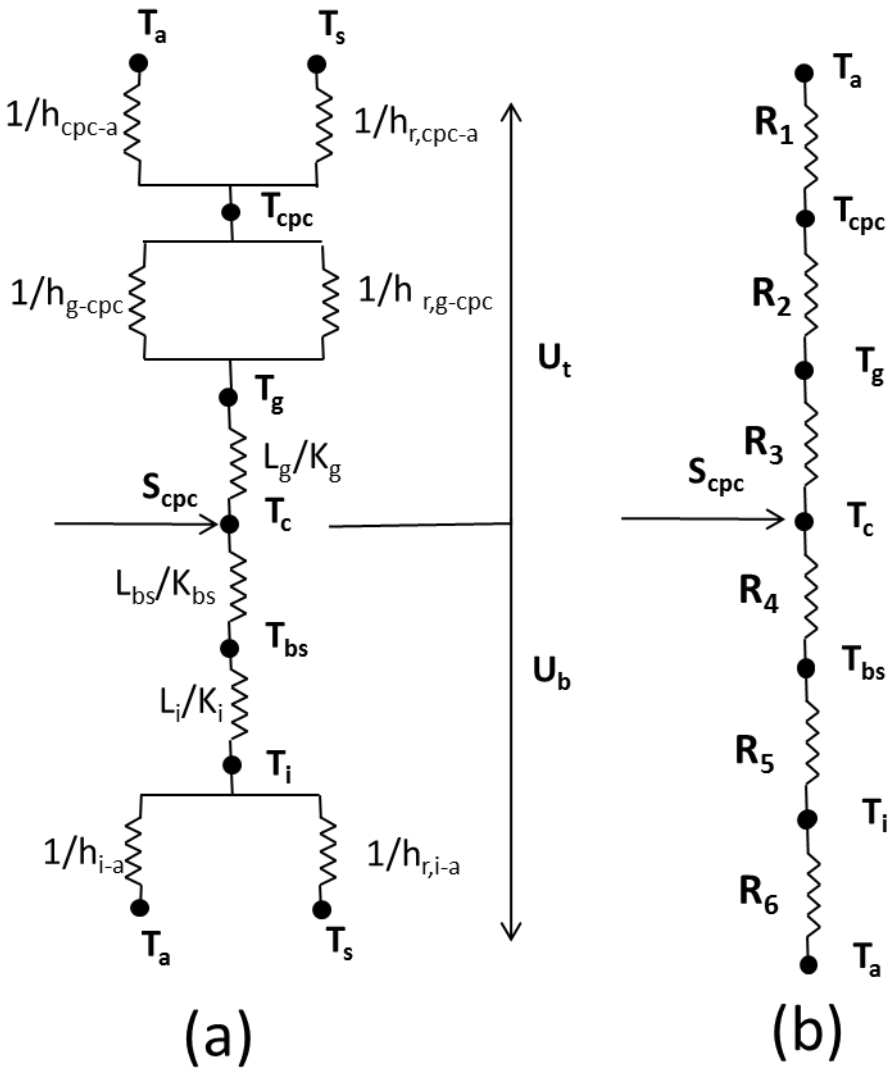

Figure 3.5: Thermal network for glazed PV-CPC without cooling (a) in terms of conduction, convection and radiation resistances; (b) in terms of resistances between plates.

Energy balance equations for the case of unglazed PV-CPC system are written as follows:

(1) PV cell

$$S = U_t(T_c - T_a) + h_T(T_c - T_{bs}) \tag{3.35}$$

(2) Cell Glass cover

$$U_{cg}\left(T_c - T_g\right) = U_{ga}\left(T_g - T_a\right) \tag{3.36}$$

(3) Back Sheet

$$U_{cbs}\left(T_c - T_{bs}\right) = U_{bsf}\left(T_{bs} - \bar{T}_f\right) \tag{3.37}$$

(4) Fluid flowing in the heat exchanger

$$U_{bsf}(T_{bs} - \bar{T}_f) = \dot{m}C_p \frac{dT_f}{dx}dx + U_{fa}(T_f - T_a) \tag{3.38}$$

The thermal networks for the unglazed PV-CPC system with cooling and without cooling are shown in Figure 3.6 and Figure 3.7 respectively. Conductive, convective and radiative resistances between different components are calculated in order to estimate the temperature variation in different components of the unglazed PV-CPC system.

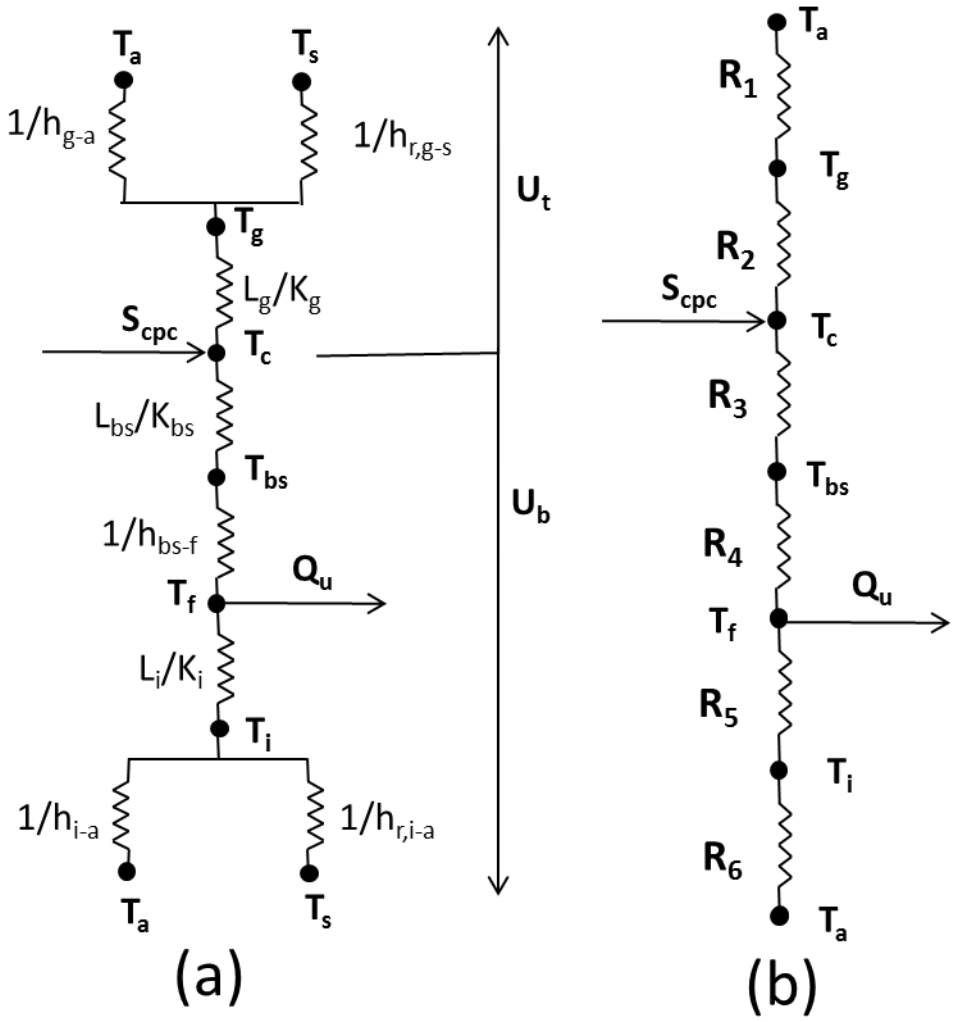

Figure 3.6: Thermal network for unglazed PV-CPC with cooling (a) in terms of conduction, convection and radiation resistances; (b) in terms of resistances between plates.

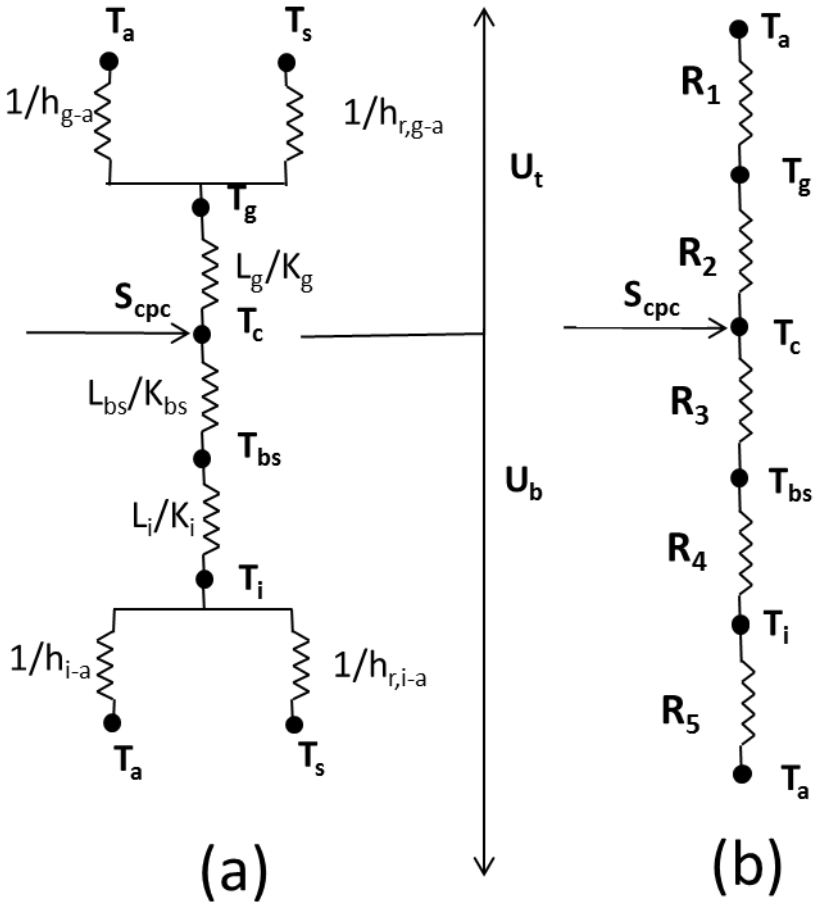

Figure 3.7: Thermal network for unglazed PV-CPC without cooling (a) in terms of conduction, convection and radiation resistances; (b) in terms of resistances between plates.

3.3.2 V-trough PV system

Energy balance equations for V-trough PV system are similar to unglazed PV-CPC system as the reflectors are assumed not be in perfect contact between the solar cell/panel. Absorbed radiation obtained from the optical modeling of V-trough PV system is used to estimate the temperature across the different components of V-trough PV system. The thermal network for cooled and uncooled V-trough PV system is same as shown in Figure 3.5 and Figure 3.6 respectively.

3.3.3 Heat Transfer Coefficients

The heat transfer coefficients required to solve the thermal network are explained as follows:

Radiation Heat Transfer coefficient

In the analysis the radiation heat transfer coefficient is given by [91]

$$h_{ra} = \varepsilon\sigma\left(T_p^{\,2} + T_s^{\,2}\right)\left(T_p + T_s\right)\left(\frac{T_p - T_s}{T_p - T_a}\right) \tag{3.39}$$

where ε is the emissivity of the plate or cover radiating its energy to the atmosphere and σ is the Stefan-Boltzmann constant. T_s is the sky temperature which is given as [91]

$$T_s = T_a\left(0.711 + 0.0056 \times T_{dp} + 0.000073 \times T_{dp}^{\,2} + 0.013 \times \mathrm{Cos}(15t)\right)^{0.25} \tag{3.40}$$

where T_{dp} is the dew point temperature in degree Celsius, and *t* is the hour from midnight. The range of difference in sky and atmosphere temperature is from 5°C in a hot, humid climate to 30°C in a cold dry climate.

The mode of radiation heat transfer between the glass cover and the glazing of the CPC is taken by assuming the heat transfer between two flat parallel plates which is given as [91]

$$h_{rcpc} = \frac{\sigma\left(T_{cpc}{}^2 + T_g{}^2\right)\left(T_{cpc} + T_g\right)}{\frac{1}{\varepsilon_{cpc}} + \frac{1}{\varepsilon_g} - 1} \tag{3.41}$$

where ε_{cpc} is the emissivity of the glazing.

Convection Heat Transfer

In the case when PV-CPC system is covered by glazing there is air enclosed in the CPC cavity which gets heated up and there is natural convection being taking place from the glass cover of the cell to top glazing through air. The CPC cavity is a bit complicated, therefore in order to simplify the analysis natural convection is assumed to be between parallel flat plates which is given as [91]

$$\begin{aligned} Nu &= \frac{hL}{k} \\ Ra &= \frac{g\beta'\Delta TL^3}{\nu\alpha} \\ \Pr &= \frac{\nu}{\alpha} \end{aligned} \tag{3.42}$$

The analytical expression for Nusselt number was given for tilt angles from 0 to 75^0 as [91]

$$Nu = 1 + 1.44\left[1 - \frac{1708\left(sin\left(1.8\beta\right)^{1.6}\right)}{Ra.\mathrm{Cos}\beta}\right]\left[1 - \frac{1708}{Ra.Cos\left(\beta\right)}\right]^{+} + \left[\left(\frac{Ra\mathrm{Cos}\beta}{5830}\right)^{.3333} - 1\right]^{+} \quad (3.43)$$

where the +ve sign on the terms indicate that only positive values are to be considered.

The data reported for a $0.5m^2$ plate in which the wind-related heat transfer coefficient h_w is given by the dimensional equation as [91]

$$h_w = 5.7 + 3.8V_w \quad (3.44)$$

. The fluid flow in the rectangular heat exchanger is assumed to be hydro dynamically fully developed at the collector inlet. With fully developed hydrodynamic and thermal profiles, the Nusselt number is 4.4 for constant heat flux. The inner surface convective heat transfer coefficients were modeled according to the flow regime.

3.4 ELECTRICAL MODELING

The main objective in modeling the PV device is that the model should be able to regenerate the output characteristics of the PV panel at different ambient condition with high precision. Several PV electrical models have been proposed and developed by researchers including the models that are based on the simple idealized model and the models that replicate the actual physics of the PV cell [91]. Some of these models are described vaguely and some of them are much complex for the simple power system studies like load flow, maximum power point tracking, load frequency match, etc. These models also have the implementation issue on several softwares. Electrical characteristics of the PV panel can be modeled by representing it with equivalent electrical circuit. This model has the advantage over other models due to its electric circuit nature and behavior of the PV array can easily be understood in the circuit connected. Power electronics design engineers require an efficient PV panel model for the simulation study of the power electronics before any experimental verification. This model is best suited for the dynamic and transient study of the power electronics converters.

The well-known five parameters electric circuit model of PV device is used and shown in Figure 3.8 [93]. It consists of light depended current source, a p-n junction diode and two resistances one in series and another in parallel. The current source (I_L) represents charge carrier generation in the semiconductor caused by incident radiation. The shunt diode represents recombination of these charge carriers at a high forward-bias

voltage ($V+IR_s$). The shunt resistor (R_{sh}) signifies high-current paths through the semiconductor along mechanical defects and material dislocations.

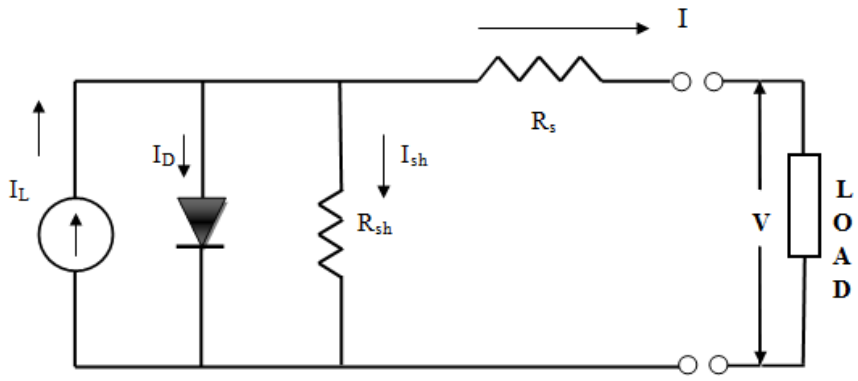

Figure 3.8 : Equivalent circuit for an individual PV cell

At a fixed temperature and solar radiation, the I-V characteristic of this model is given by [91],

$$I = I_L - I_o\left[\exp\left(\frac{V+IR_s}{a}\right)-1\right]-\frac{V+IR_s}{R_{sh}} \tag{3.45}$$

where I and V represent the current and voltage respectively at the load condition. The circuit requires that five parameters be known and they are: light generated current, diode reverse saturation current, series resistance, shunt resistance and ideality factor. The five parameters in the model are obtained using I-V characteristics of a module at reference condition supplied by the manufacturer and other known PV characteristics. Measurements of PV electrical characteristics are made at standard reference condition: incident radiation of 1000 W/m^2, a cell temperature of 25^0 C, and a spectral distribution corresponding to an air mass of 1.5.There are five parameters to be estimated and hence

we need five conditions to calculate these parameters simultaneously. These conditions are presented in the Table 3.1. The methodology adopted here is to know three I-V points on the I-V curve (i.e. short circuit current, open circuit voltage and maximum power point) as shown in Figure 3.9.

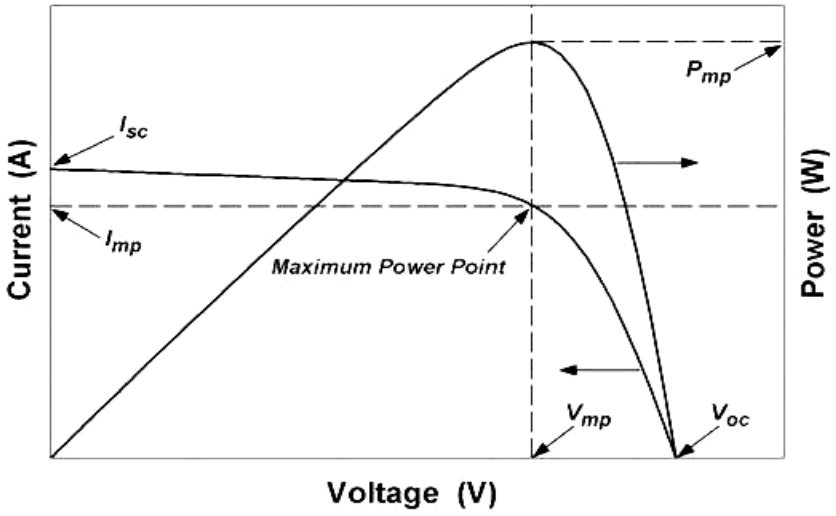

Figure 3.9: I-V and P-V curves for a PV module

Table 3-1 : Conditions used to estimate five parameters

At short circuit	$[dI/dV]_{sc} = -1/R_{sh,ref}$
At open circuit voltage	$I=0,\ V=V_{oc,ref}$
At short circuit current	$I=I_{sc,ref}\ ,\ V=0$
At the maximum power point	$I=I_{mp,ref}\ ,\ V=V_{mp,ref}$
At the maximum power point	$[dVI/dV]_{mp} = 0$

By applying all these above described five conditions into Equation (3.45), the following equations are obtained [91]

$$I_{sc,ref} = I_{L,ref} - I_{o,ref}\left[\exp\left(\frac{I_{sc,ref}R_{s,ref}}{a_{ref}}\right)-1\right]-\frac{I_{sc,ref}R_{s,ref}}{R_{sh,ref}} \tag{3.46}$$

$$I_{L,ref} = I_{o,ref}\left[\exp\left(\frac{V_{oc,ref}}{a_{ref}}\right)-1\right]+\frac{V_{oc,ref}}{R_{sh,ref}} \tag{3.47}$$

$$I_{mp,ref} = I_{L,ref} - I_{o,ref}\left[\exp\left(\frac{V_{mp,ref}+I_{mp,ref}R_{s,ref}}{a_{ref}}\right)-1\right]-\left[\frac{V_{mp,ref}+I_{mp,ref}R_{s,ref}}{R_{sh,ref}}\right] \tag{3.48}$$

$$\left[dI/dV\right]_{sc} \cong -\frac{1}{R_{sh,ref}} \tag{3.49}$$

$$\frac{I_{mp,ref}}{V_{mp,ref}} = \frac{\left(\frac{I_{o,ref}}{a_{ref}}\right)exp\left(\frac{V_{mp,ref}+I_{mp,ref}R_{s,ref}}{a_{ref}}\right)+\frac{1}{R_{sh,ref}}}{1+\left(\frac{I_{o,ref}R_{s,ref}}{a_{ref}}\right)exp\left(\frac{V_{mp,ref}+I_{mp,ref}R_{s,ref}}{a_{ref}}\right)+\left(\frac{R_{s,ref}}{R_{sh,ref}}\right)} \tag{3.50}$$

Solving these simultaneous equations from (3.46) to (3.50) gives the value of five parameters ($a_{ref,}$ $I_{L,ref}$, $I_{o,ref}$, $R_{s,ref}$ and $R_{sh,ref}$) at the reference conditions. The ideality factor which is assumed to be independent of the cell temperature is related to reference condition by,

$$\frac{a}{a_{ref}} = \frac{T_c}{T_{c,ref}} \tag{3.51}$$

The effect of each of the five parameters on the behavior of the I-V curve is shown in Figure 3.10. The effect is shown for the current monocrystalline solar panel around the STC condition, although the effect of each parameter on the I-V curve is similar for all panels and operating conditions.

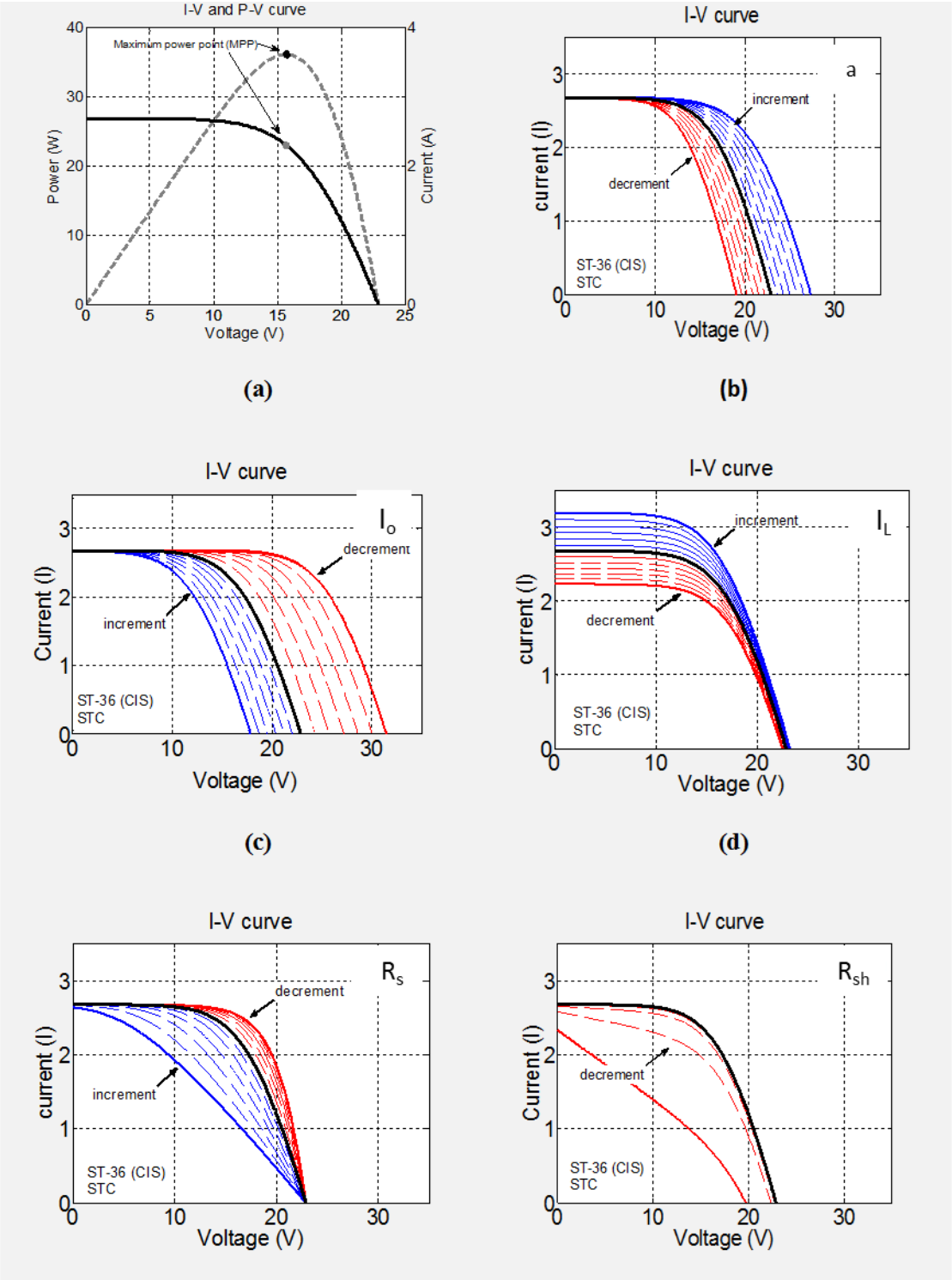

Figure 3.10: Effect of five parameters on I-V curve

The bold I-V curve in each of the following plots is the result of using parameters calculated at Standard Test Condition (STC) data while the other two are the result of adjusting one specified parameter above and below the original value. The above figures show that both a and I_o adjust the predicted voltage at all points on the I-V curve and I_L adjusts the predicted current. R_s and R_{sh} have a more localized influence around the maximum power point; R_s adjusts the maximum power voltage and R_{sh} adjusts the maximum power current.

The light current for any operating conditions is related to its reference conditions by,

$$I_L = \frac{S}{S_{ref}}[I_{L,ref} + \mu_{I_{sc}}(T_c - T_{c,ref})] \tag{3.52}$$

where $\frac{S}{S_{ref}}$ is the ratio of absorbed radiation to the absorbed radiation at reference condition . It is given by,

$$\frac{S}{S_{ref}} = M\left(\frac{G_b}{G_{ref}}R_b K_{\tau\alpha,b} + \frac{G_d}{G_{ref}}K_{\tau\alpha,d}\left(\frac{1+\cos\beta}{2}\right) + \frac{G}{G_{ref}}\rho_g K_{\tau\alpha,g}\left(\frac{1-\cos\beta}{2}\right)\right) \tag{3.53}$$

The diode reverse saturation current is related to reference conditions by,

$$I_0 = I_{oref}\left(\frac{T_c}{T_{c,ref}}\right)^3 \exp\left(\frac{\varepsilon}{kT_{c,ref}} - \frac{\varepsilon}{kT_c}\right) \tag{3.54}$$

The following relationship is used to relate the shunt resistance (R_{sh}), (which is assumed to be finite and independent of temperature but varies with the absorbed radiation) at reference conditions to that at operating conditions:

$$\frac{R_{sh}}{R_{sh,ref}} = \frac{S_{ref}}{S} \tag{3.55}$$

The model is now complete. These equations are a set of nonlinear equations that cannot be solved unless good initial guesses and variable limits are used. The following guess values are used for determining the parameters.

$$a_{ref,guess} = 1.5KT_{c,ref}N/q \tag{3.56}$$

$$I_{o,ref,guess} = I_{sc,ref}\exp(-V_{oc,ref}/a_{ref,guess}) \tag{3.57}$$

$$I_{L,ref,guess} = I_{sc,ref} \tag{3.58}$$

The series resistance is assumed to be independent of both temperature and solar radiation so that,

$$R_s = R_{s,ref} \tag{3.59}$$

Once the values of reference parameters are obtained, the characteristics curve can be found at any operating conditions. In order to estimate the maximum power point (MPP) from the model, the following equations are used.

$$\frac{I_{mp}}{V_{mp}} = \left[\frac{\frac{I_o}{a}\exp\left(\frac{V_{mp}+I_{mp}R_s}{a}\right)+\frac{1}{R_{sh}}}{1+\frac{R_s}{R_{sh}}+\frac{I_oR_s}{a}\exp\left(\frac{V_{mp}+I_{mp}R_s}{a}\right)}\right] \tag{3.60}$$

The general I-V equation at the MPP must also be satisfied:

$$I_{mp} = I_L - I_o\left[\exp\left(\frac{V_{mp}+I_{mp}R_s}{a}\right)-1\right]-\left[\frac{V_{mp}+I_{mp}R_s}{R_{sh}}\right] \tag{3.61}$$

The simultaneous solution of the equations (3.60) and (3.61) yields the MPP current and voltage. The maximum power output can be obtained as.

$$P_{mp} = I_{mp} V_{mp} \tag{3.62}$$

In estimating the PV module performance, the temperature dependance of the maximum power point efficiency (η_{mp}) is an important parameter and is given by,

$$\eta_{mp} = \frac{I_{mp} V_{mp}}{G_T A_m} \tag{3.63}$$

CHAPTER 4 EXPERIMENTAL STUDY

4.1 DESCRIPTION OF V-TROUGH PV/T SYSTEM

Experimental setup was designed and fabricated to investigate the thermal and electrical performance of V-trough PV system. This setup was built outside building 26 at King Fahd University of Petroleum and Minerals. The present setup was designed to investigate the performance of electrical efficiency and power output from the PV panel during operation under concentrated sunlight (CR>1).

There are various design models for V-trough PV system which are categorized according to tracking modes. The different tracking modes are seasonal tracking, one axis north-south tracking and diurnal tracking. V-trough parameters are evaluated for geometric concentration ratio of 2 as shown in Figure 4.1 below.

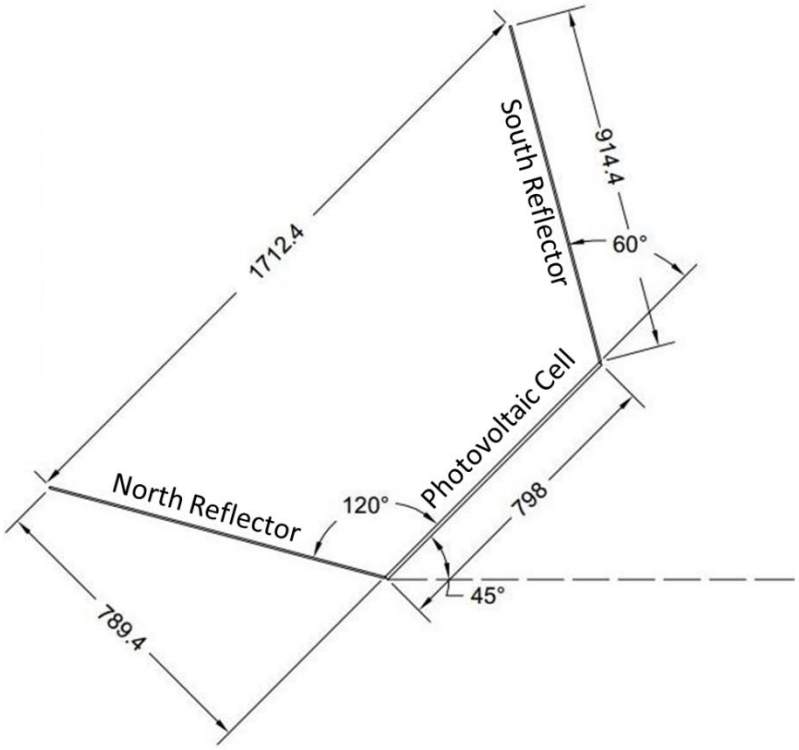

Figure 4.1 Dimensions (mm) of V-trough PV system

Commercially available SUN POWER 230W module was used for the V-trough PV system. The detail of the panel can be found in Appendix-A. Glass mirror was used as the reflector material with reflectivity around 79%. The thickness of the mirror used for the experiments was 5mm. When the solar intensity is enhanced by reflectors, the temperature of the panel rises up and it affects the electrical efficiency of the system. For this purpose cooling system was integrated with the V-trough PV system to lower the module temperature and increase the electrical efficiency of the system. A storage tank with proper insulation was used to supply cooling water to the system. For lowering the operating temperature of the module, SDM100 collector (heat exchanger) was placed at the bottom of the panel with insulation of about 20mm. Pump and bypass system was

used in order to maintain the pressure of water supplied to the collector. The electricity which is generated by the solar panels is stored in two batteries of 12 V each connected in series. The schematic diagram of the entire setup is shown in Figure 4.2.

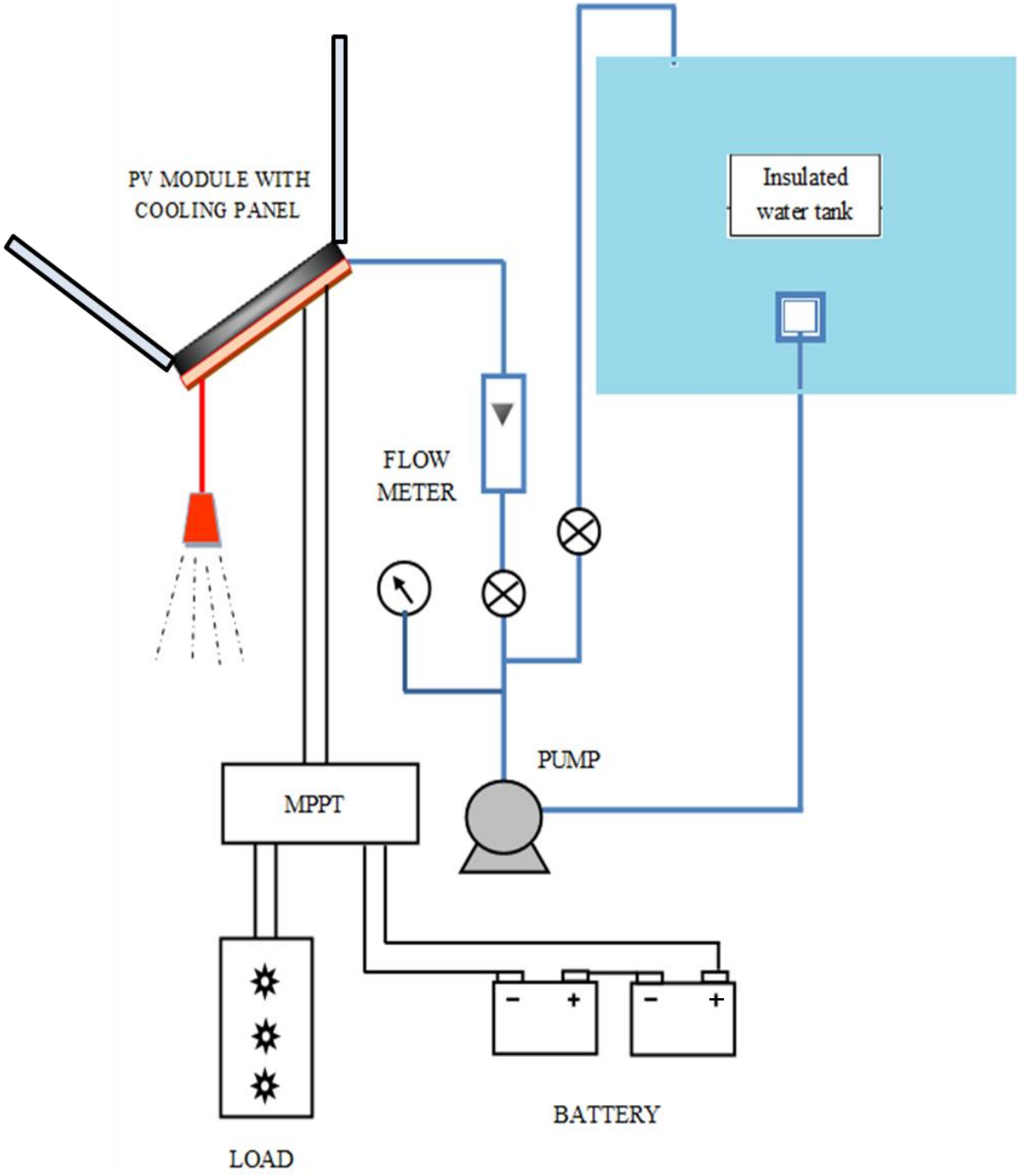

Figure 4.2: Schematic diagram of V-trough PV system

During the operation, a maximum power point tracker (MPPT) was used to extract the maximum power from the panel at different operating conditions. Solar radiation was measured by using pyranometer which was installed horizontally. In this setup the air speed was recorded by the anemometer. K-type thermocouple was used in order to measure the ambient temperature, PV module temperature, water inlet and outlet temperatures. The voltage and current of the panel was recorded with ammeter and multimeter from the MPPT. The experimental setup is shown in the Figure 4.3.

Figure 4.3: Experimental setup of V-trough PV system

The experimentation was performed from 9am to 4 pm. During the operation of the experimental setup, PV current and voltage, inlet and outlet temperature, temperature of the module, wind speed and irradiation of sunlight were recorded on the hourly basis.

4.1.1 Experimental Components

Photovoltaic Module

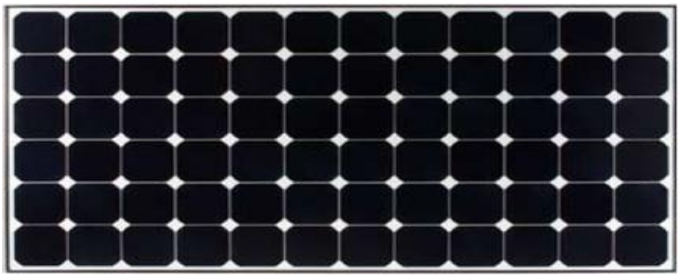

Figure 4.4: Monocrystalline silicon photovoltaic panel

Monocrystalline Silicon Solar cells are used in the current experimental setup. The SunPower 230 Solar Panel was used which utilizes 72 all back-contact solar cells. The specifications of the panel are given in Table 4-1 and Appendix-A. According to the manufacturer data the total panel conversion efficiency is about 18.5%.

Figure 4.5 shows the structure of a crystalline silicon solar cell [50]. EVA is a type of copolymer of ethylene and vinyl acetate. The function of polymer encapsulate in PV modules is to provide structural support, electrical insulation, physical isolation and thermal conduction for the solar cell circuit.

Table 4-1: Specifications of SunPower 230 PV module

Solar PV module parameters	**Value**
Module type	SUN POWER SPR-230WHT-U
Maximum Power (P_{mp})	230 Watts
Maximum Power Voltage (V_{mp})	41 V
Maximum Power Current (I_{mp})	5.61 A
Maximum Power point efficiency(η_{mp})	18.5%
Open Circuit Voltage (V_{oc})	48.7 V
Short Circuit Current (I_{sc})	5.99 A
Area of the module (A)	1.24 m^2
Temperature co-efficient of Short-circuit current (μ_{Isc})	3.5mA/K
Number of solar cells	72 (mono crystalline type)

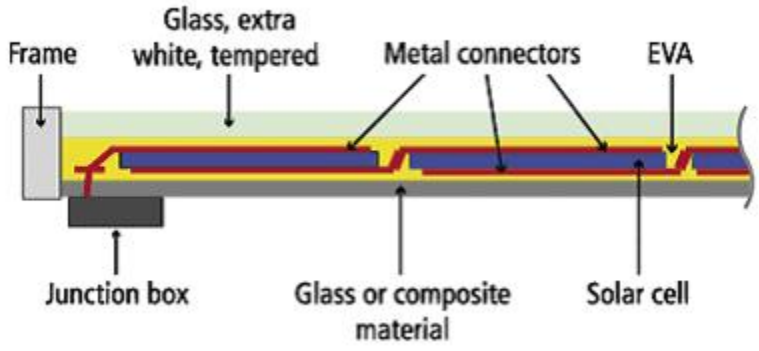

Figure 4.5: Structure of photovoltaic panel

The backsheet of the photovoltaic module mostly consists of Tedlar. The main purpose of the Tedlar is to prevent the ingress of water vapor. It also provides functions like strength and durability, electrical insulation, resistance of weathering, mechanical properties and UV resistance. Due to these added advantages, Tedlar helps the PV panel to sustain at least 20 years and above. Sometimes the part of backsheet is made as a laminated film composite and most common structure is the tri-layer structure of Tedlar/Polyester/Tedlar, also known as TPT. This type of structure can enhance the functions of abovementioned characteristics.

The reflection of the front surface of PV panel should low as well, besides the transmission issues. A low iron glass is mostly used in the PV industry because it is of low cost, strength & stability, highly transparent, resistant to water and gases and the front contact glass also has self-cleaning properties after raining.

Maximum Power Point Tracker (MPPT)

A maximum power point tracker (MPPT) is utilized to maximize the power output of PV module and it is also a high efficiency DC to DC converter. The SunSaver MPPT is used for this study which proves an efficient device for professional and consumer applications. The specifications of the SunSaver MPPT is given in Table 4-2.

Table 4-2: Specifications of SUNSAVER MPPT

SUNSAVER MPPT	**SSMPPT-15L**
Maximum Battery Current	15A
Maximum Open Circuit Voltage	75V
Maximum PV Input	200Wp (12V Battery) 400Wp (24V Battery)
System Voltage	12/24V

Using a conventional charge controller to charge a discharged battery, it connects the PV modules to the battery directly, forcing the PV module to work at the battery voltage. Generally speaking, this voltage is always not the ideal voltage for the maximum power output of PV module. However, the MPPT is not simply the bridge between the module and battery.

The MPPT controller is able to calculate the voltage at which modules can produce the maximum power output and the working voltage of PV module is at maximum power output voltage rather than battery voltage. If the whole system wiring is assumed to be 100% efficient, the battery charge current would be V_{module} /$V_{battery}$ x I_{module}. There is a significant increase in the current supplied to the battery by using the MPPT controller rather than the conventional converter. Figure 4.6 show that there is always a single operating point which will produce the maximum power output of the PV cell. This point is called the maximum power point.

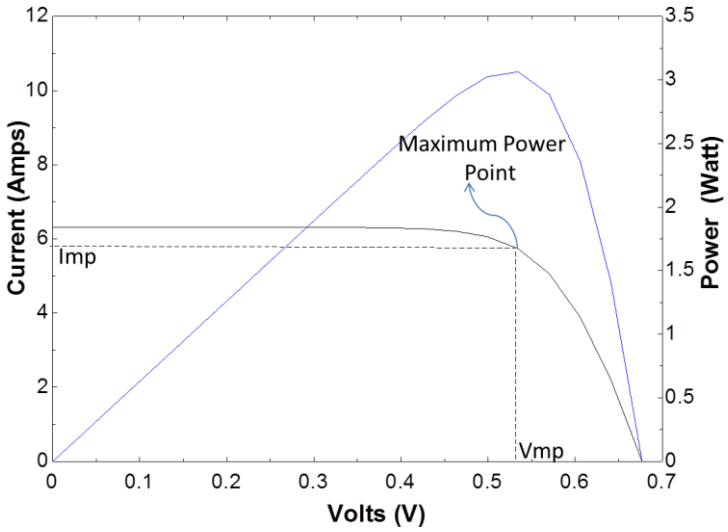

Figure 4.6: *I-V* curve and the maximum power point

The MPPT is used to seek this point in order to maximize the power output of the panels under the different irradiation. The power from the solar panel passes through the MPPT, which modulates to the best level that the module can produce and converts it to get maximum current from the deep cycle battery. Figure 4.7 shows the MPPT being used in this experiment.

Figure 4.7: SunSaver MPPT controller

Electrical Circuit

In order to store the excess electrical energy produced from the PV panel, two batteries (12V, 80 AH connected in series) are used. The electricity generated from the panel is used to drive the load which consists of DC bulbs rating 24V and 70W.An ammeter and voltmeter is used for measuring the maximum current and voltage from the output terminals of the MPPT. The detail of the connections between load, MPPT and batteries is shown in the Figure 4.8 below. Multimeter was used to measure the voltage from the panel through the terminals of the MPPT.

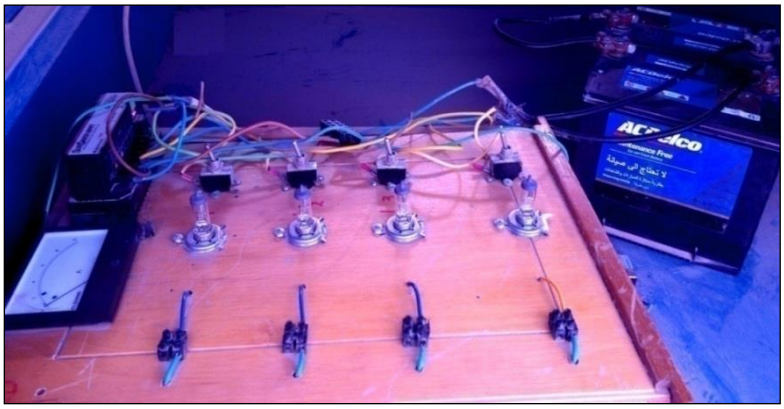

Figure 4.8: Electrical setup showing the connections to load, MPPT and batteries.

Integrated Cooling System

The PV module is integrated with a cooling panel followed by insulation with thickness of about 20mm attached on the rear side of the module. Figure 4.9 shows the test setup of the combined PV with the cooling panel.

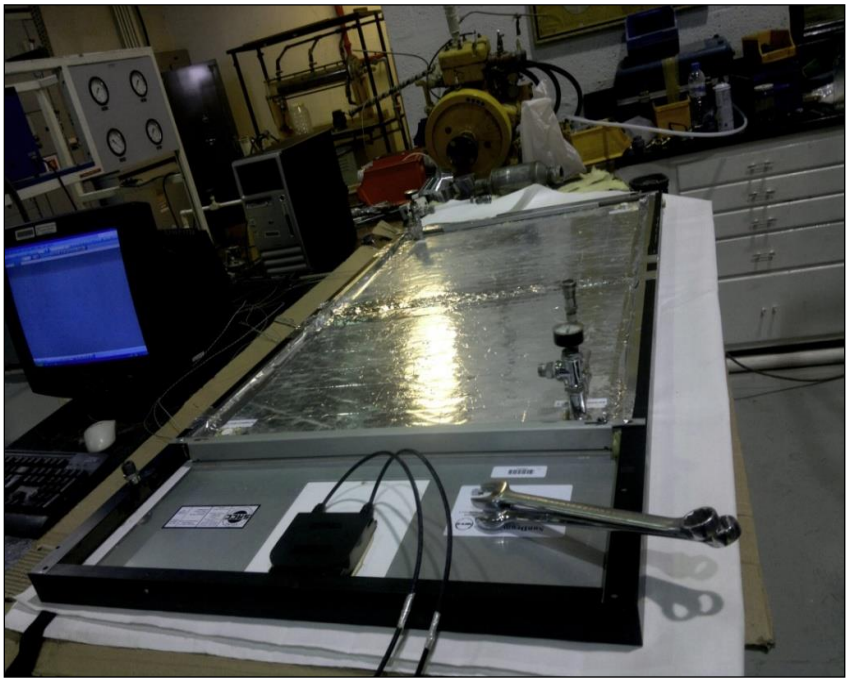

Figure 4.9: PV module integrated with the cooling panel and back insulation.

The water to be supplied to the cooling panel is stored in a well insulted storage tank with insulation thickness of 10mm as shown in Figure 4.2. The outlet of the tank is connected to a pump for circulating water at the required pressure. The pump delivers the water to the cooling panel only after adjusting the required flow rate and pressure using a bypass system. The maximum pressure allowed for the cooling panel is 41.4 kPa.

The outlet and inlet ports for water flow are shown in Figure 4.10. Various configurations of water inlet/outlet are provided by the manufacturer. In order to maintain the water pressure to an adequate level, a bypass system is created. The bypass system which regulates the pressure by pumping the water back to the storage tank (with pressure gauge and valve arrangement) ensures the pressure does not exceed 41.4 kPa. To regulate the water flow inside the cooling panel, a flow-meter with maximum flow rate of 3.6 L/min was used. The cooling water flows through the collector, captures the waste heat from the PV module and producing hot water which is collected at the collector outlet. To take the measurements of the temperature of the PV/T system, K-type thermocouples were used.

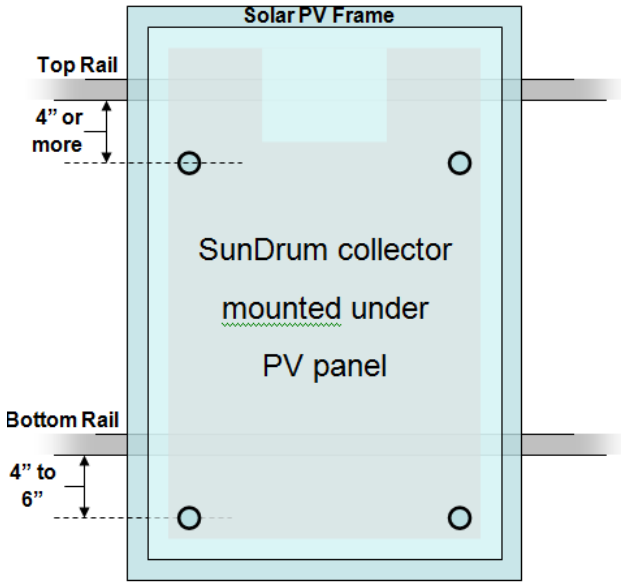

Figure 4.10: Thermal collector with water inlet/outlet ports

The water temperature is measured using standard type-K thermocouples attached at the inlet and outlet of the cooling panel. Temperatures at the various points of the system are measured with the help of thermocouple thermometer using a digital switch (front and back). Hygro thermo-anemometer was used to record the ambient temperature and wind speed and is shown in Figure 4.11.

Figure 4.11: Hygro-thermo anemometer

The accuracy and sensitivity of the instruments used in the setup is given in the Table 4-3.

Table 4-3: Accuracy/sensitivity of the instruments

Instrument Used	Accuracy/Sensitivity
Sunsaver MPPT	Current: 1%; Voltage: 2%
Pyranometer	30.1μV/(W/m^2)
Hygro Thermo-Anemometer	2% ±0.2 m/sec
Thermocouple	±1°C

Figure 4.12 shows the SDM 100 collector (heat exchanger) with thermocouples attached on it. The collector after being attached to the panel is mounted on the stand shown in Figure 4.13. Different views of the experimental setup are shown in Figure 4.14 and Figure 4.15.

Figure 4.12: Sundrum SDM 100 collector used for cooling the panel.

Figure 4.13: Back view of the hybrid PV with cooling panel.

Figure 4.14: Front view of the V-trough PV test setup

Figure 4.15: Side view of the experimental setup

4.2 DESCRIPTION OF PV-CPC SYSTEM

The CPC contains two parabolic reflectors and the absorber/solar cell is located between the distances of two foci of parabolas. CPC troughs are usually mounted in east–west direction with the aperture inclined from the horizon. For fixed CPC's, the smaller the acceptance half-angle, the greater the geometrical concentration factor. Three cases with and without cooling are considered for the present study.

- Case1: Glazed PV-CPC system
- Case2: Unglazed PV-CPC system
- Case3: PV strings without CPC

Experimental setup was designed and fabricated to investigate the thermal and electrical performance of PV-CPC system. This setup was built on the open space of building 26 at King Fahad University of Petroleum and Minerals. The present setup is designed to investigate the performance of electrical efficiency and power output from the PV strings during operation.

4.2.1 Design & Fabrication of PV-CPC system

Integration of CPC with the PV strings can be done in different ways. One of the methods is to design parabolic shape supports for the CPC and place the parabolic reflectors onto the supports. The fabrication of such reflector supports needs special arrangements. In order to simplify the fabrication and provide the insulation for the reflectors wooden block was selected as the base material for the parabolic reflectors. In order to design and fabricate the PV-CPC for specific concentration ratio of 2.3X,

equations presented in chapter 3 were used. For this purpose the solar strings available had width of 125 mm, and the design was made by considering the tolerance and back sheet width of 129 mm. The width for the panel after considering the tolerance was taken as 134 mm.

Equations 3.12-3.25 were used to evaluate the required parameters for the geometry of the PV-CPC system including the concentration ratio, height and width of the reflectors etc. After estimating the parameters for the full CPC it was found that the surfaces become parallel to central plane of symmetry at the upper end points of CPC, thus contributing little to the radiation reaching the absorber. Therefore 38% truncation was applied to save the reflector area and along with a little compensation in the performance. After truncation, the half acceptance angle was 41.75° and the concentration ratio was 2.33X. Stainless Steel (mirror type) was used as reflecting material for the walls of CPC which has good reflectivity and provides better resistance to corrosion.

For fabricating the desired configuration of PV-CPC in a wooden block, a 3D model was made in SolidWorks as shown in Figure 4.17. Two blocks were made in order to study the effect of glazing in the performance of PV-CPC system. A single block consisted of two set of systems; one PV-CPC system with active cooling and the other one PV-CPC system without cooling. To ensure the complete filling of the rectangular heat exchanger, the inlet was kept at the lower side and the outlet of the fluid at the upper side as shown in Figure 4.18. In order to fabricate the modeled system by CNC milling machine, a G-code is required which was formulated from the 3D SolidWorks model. This

generated G-code was supplied to a manufacturing company for the CNC cutting of the CPC wooden blocks. A special weatherproof coating was applied onto the CPC blocks in order to withstand the environmental conditions as the setup was exposed to harsh atmosphere. When the solar intensity is enhanced by reflectors, the temperature of the panel rises up and it affects the electrical efficiency of the system. For this purpose cooling system was integrated with the PV-CPC system (Figure 4.18) to lower the module temperature and increase the electrical efficiency of the system. A storage tank with controlled inlet temperature was used to supply cooling water to the system. For lowering the operating temperature of the module, a rectangular channel heat exchanger (W130mm×L1016mm×d13mm) was placed at the bottom of the cells. The schematic diagram for the rectangular heat exchanger is shown in Figure 4.16. A Pump and bypass system was used in order to maintain the pressure of water supplied to the heat exchanger. The electricity which is generated by the solar panels is stored in batteries of 12 V.

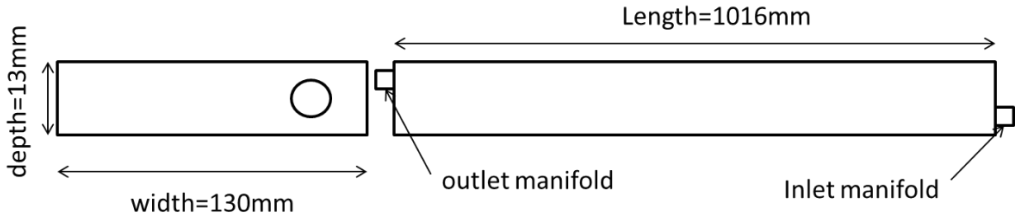

Figure 4.16: Schematic diagram for heat exchanger

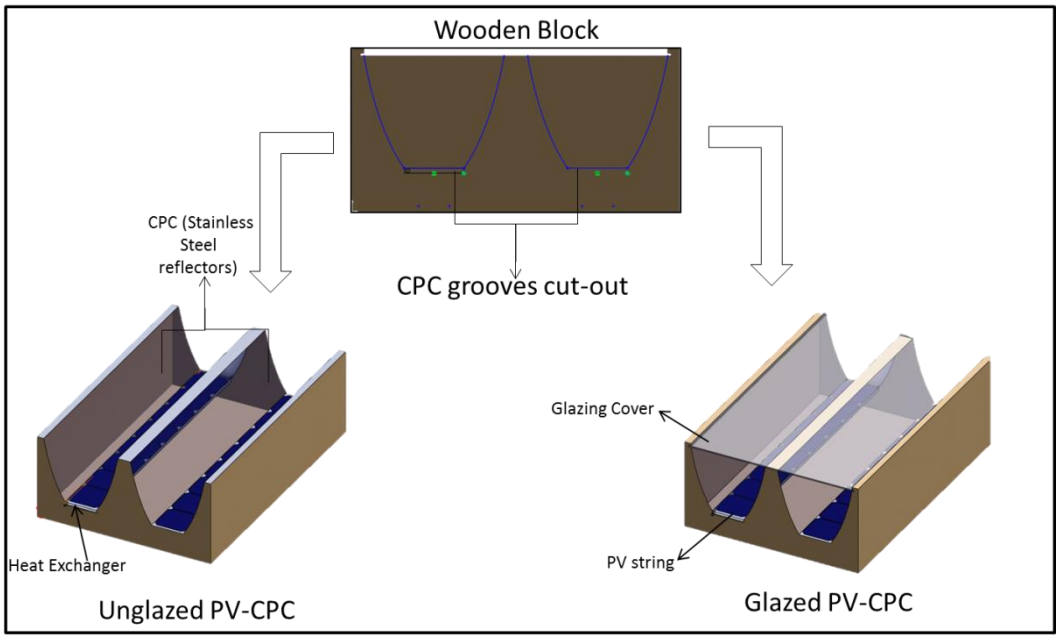

Figure 4.17: Modeling of PV-CPC in SolidWorks

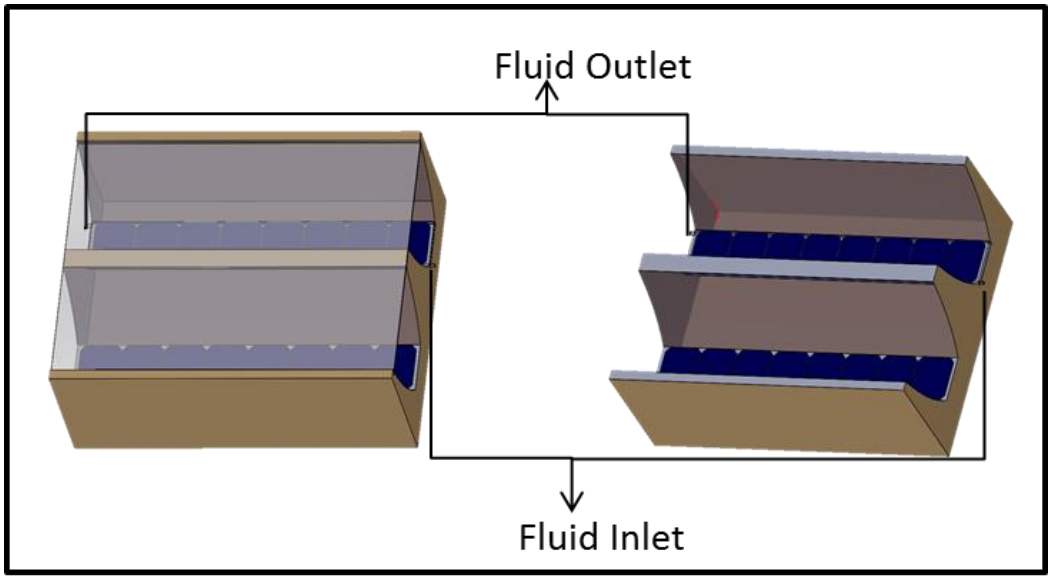

Figure 4.18: Orientation of the inlet and outlet manifold

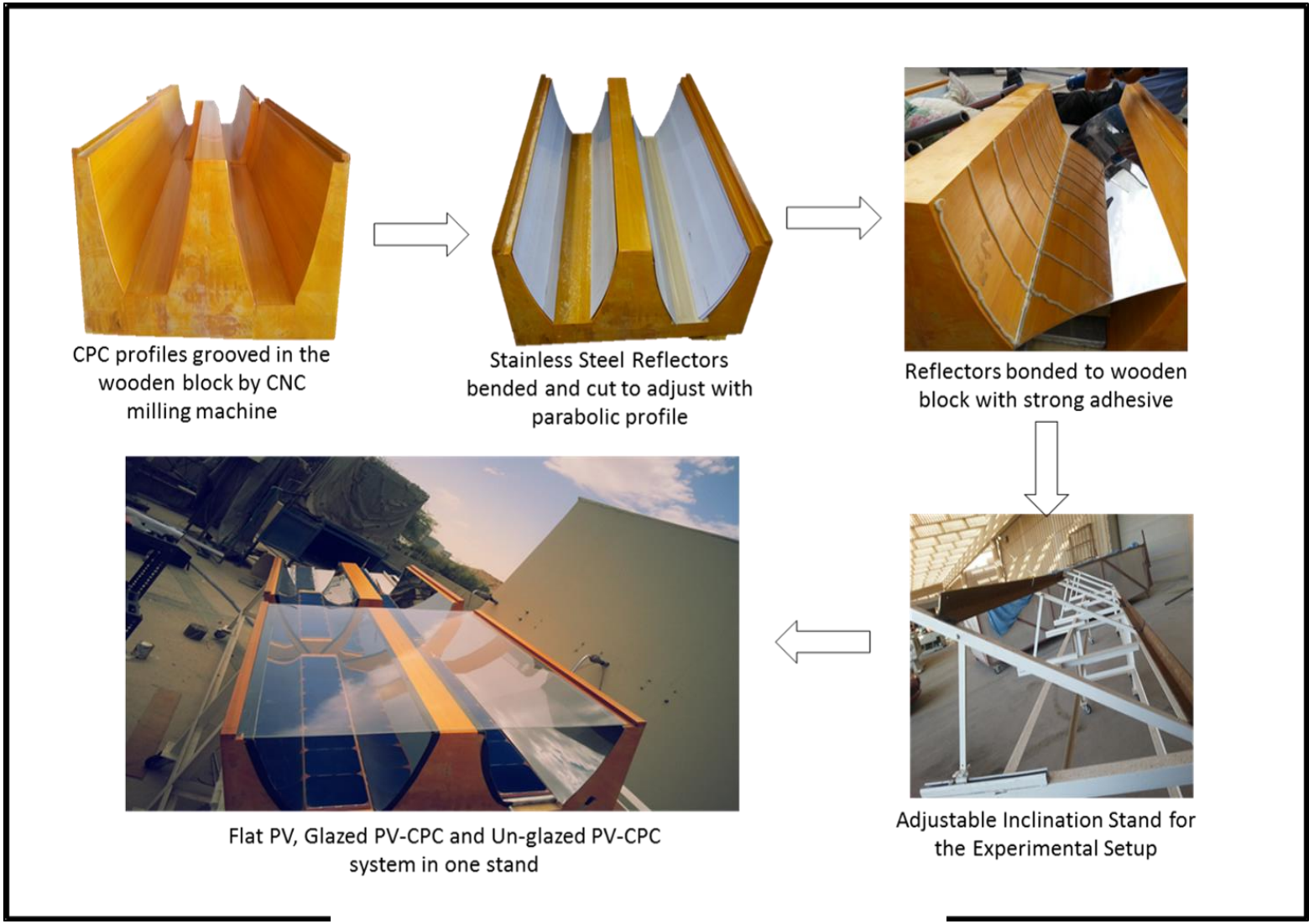

Figure 4.19: Manufacturing of PV-CPC system

Various stages involved in the manufacturing of PV-CPC system are shown and explained in Figure 4.19.

A PV string is fabricated by connecting eight C60 monocrystalline silicon solar cells in series with bottom contacts as shown in Figure 4.20. In the present setup there are six PV strings which are tested under different conditions. The specification of single C60 monocrystalline silicon solar cell is given in Table 4-4 and Appendix-B. The schematic diagram of the complete setup including all of the configurations considered is shown in Figure 4.21.

Table 4-4: Electrical characteristics of C60 cell at Standard Test Conditions (STC)

Open Circuit Voltage	0.680 V
Short Circuit Current	6.28 A
Maximum Power Voltage	0.575 V
Maximum Power Current	5.92 A
Rated Power	3.40 W

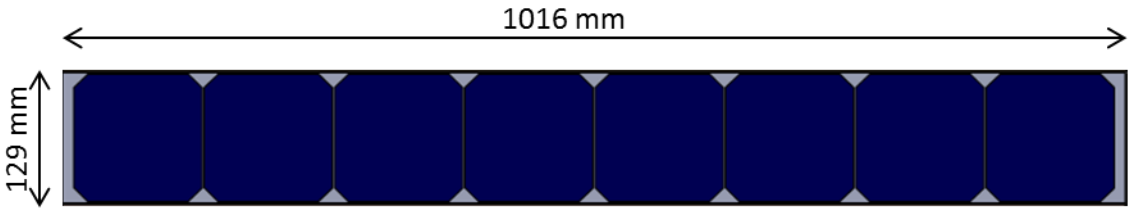

Figure 4.20: Monocrystalline silicon cells connected in series

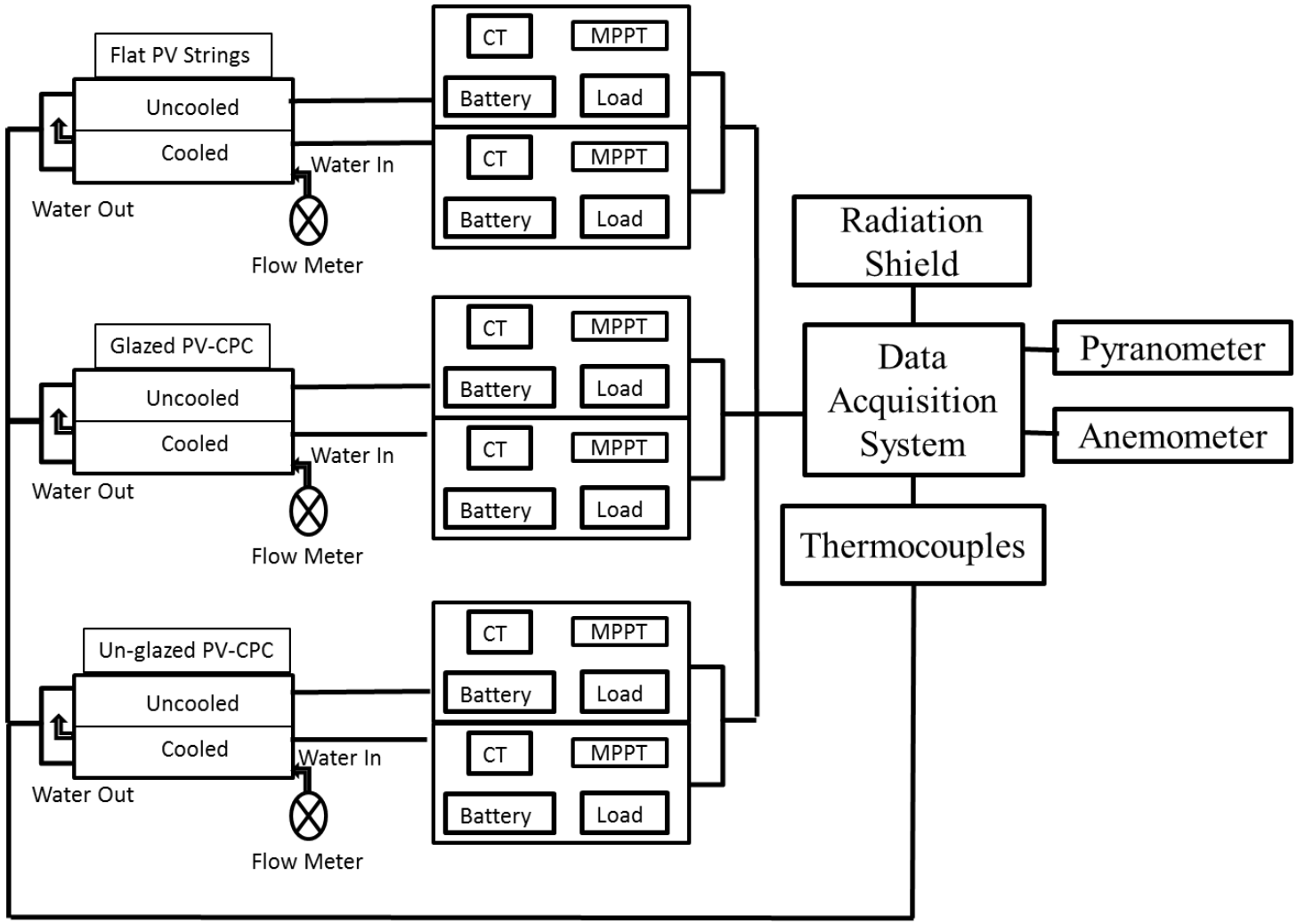

Figure 4.21: Schematic diagram of PV-CPC system

All the panels are aligned along east west direction and facing due south. Inclinations of the panels are adjustable for optimization of the collectible solar radiation in different seasons. Figure 4.22 shows the actual arrangement of the panels located in the outside of Bldg. 26 in KFUPM, Dhahran, KSA. The experimental setup is shown in the Figure 4.22 and Figure 4.23.

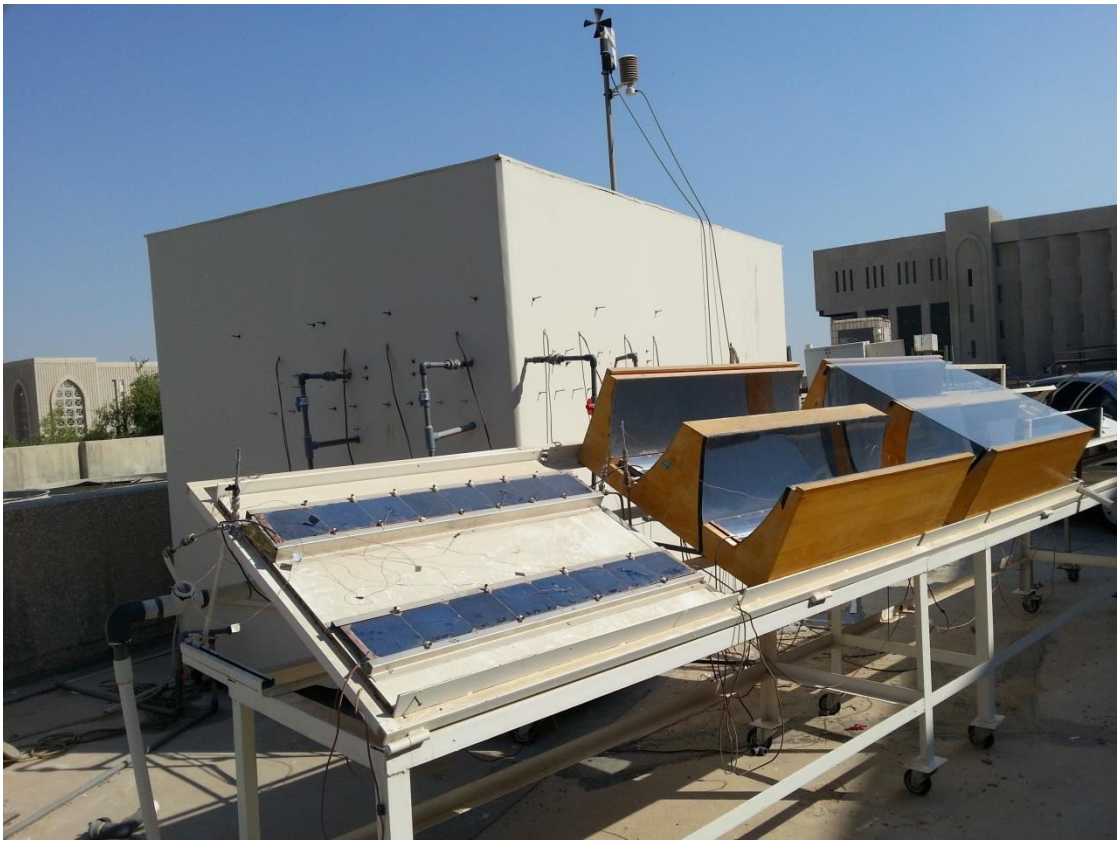

Figure 4.22: PV-CPC experimental setup

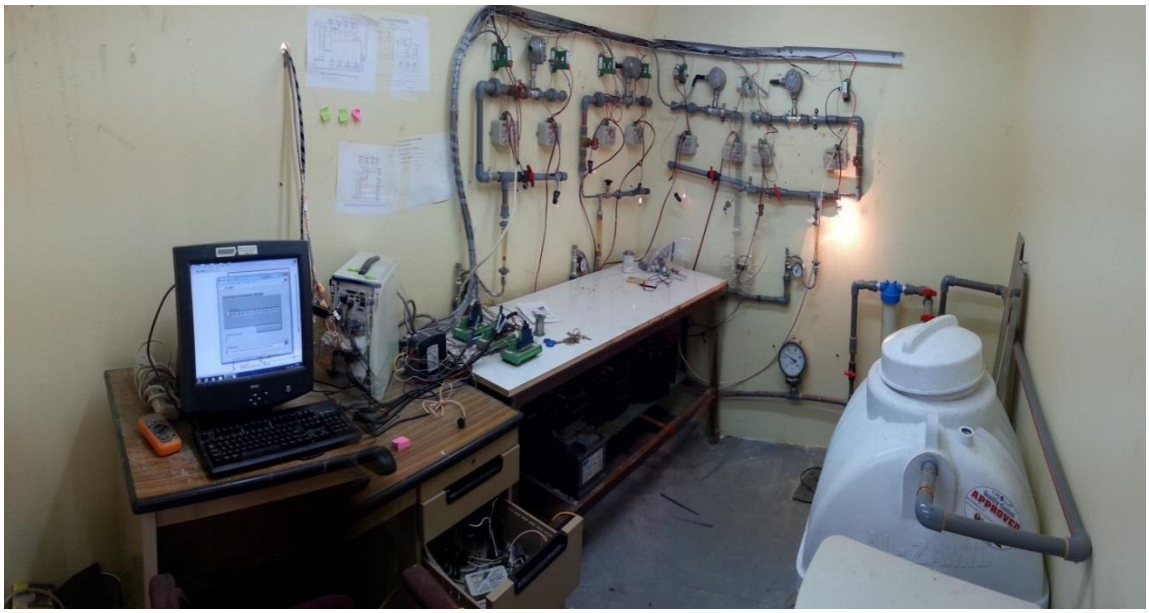

Figure 4.23: Inside view of the PV-CPC experimental setup

4.2.2 Experimental Components

Instruments used for investigating the performance of the photovoltaic are as follows.

Maximum Power Point Tracker (MPPT)

Maximum power point tracker is necessary for operating the photovoltaic at maximum available power. MPPT has a variable load which is adjusted to extract the maximum current from the panel. Without MPPT the output of the panel solely depends upon the resistance (load) attached with the panel. The SOL-1 series, as shown in Figure 4.24 utilizes a Maximum Power Point tracking software algorithm which efficiently optimizes the operation of the solar panel. Through the MPPT functionality the solar system can achieve up to 40% more output of the solar panel compared with standard solar battery chargers. The decoupling of the best operating point for the solar panel

(MPP) from the actual battery voltage by Switch Mode Power Supply (SMPS) technology and state-of-the-art microprocessor technology for efficient MPPT are the main features of the SOL-1 solar battery charger systems. The typical, highly temperature dependent MPP voltage of solar panels is around 16.8V at 25°C and 1000W/m^2 of solar irradiation intensity under reference conditions.

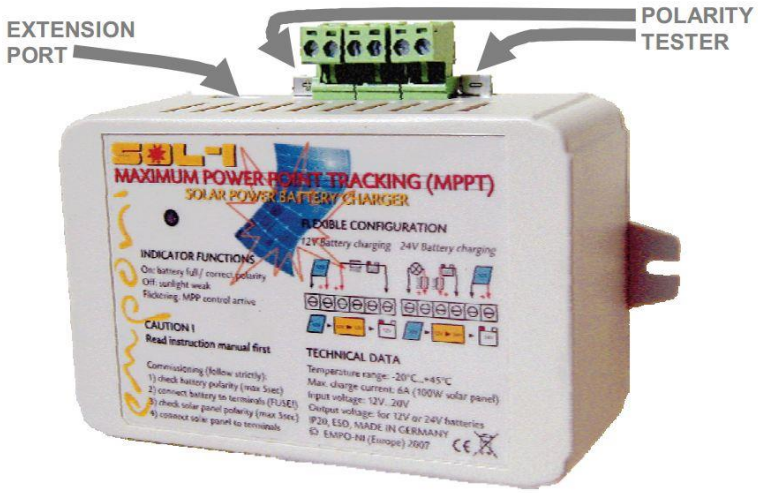

Figure 4.24: Sol-1 MPPT

Assuming an empty battery at 12V the difference in the achievable performance between conventional and the SOL-1's MPP technology becomes apparent by the following graph (Figure 4.25) showing an example of a V/I characteristic of a solar panel charging an empty battery. For the current setup, a special custom made MPPT is used which functions in the operating range of 1-6V and 0-6A. The MPPT used in the setup steps up the voltage and charges the battery of 12V. The load terminal is programmed in such a way that it turns ON when the battery voltage reaches 12V and it turns OFF when

the battery voltage falls below 11V. A 12V lamp is used as electric load which ensures the continuous extraction of maximum power even if the batteries are fully charged. In the absence of the load, the maximum power of the panel could not be recorded when the batteries are fully charged.

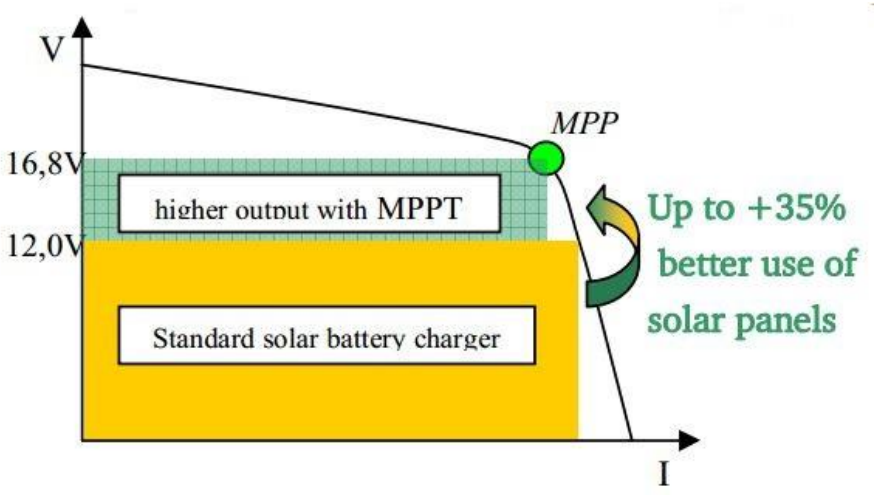

Figure 4.25: V/I characteristics of a solar panel

Current Transducer

In order to measure the maximum power point current I_{mp} from the panel at different operating conditions, current transducer (CR5200 Series) is used as shown in Figure 4.26. It is connected to the wire coming from the panel before the MPPT. The CR5200 Series, DC Current Transducers are designed to provide a DC signal which is proportional to a DC sensed current. These devices are designed for direct current only, targeting them towards general and daily applications. The ranges 2 to 10 A utilize an advanced Magnetic Modulator technology and the ranges 20 amps.

Figure 4.26: Current transducer

Radiation Shield & Relative Humidity/Temperature Probe

Radiation Shield is used in the current setup for measuring the ambient temperature and relative humidity. It is fixed at the top roof of the equipment room as shown in the Figure 4.27. The Multi-Plate Radiation Shield protects temperature and relative humidity sensors from error-producing solar radiation and precipitation. This shield relies on a combination of plate geometry, material and natural ventilation to provide effective shielding. The Multi-Plate Radiation Shield is designed to be mounted on a relatively flat open area. For best performance, the shield should be placed in a location with good air circulation clear of large thermal masses (buildings, pavement, solar panels, etc.), exhaust vents, electrical machinery and motors, water fountains and sprinklers.

The Model 41382LC2 Relative Humidity/Temperature Probe combines high accuracy humidity and temperature sensors in a single probe. The output signal is 4-20 mA. RH range is 0-100%. Temperature range is -50 to +50°C.

Figure 4.27: Multi-plate radiation shield with relative humidity/temperature probe

Anemometer

Wind velocity and wind direction are very fluctuating parameters. In order to accurately record the measurement 05103L Wind Monitor is used and it is also installed on the roof top of the measuring room as shown in the Figure 4.28. The 05103L wind monitor measures wind speed and direction and provides calibrated wind speed and

direction signals via independent loop-powered 4-20 mA analog transmitters. Sensor housing, nose cone, propeller, and other components use molded UV-stabilized plastic for strength, corrosion resistance, light weight, and fast response. Both the propeller and vertical shafts use stainless steel precision grade ball bearings. The sensor mounts directly on standard one inch pipe, outside diameter 34 mm. An orientation ring allows sensor removal without loss of wind direction reference. Both sensor and orientation ring are secured to the mounting pipe by stainless steel band clamps. Electrical connections are made in a junction box on the mounting post.

Figure 4.28: Wind monitor

Pyranometer

Solar radiation intensity is measured with the help of CMP 22 pyranometer as shown in the Figure 4.29 CMP 22 uses very high quality quartz domes for a wider spectral range, improved directional response, and reduced thermal offsets. Because of the high

optical quality of these domes the directional error is reduced below 5 W/m². A waterproof socket is fitted for the signature yellow signal cable, which is available in a range of lengths pre-wired to the waterproof plug. The integral bubble level is raised to the top of the housing and can be viewed without removing the redesigned Snap-On sun shield, which also covers the connector. The screw-in drying cartridge is easy to remove and the replacement desiccant is supplied in convenient refill packets.

Figure 4.29: CMP 22 pyranometer

The pyranometer does not require any power; it supplies a low voltage of 0-20mV in relation to the amount of incoming radiation. When a higher voltage level or a 4-20mA signal is required, the AMPBOX is the perfect solution.

Flow Meter

In order to regulate the desired flow of water through the heat exchangers, electronic flow meters are used. Turbine flow meter (FTB-1300 Series) is used for the current setup

as shown in the Figure 4.30. The FTB-1300 series of turbine flow meters is designed with a wear resistant rotor assembly to provide trouble free operation and a long service life. Fluid moving through the flow meter causes the rotor to turn at a speed proportional to the flow rate, and as the rotor blades cut through the magnetic field of the pickup, an electronic pulse is generated. The pulse train is used to represent the actual flow or total amount of fluid passing through the flow meter. The number of electronic pulses generated per unit volume is known as a K-factor. The value is constant over each flow meter's operating range, and is unique to each meter.

Figure 4.30: Turbine flow meter FTB-1300 series

The data for the temperature of the different components was recorded by using the same thermocouples as stated in the V-trough experimental setup. A card for measuring readings from thermocouple was inserted into NI-DAQ and the readings were recorded automatically after specified interval of time. There were three terminal blocks which were connected to the DAQ and each contained eight channels for analogue input. The wiring diagrams for all the devices to these terminal blocks are shown below. Figure 4.31 shows the exact color coding of the wires used in the setup for the current transducers. Similarly for other instruments like pyranometer, radiation shield, flow meters and anemometer is shown in Figure 4.32. Voltage of the strings are measured by measuring the voltage from the MPPT (SOL) as shown in Figure 4.33

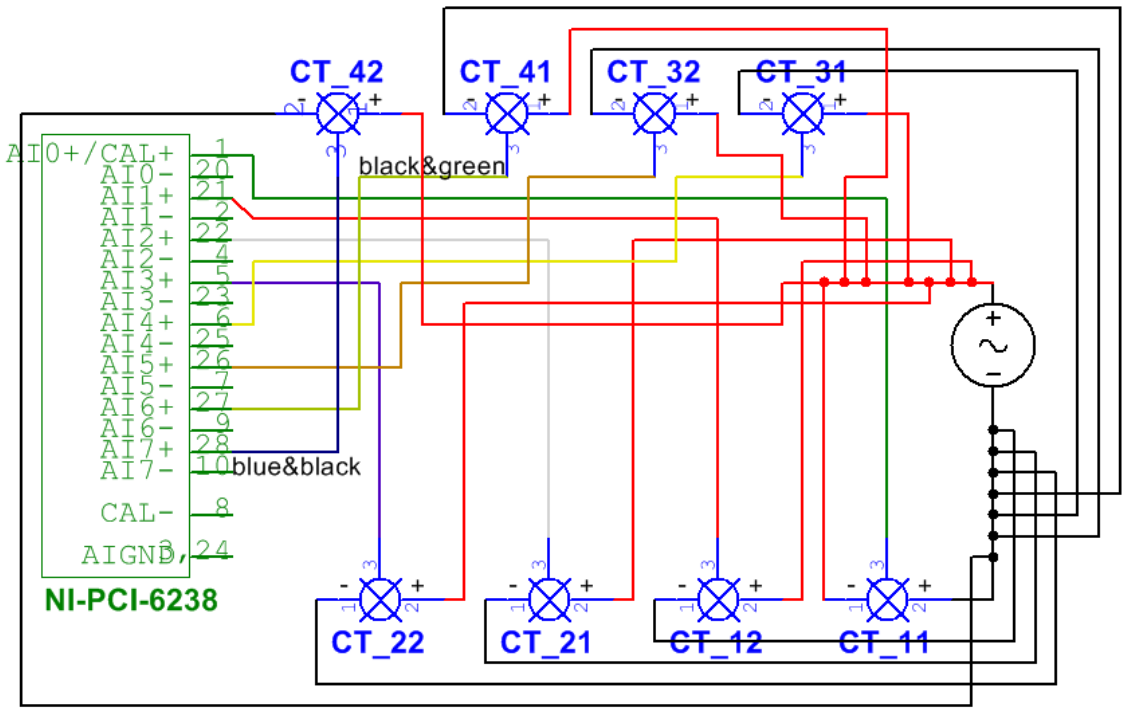

Figure 4.31: Wiring layout for current transducers (CT)

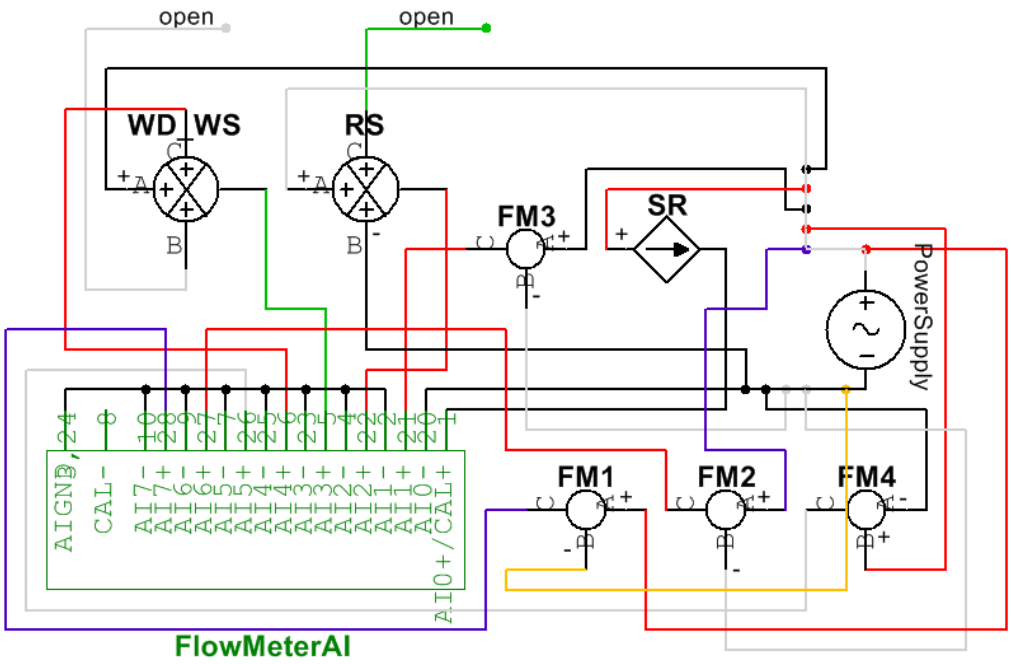

Figure 4.32: Wiring layout for flow meters (FM), radiation shield (RS), pyranometer (SR) and anemometer (WD)

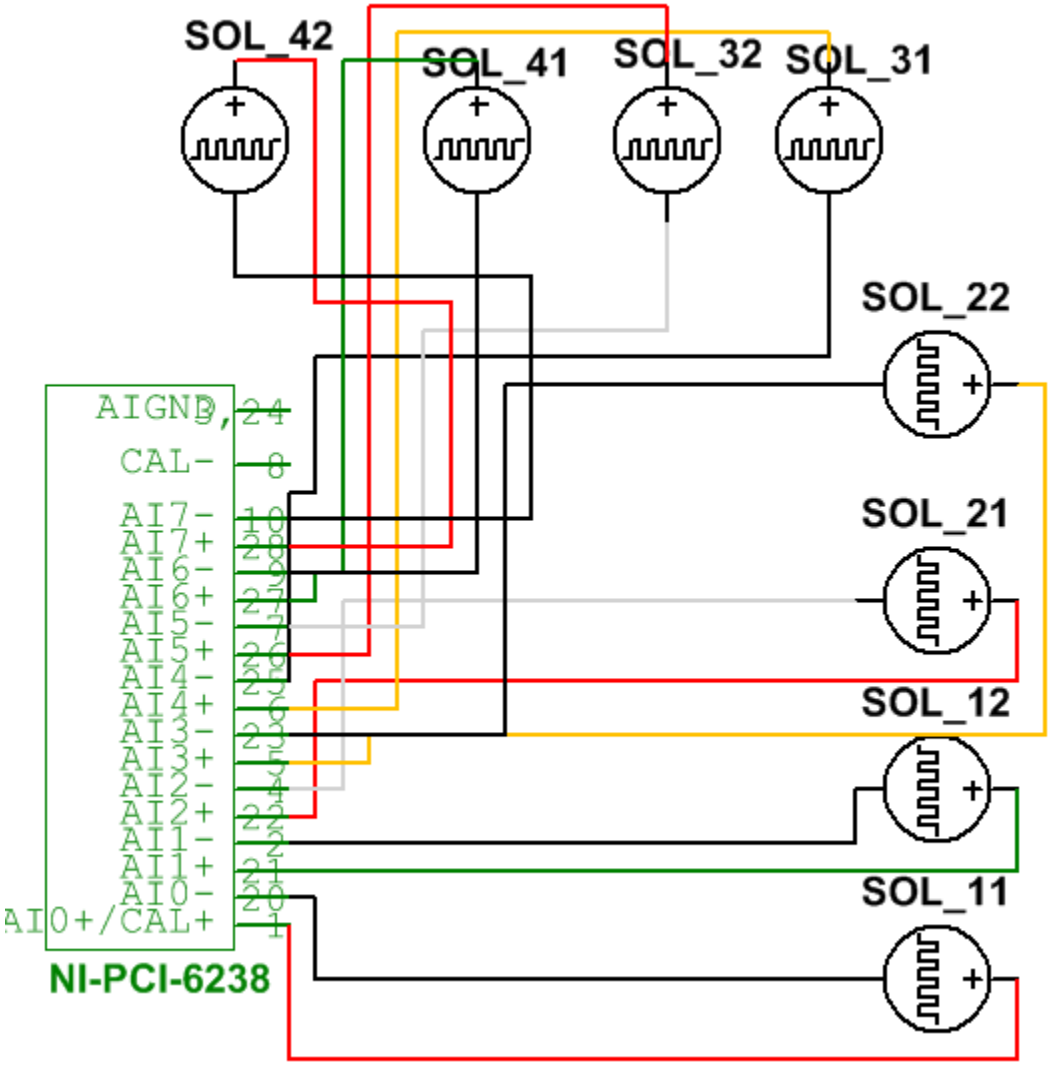

Figure 4.33: Wiring layout for voltage block

4.3 UNCERTAINTY AND ERROR ANALYSIS

Uncertainty in measurements arises from many sources including the limited precision of the measurement tool, the manner in which the measurement is performed, and the person performing the measurement. There is possibility of uncertainty/error in every measurement. Uncertainty analysis is the method used to estimate the limits of the unknown error and also describe the credibility of the experimental data. During the experimental measurements, various forms of uncertainty are liable to be included in the measured values. These uncertainties range from the precision and accuracy of the liquid flow meters, uncertainty in the readings of maximum power output and that from human. In the present study, the temperatures, pressures, mass flow rate of water and photovoltaic current and voltage are measured using the instruments with respective instruments errors.

4.3.1 Reporting Measurements

If multiple trials are performed to measure X, the best estimate is the average value, X, of all the trials (the bar over the variable denotes an average value). The average value is computed by summing up all the measured values and then dividing by the number of trials, N. Mathematically, we write this as [94]

$$\overline{X} = \frac{\sum_{i=1}^{N} X_i}{N} = \frac{X_1 + X_2 + X_3 + ... + X_N}{N} \tag{4.1}$$

When experimental or time limitations only permit one trial for a measurement, as in the present case, then the best estimate is the most careful measurement we can perform. Even the best measurements have some degree of uncertainty associated with them. The inclusion of an estimate of the uncertainty when reporting an experimental measurement permits others to determine how much confidence should be placed in the measured value. Additionally, measurements should also be accompanied by a statement of how the uncertainty was determined. Without uncertainties and an explanation of how they were obtained, measured parameters have little meaning.

A simple approach for estimating the uncertainty in a measurement is to report the limiting precision of the measurement tool. For example, if a Voltmeter is used to measure the voltage of the photovoltaic cell as 4.23 V, then the actual voltage of the cell could be 0.005 V greater or less than the measured voltage, and the voltmeter would still give the same value. Thus, the uncertainty associated with voltage measurements using this voltmeter would be ±0.005 V. This method for estimating the uncertainty of a measurement is a good choice when only a single trial is performed.

If on the other hand, the best estimate of a parameter is determined by making repeated measurements and computing the average value from the multiple trials, the uncertainty associated with random error of any quantity is determined using the standard deviation (σ), mean as follows:

$$Uncertainty = \sqrt{\frac{\sum_{i=1}^{N}(X_i - X)}{N(N-1)}} \quad (4.2)$$

Based on the above mentioned procedure, uncertainties for the current experimental data are presented below.

Table 4-5: Uncertainty of the instruments

Parameter	**Uncertainty Value**
Temperature	±0.05 ^{o}C
Liquid flow rate	Uncertainty = ± 0.2
Voltage	±0.005 V
Current	±0.005 A
Solar Intensity	± 5 W/m^2
Anemometer	± 0.02 m/s

4.3.2 Error Analysis

In order to investigate how well the predicted power output obtained by the analytical model fits the experimental measured power, the two cases are compared. Further, in order to compare the computed results with the experimental measurements, root mean square per cent deviation (e) has been evaluated by the following equation [95]

$$e = \sqrt{\frac{\sum \left[100 \times \left(X_{sim,i} - X_{\exp,i} \right) / X_{sim,i} \right]^2}{n}} \tag{4.3}$$

CHAPTER 5 RESULTS AND DISCUSSION

In this chapter the experimental and numerical results will be discussed for various parameters which determine the overall performance of the low concentration photovoltaic systems. In the first part of the chapter several numerical and experimental results of different configurations of PV-CPC system will be discussed in detail. Then in the second half similar results will be discussed for different configuration of V-trough PV system in detail.

5.1 PV-CPC SYSTEM

5.1.1 Optical Modeling

In order to enhance the electrical performance of the PV system and to reduce the cost of electric power produced per unit area, the solar flux should be maximized on the given cell area. Increase in the solar flux is the main key parameter that enhances the electric power output from a PV system. As the solar flux will increase more photons will strike the PV cell and more electron hole pairs will be generated. As a result more electricity is generated from the same PV cells by increasing the solar flux. In PV-CPC system low cost parabolic reflectors are used for this purpose of enhancing the solar flux onto the PV cell area.

PV-CPC performance analysis was made for the location of Dhahran with latitude of 26.5°. To capture the maximum amount of solar radiation, the slope of the collector was varied seasonally. It was increased 15° from latitude in winters and in summers it was decreased 15°. The slope of the collector was kept to be 11.5° for June and 41.5° for December. For the months of March and September it was kept equal to the latitude of the site as 26.5°. Incident solar radiation over a geographic location varies with different months in a year. Figure 5.1 shows the solar irradiance absorbed in glazed PV-CPC system, unglazed PV-CPC system and flat PV system for different climates around the year in location of Dhahran. In glazed PV-CPC system, the incident radiation is effected by the transmittance of the glass cover. Absorbed radiation is higher for unglazed PV-CPC system because there is no glass cover present and the incident radiation directly strikes the solar cells. In June the maximum amount of absorbed radiation absorbed by flat PV string is about 885 W/m^2. When glazed CPC is integrated with the flat PV string, the amount of absorbed radiation increases up to 1326 W/m^2 .This shows the percentage increase of about 49.8%. In unglazed PV-CPC system the amount of absorbed radiation for the same ambient conditions is estimated from the optical model to be about 1597 W/m^2. Similarly for other climates around the year, maximum absorbed radiation is for the case of unglazed PV-CPC system. The amount of energy absorbed is needed to calculate the thermal and electrical performance of the PV system, as part of the absorbed energy is used to generate electric current and the rest of it increases the temperature of the cell. This amount of absorbed energy is then given as the input parameter to the thermal and electrical model.

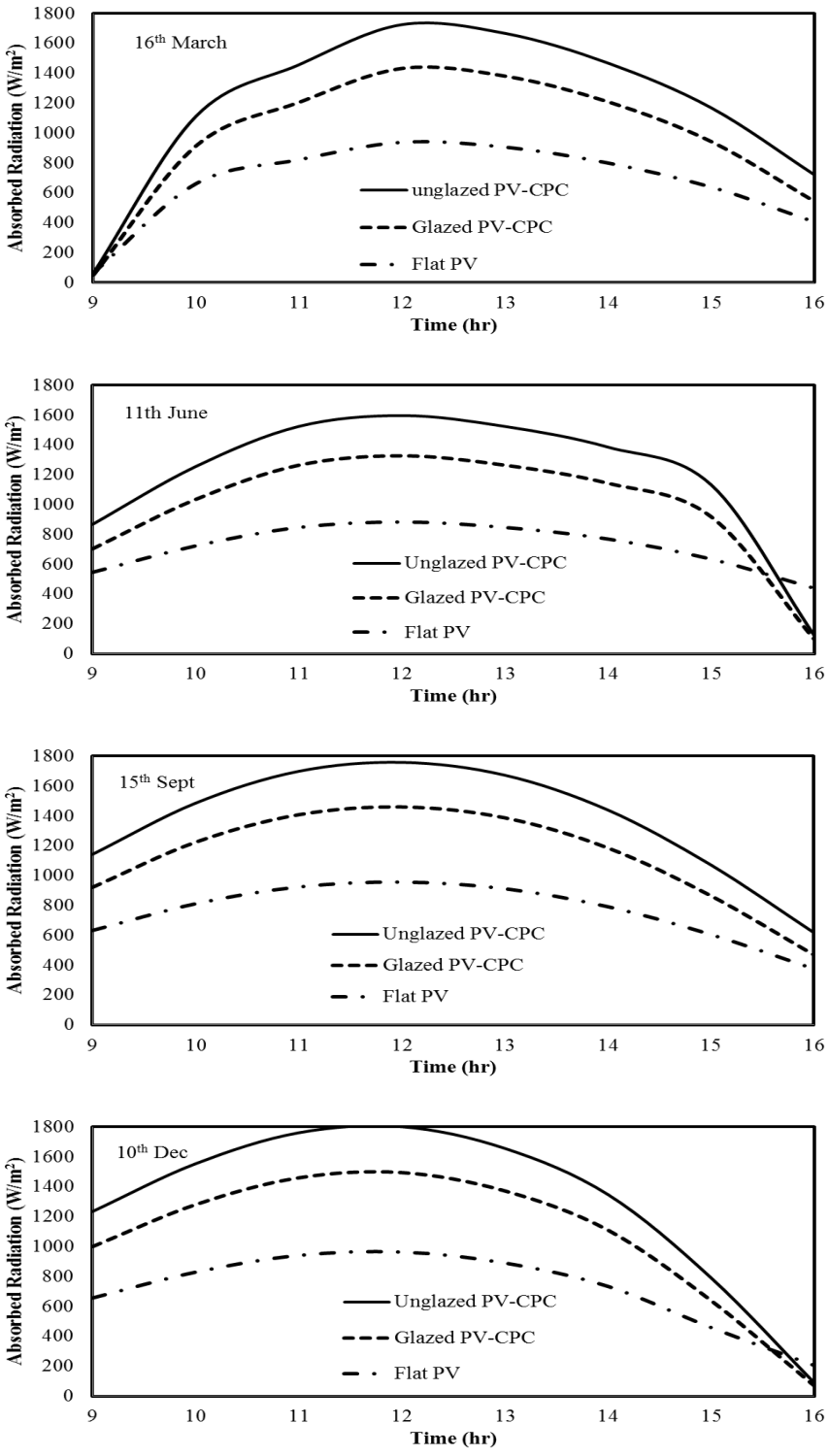

Figure 5.1: Absorbed radiation

5.1.2 Thermal Modeling

. Operating temperature of a PV module plays an important role in deciding the efficiency and thermal degradation of the PV module. Temperature effects are the result of an inherent characteristic of crystalline silicon cell based modules as the front and the back surface gets heated up with the irradiance which results in increase of cell temperature. The operating temperature of the module depends on the equilibrium maintained between the heat generated by the module and the heat lost to surrounding environment. Simulations were performed and cell temperatures for different configurations were calculated by thermal model discussed in Chapter 3. Figure 5.2 indicates that the maximum cell temperature is observed in the case of glazed PV-CPC system. Cell temperature goes up to 82°C for glazed PV-CPC system whereas for unglazed PV-CPC system it is estimated to be 72°C for the month of June. For flat PV the temperature remains under the range of 58°C. Increase in cell temperature for glazed and unglazed PV-CPC system is due to increased amount of absorbed radiation compared to flat PV panels. This unwanted heat lowers the electrical efficiency of the system.

Since the PV panels interact with the environment and their efficiency is so low, they passively absorb about 80% of the incoming solar irradiance as heat. The electrical efficiency of PV module declines with the increase in temperature of the PV module.

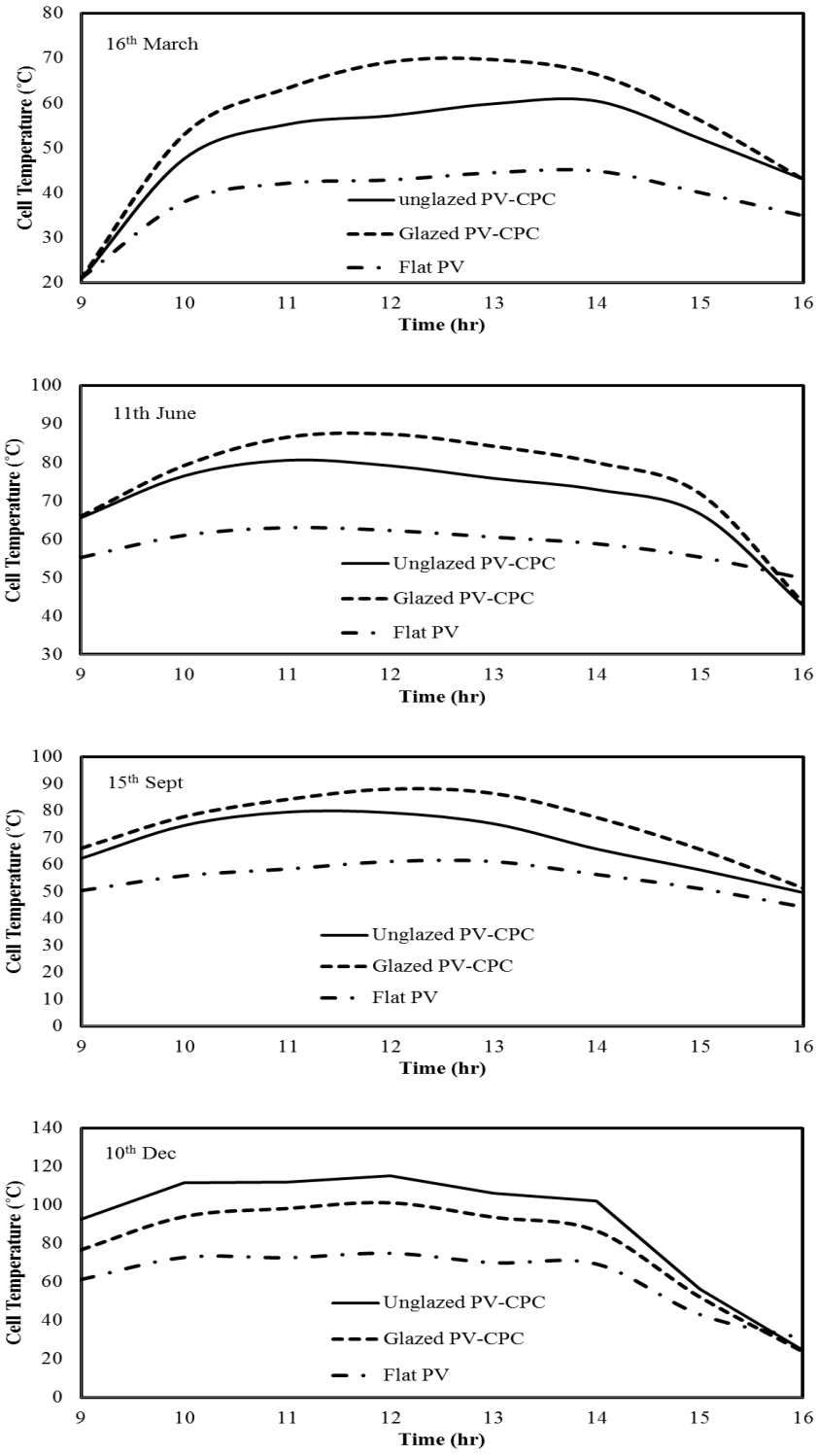

Figure 5.2: Comparison of cell temperatures without cooling

In order to increase the efficiency and to reduce the thermal degradation, an effective technique is to lower the operating temperature of the PV module. This can be accomplished by applying cooling techniques which reduce the heat stored inside the PV panel during operation. It is reported that water cooled PV/T system can produce electricity at higher efficiencies than the PV/T air cooled systems, as the operating range of temperature is less in the case of water cooling. As the specific heat at constant pressure of water is greater than air, therefore water has more capacity to absorb heat as compared to air. For the present study, water cooling is applied to lower the operating temperature of the PV panel and consequently improve the efficiency of the PV system.

The effect of cooling in the performance of PV systems is studied in this study. In order to extract the unwanted heat from the cells, active cooling system is applied. A rectangular heat exchanger is attached at the bottom side of the panels and then compared with the uncooled panels. Figure 5.3 shows the estimation of the cell temperatures by circulating cooling water in the rectangular channels (W130mm×d13mm×L1016mm) attached at the bottom of the PV strings. There is significant reduction in the cell temperatures and the maximum cell temperature for the glazed PV-CPC system is reduced to 58°C for the ambient conditions of June. There is a significant reduction of 29.2% in the operating cell temperatures. Active cooling ensures the operating cell temperature range within the safe limits of the cells. Cell temperature above 80°C is hazardous to the life of standard PV cells. The operating cell temperature for unglazed PV-CPC is reduced to 54°C and for flat PV panel is 47°C. These lower operating cell temperatures ensure the increase in the overall efficiency of the system.

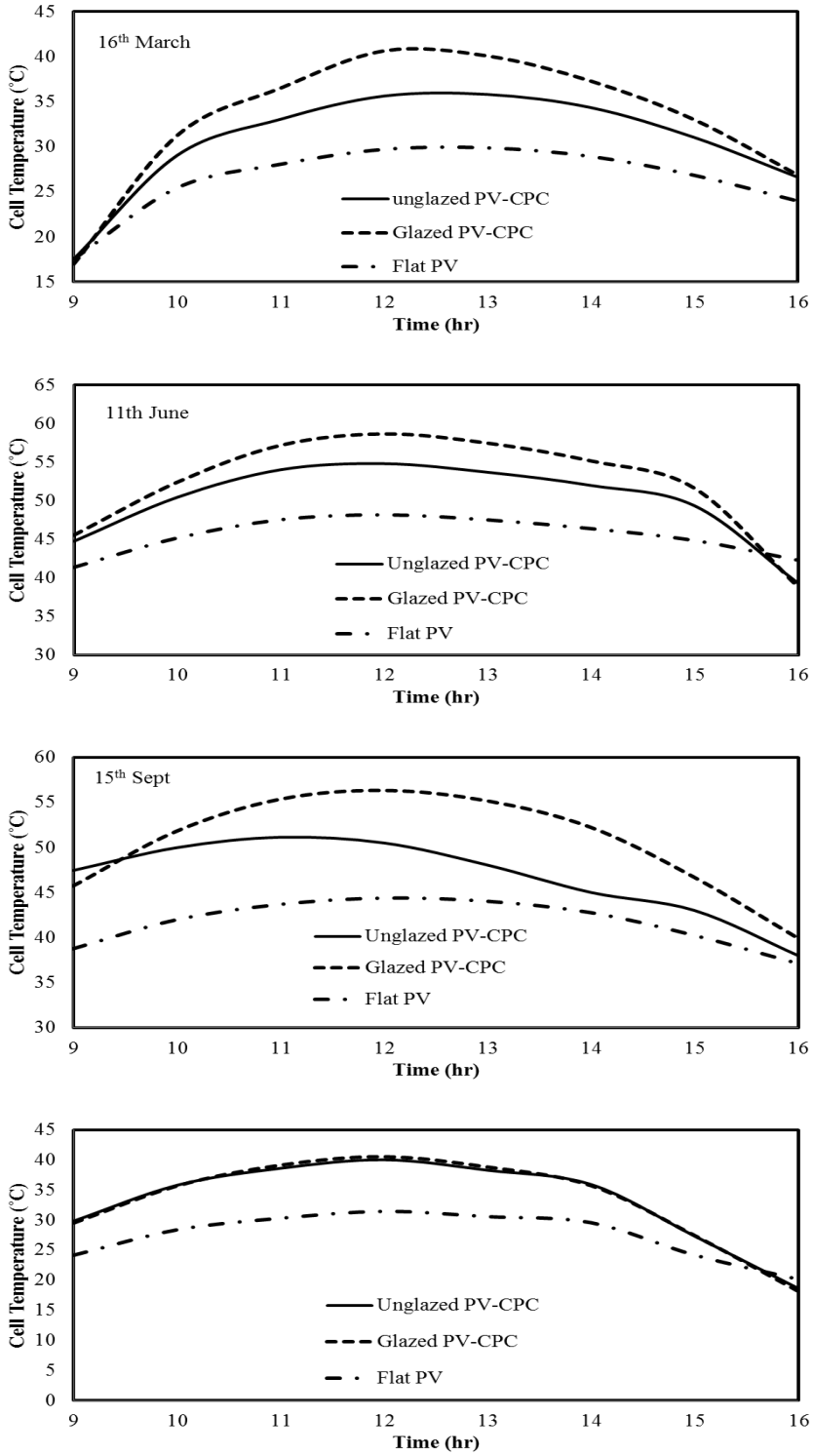

Figure 5.3: Comparison of cell temperatures with cooling

Active cooling extracts the unwanted heat from the system, stores it in the form of thermal energy and increases the electrical efficiency of the system simultaneously. The useful energy gain by extracting the thermal energy from the cells is shown in Figure 5.4. Results show that glazed PV-CPC exhibits the maximum useful energy gain compared with the unglazed PV-CPC and flat PV string. Glazing protects the cell and CPC reflecting surface from dust and moisture, but on the other hand the top loss coefficient U_t decreases and the overall losses U_L are also reduced. This acts as the barrier for the heat energy to be lost to the environment and causes the temperature of the cell to rise and consequently the electric power output is reduced. Glazing proves to be beneficial when the main objective is thermal gain from the system, because glazing reduces the overall losses and increases the useful energy gain from the system as shown in Figure 5.4. Maximum useful energy gain is for glazed PV-CPC system for all the four representative days of the month of the year. The thermal energy in the form of warm water can be used in domestic applications.

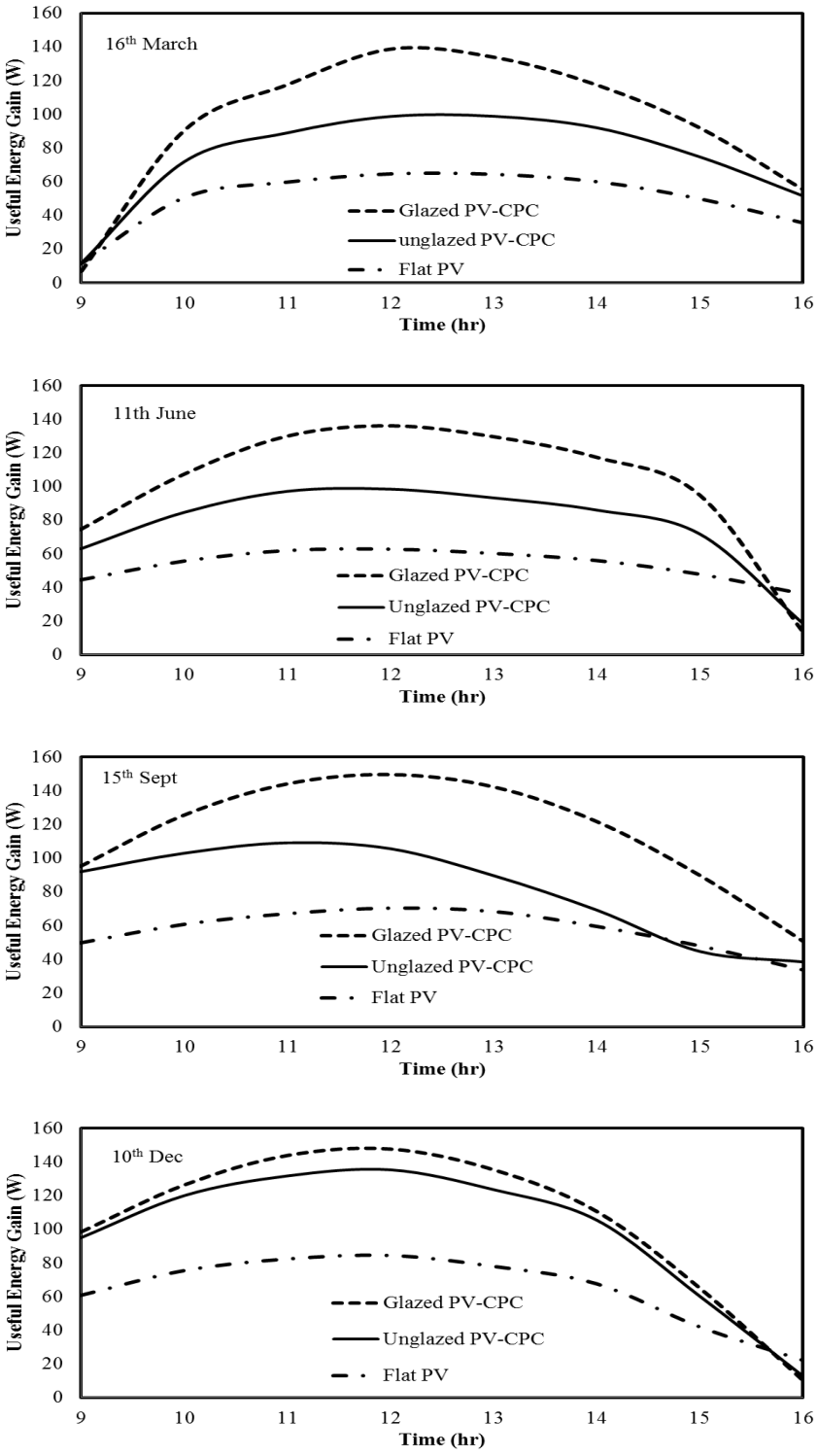

Figure 5.4: Useful energy gain for all cases

In order to analyze the amount of reduction in cell operating temperatures separately for all three cases, comparison is made for each system. The operating range of cell temperatures for glazed PV-CPC with and without cooling is shown in Figure 5.5. Water cooling is applied at the mass flow rate of 1 LPM. In the absence of active cooling, the operating cell temperature range of glazed PV-CPC is above the safe limit of operation. Therefore it is very critical to the life and safety of the PV cell to run the glazed PV-CPC system without cooling.

Similarly comparisons for unglazed PV-CPC and flat PV string are shown in Figure 5.6 and Figure 5.7 respectively.

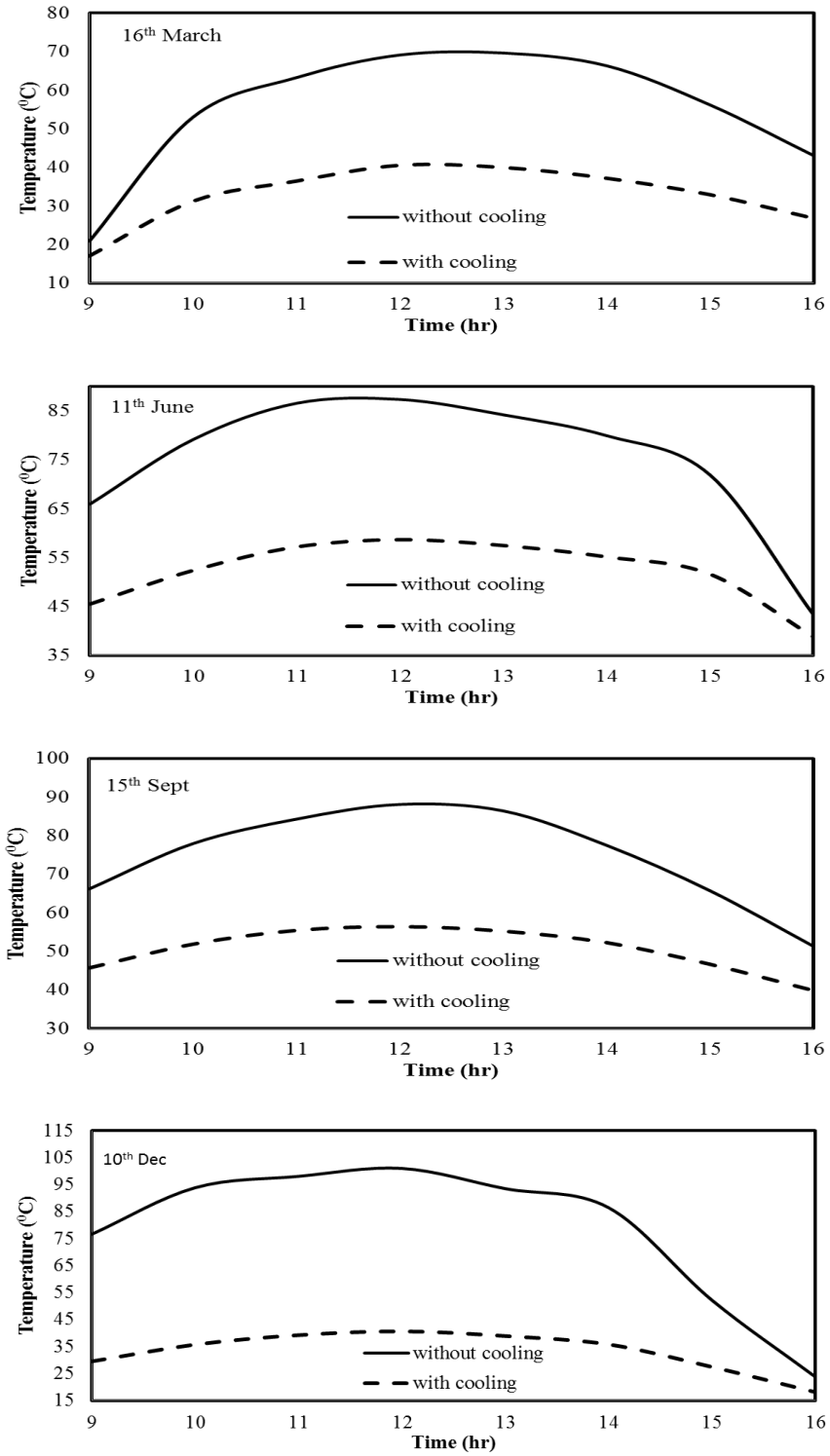

Figure 5.5: Comparison of cell temperatures with and without cooling for glazed PV-CPC system.

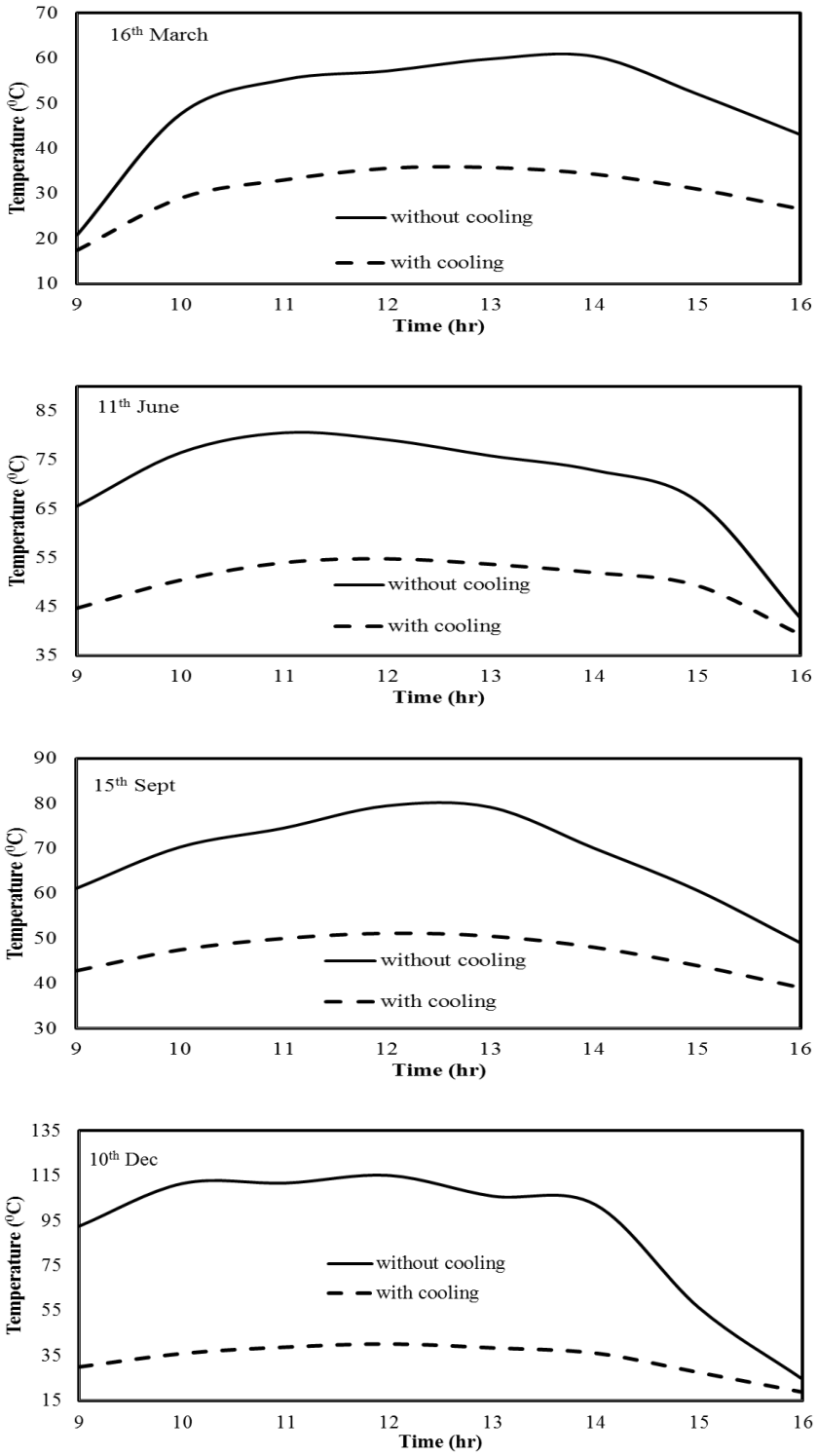

Figure 5.6: Comparison of cell temperatures with and without cooling for unglazed PV-CPC system

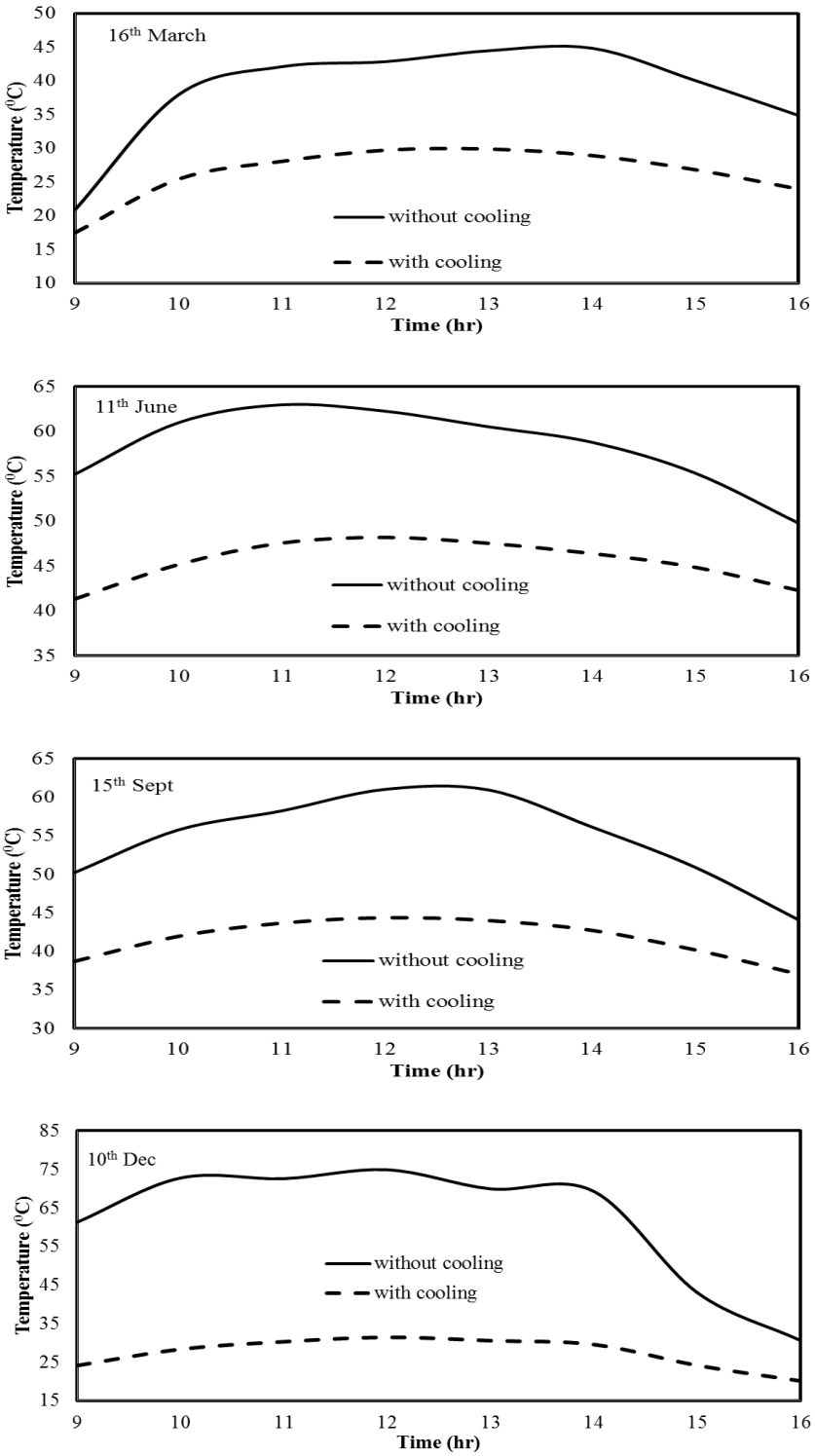

Figure 5.7: Comparison of cell temperature with and without cooling for PV string without CPC

5.1.3 Electrical Modeling

In order to analyze the electrical performance of the photovoltaic cells, five parameter model is used in the current study as discussed in chapter 3. The estimation of five reference parameters is carried out by solving highly non-linear equations using EES software. After the estimation of five parameters the electrical performance of the PV system can be analyzed by giving absorbed radiation and the cell temperature as the input parameters. The electrical performance of the glazed PV-CPC system, unglazed PV-CPC system and flat PV string is shown in Figure 5.8. Variation of electric power output for all the three cases is predicted for the four representative days of the month of the year.

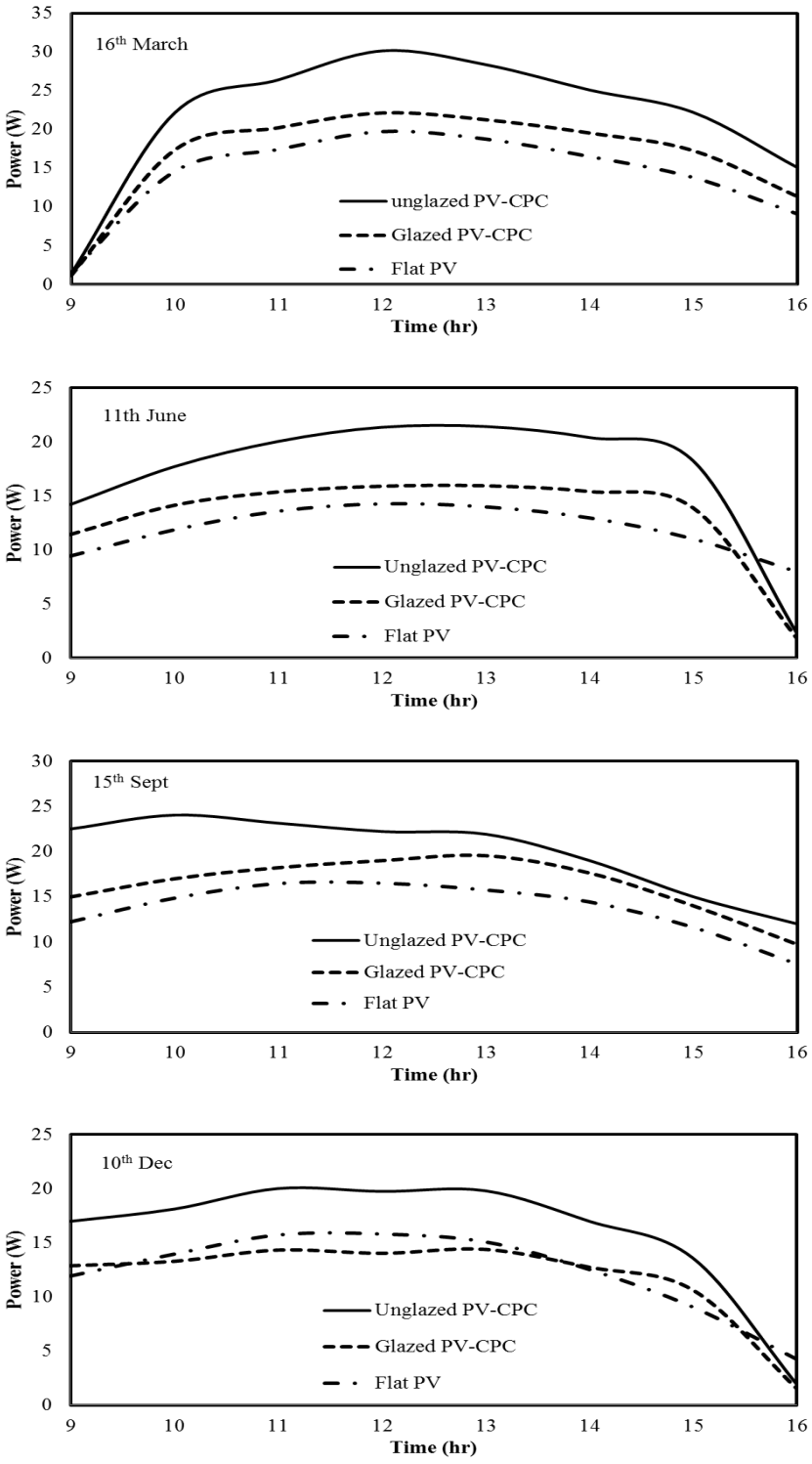

Figure 5.8: Comparison of power without cooling

Unglazed PV-CPC system produces the maximum power output compared to glazed PV-CPC system and flat PV string. As discussed earlier, the higher value of operating cell temperatures in the case of glazed PV-CPC system causes a significant reduction in electrical output of the system. Maximum power output from the flat PV string on 15th September is 15.8 W and for glazed PV-CPC system it is 16.86 W. Removing the glazing from PV-CPC system considerably increases the maximum value of power output to 22.74 W. The reason for increase in the electrical power output is the reduction in the operating module temperature by removing the glazing. This results show that there is an addition of 43.9 % in the maximum power output when CPC reflectors are integrated with flat PV strings. Similarly for the rest of the days unglazed PV-CPC system exhibits maximum power output compared with the other configurations.

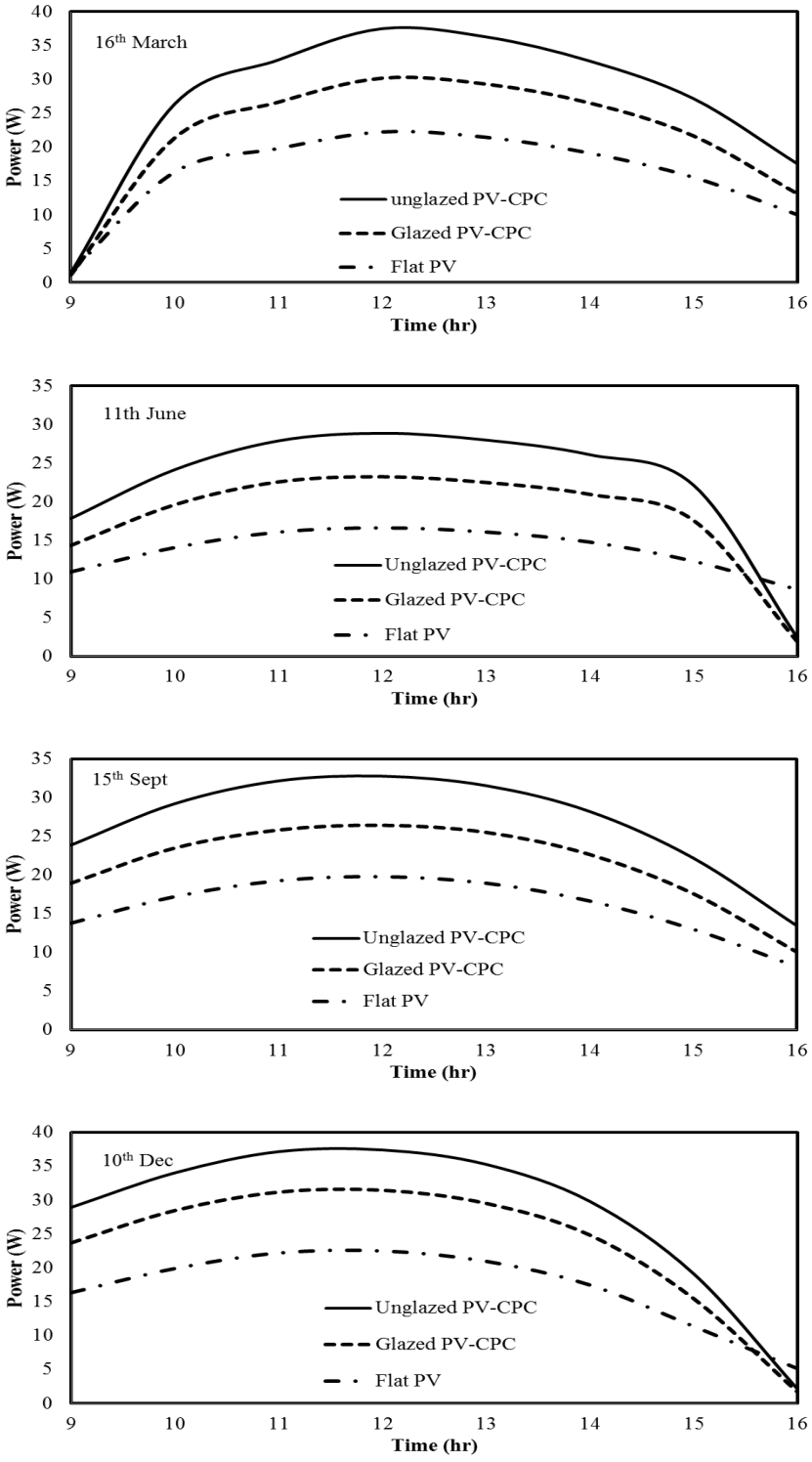

Figure 5.9: Comparison of power with cooling

There is a significant increase in the maximum value of the power output once active cooling is incorporated along with the existing system. After applying active cooling the maximum power output from the unglazed PV-CPC system reached 26.82 W for the same ambient conditions of the average day of the month of September. This shows that there is an addition of 17.94% in the value of maximum power output delivered from the unglazed PV-CPC system. In the case of glazed PV-CPC system, power is enhanced to 5.51 W which results in the percentage increase of 32.68%. Amount of power increase in each case by applying cooling is shown in Figure 5.10-Figure 5.12. As shown in these figures there is a significant amount of increase in the power output by applying cooling in these configurations.

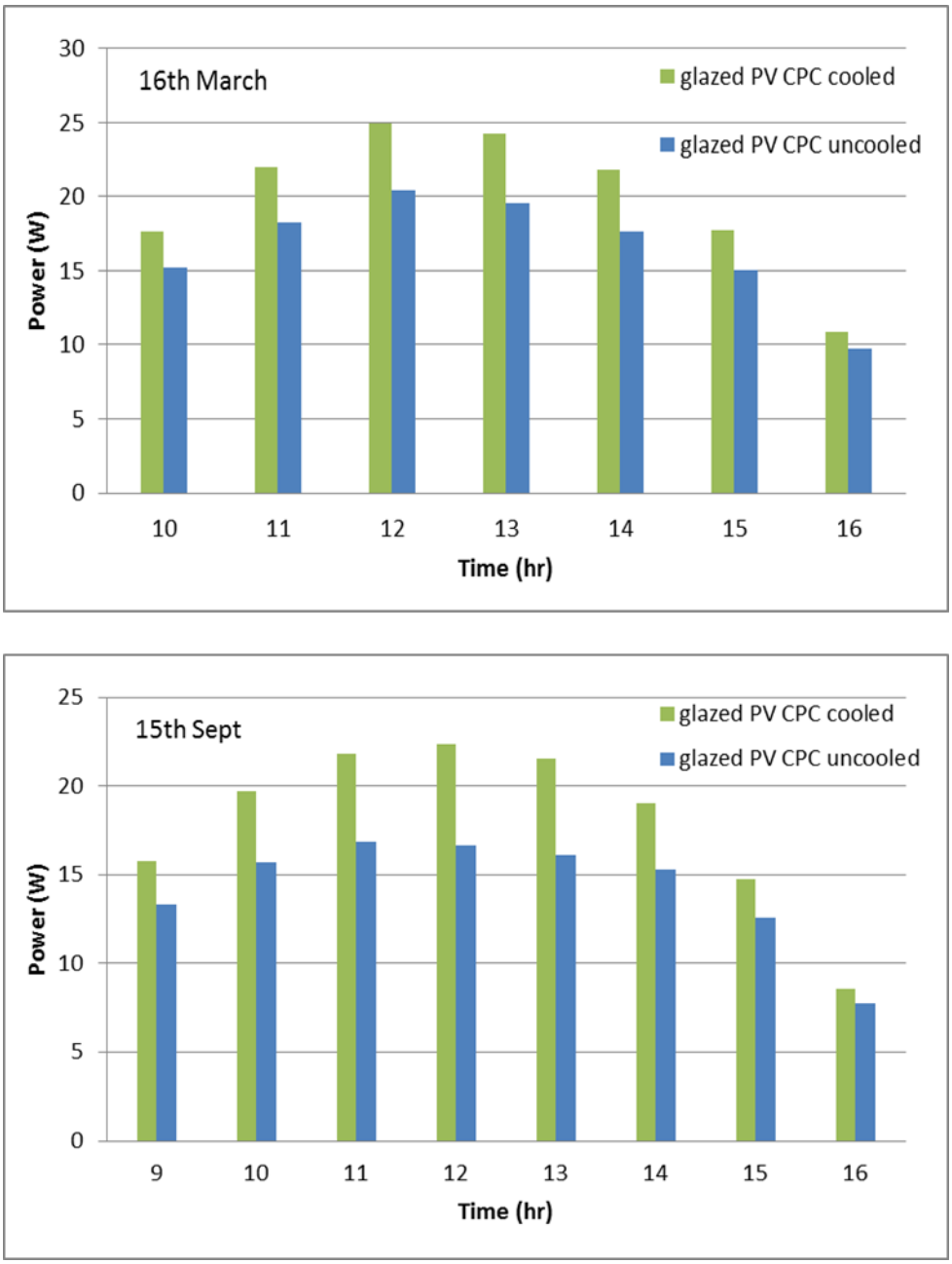

Figure 5.10: Comparison of power for glazed PV-CPC system with and without cooling

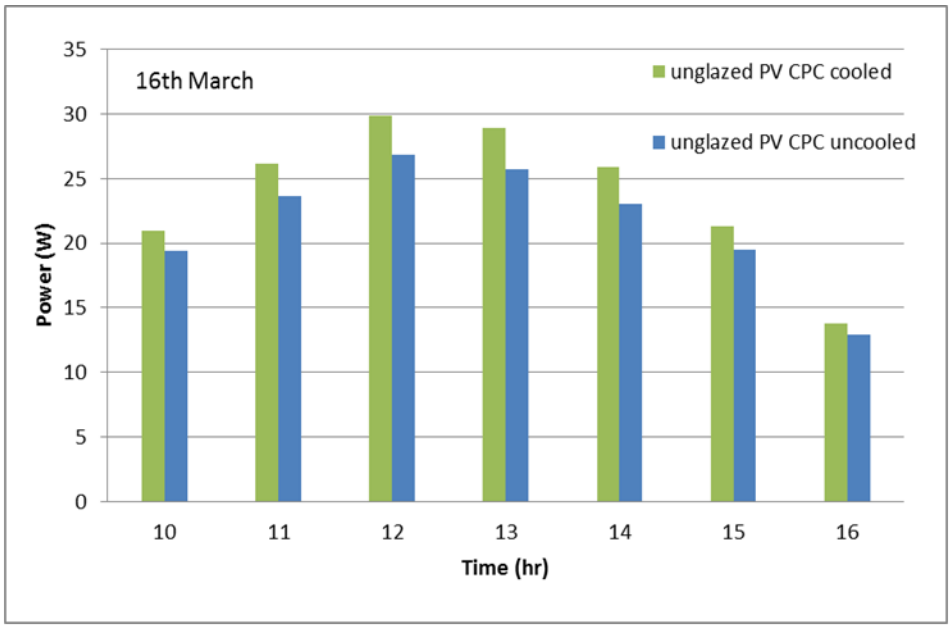

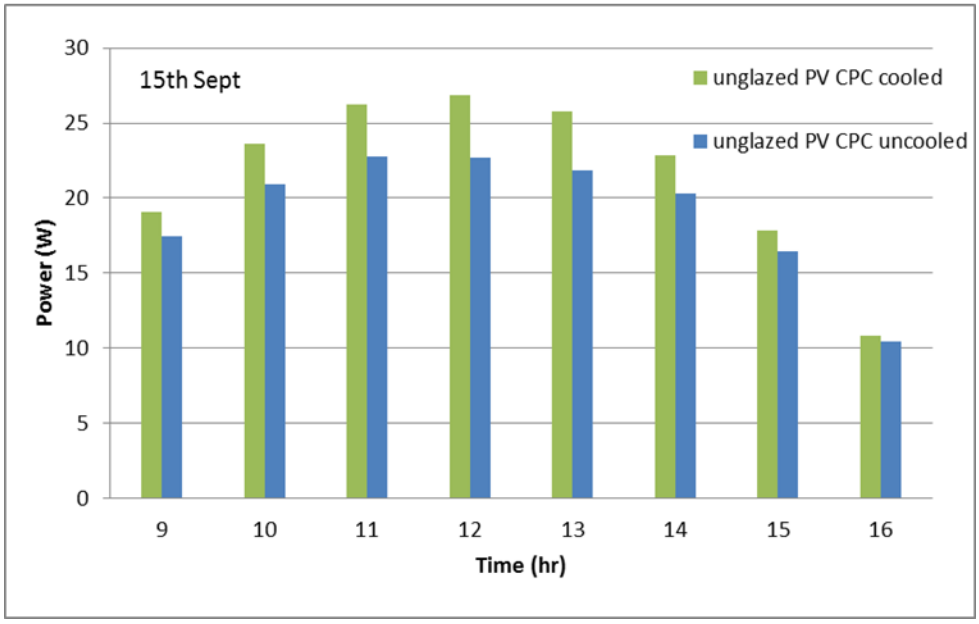

Figure 5.11: Comparison of power for unglazed PV-CPC system with and without cooling

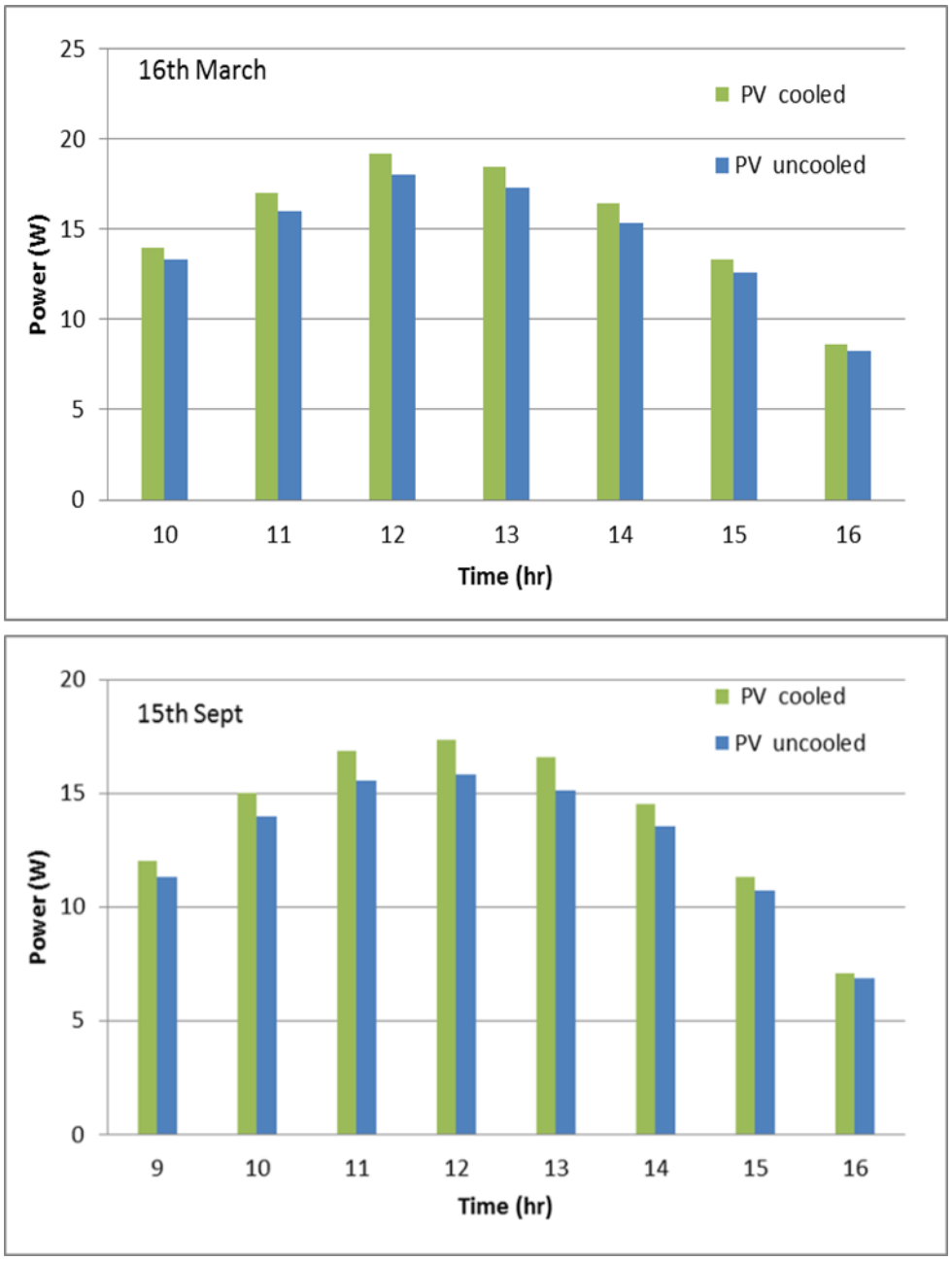

Figure 5.12: Comparison of power for flat PV string with and without cooling

5.1.4 Experimental Results of PV-CPC system

The performance of PV system depends on several climatic factors such as solar radiation, ambient temperature and wind speed since the maximum power point (MPP) on the current-voltage (I-V) performance curve varies with these factors. The experimental analysis of the PV-CPC system was carried out in two phases.

Phase I

In this phase the performance of uncooled flat PV is compared with uncooled unglazed PV-CPC system. The tests were conducted in the month of Sept. 2013. The variation of the ambient temperature and the irradiance received by the panel surface during the test days are shown in Figure 5.13 and Figure 5.14. Maximum value of radiation received is 961.22 W/m^2 at noon.

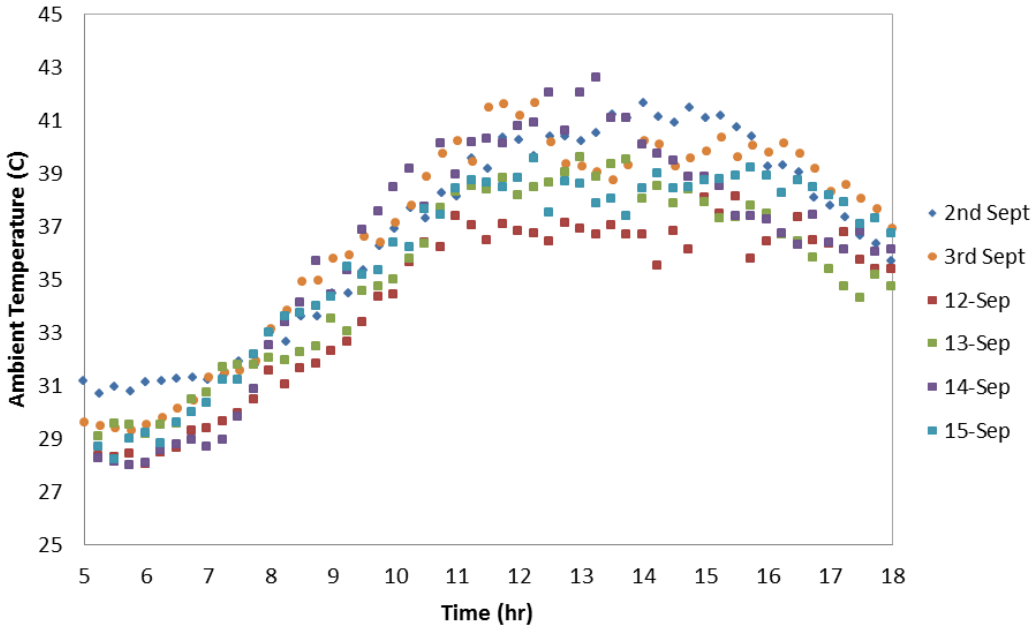

Figure 5.13: Variation of ambient temperature

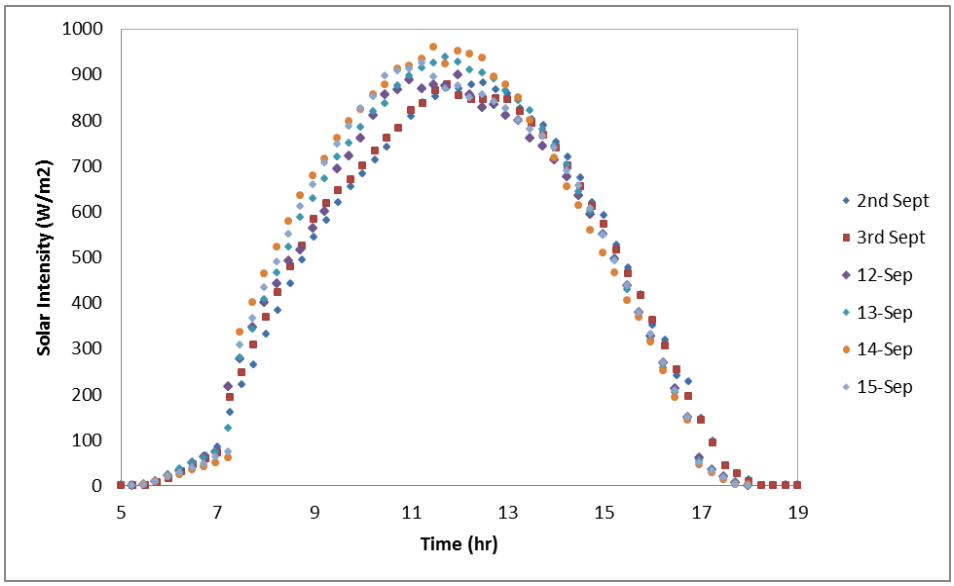

Figure 5.14: Variation of solar Intensity

Experiments were performed in order to analyze the performance of the PV-CPC system practically. Figure 5.15 and Figure 5.16 show the variation of maximum current over time for simple PV string and unglazed PV-CPC system. This result indicates that the maximum power point current for unglazed PV-CPC was about 56% higher than simple flat PV panel. This was due to effective solar radiation at the PV surface for the unglazed PV-CPC increased by its concentration ratio of 2.3 if the optics were perfect. The decrease in the output of the system as compared to its concentration ratio is due to non-uniform flux distribution on the surface of PV cell.

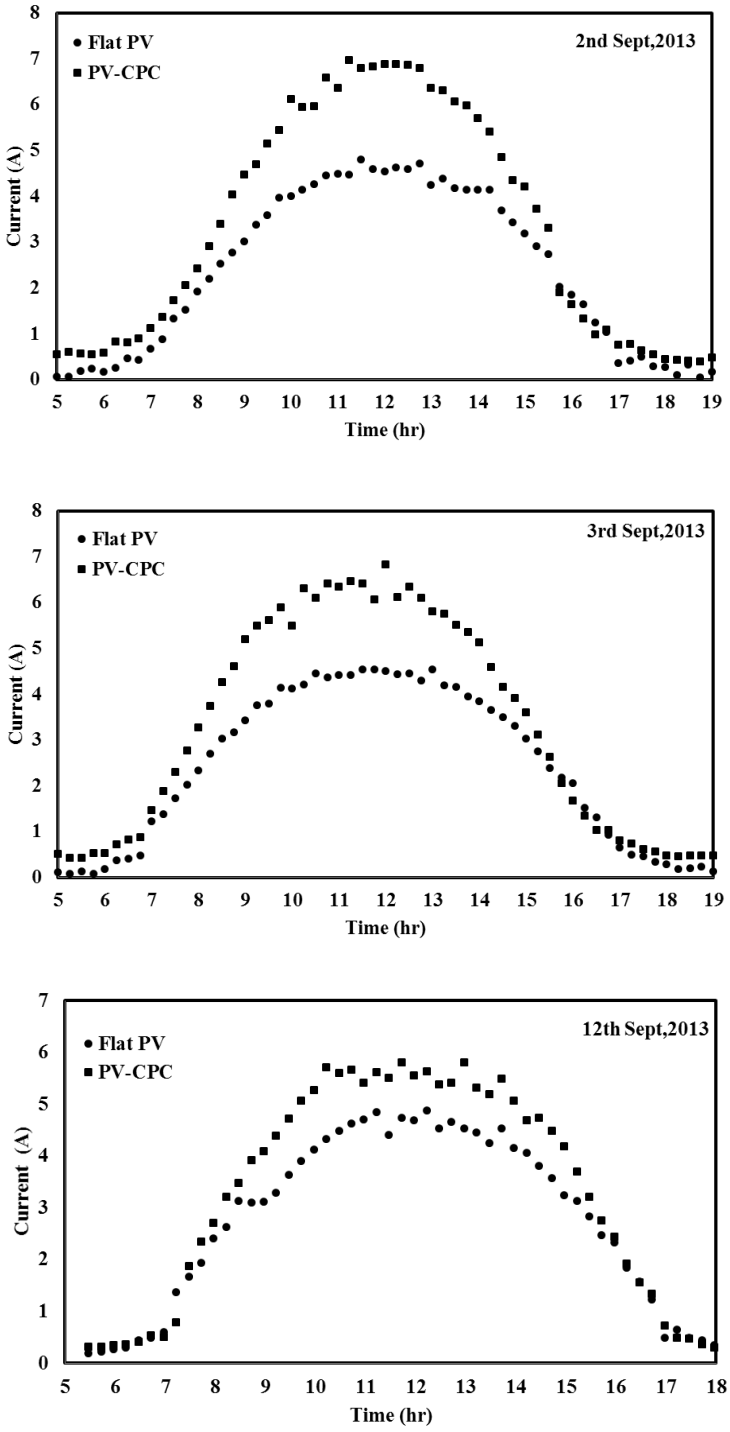

Figure 5.15: Variation of maximum power point current over time on 2nd, 3rd and 12th Sept, 2013

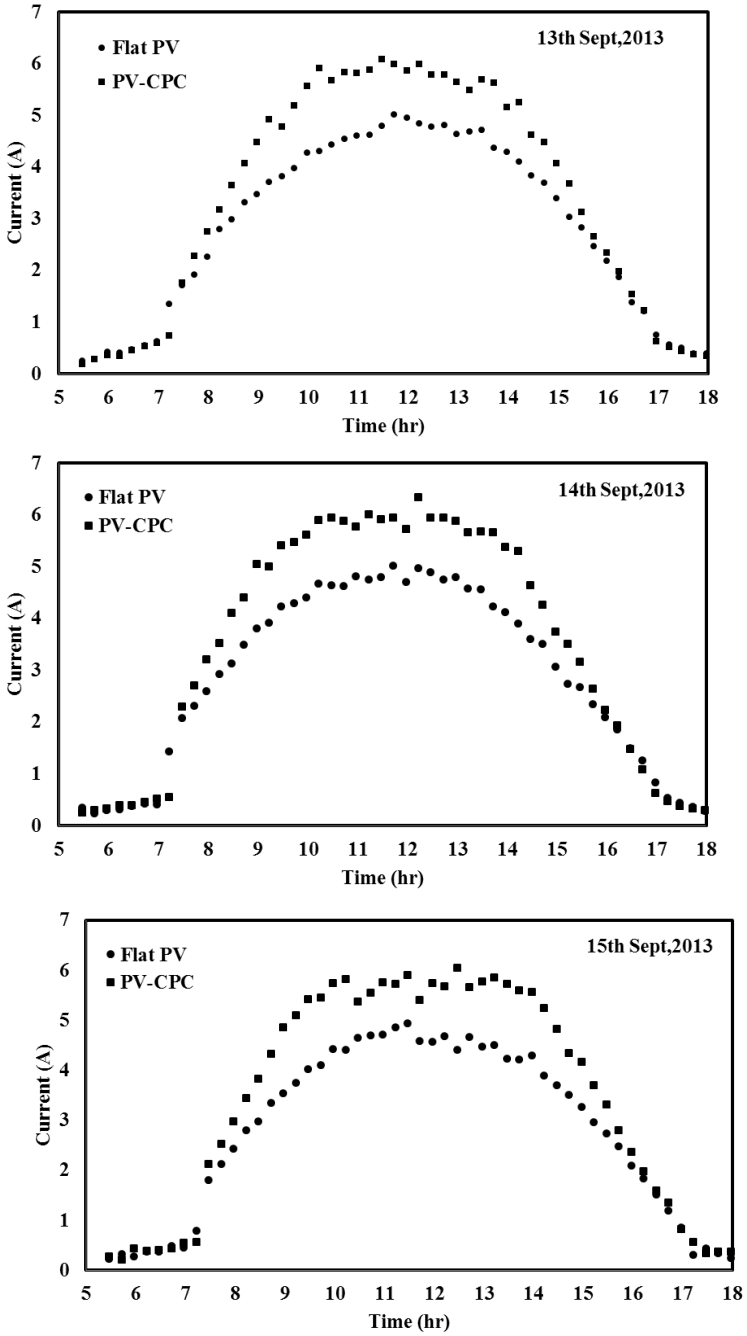

Figure 5.16: Variation of maximum power point current over time on 13,14 and 15 Sept,2013

Figure 5.17 and Figure 5.18 shows the variation of maximum power point voltage over the time for PV string and unglazed PV-CPC system. As the amount of solar radiation increases the module temperature also increases which affects the maximum power point voltage of the PV system. As shown in the figure below there is a significant reduction in the voltage of the unglazed PV-CPC system as compared to simple PV strings. The curve for the maximum power point voltage for unglazed PV-CPC system is under the curve of simple PV strings which shows that voltage is on the higher side for the case of flat PV system. This is due to the reason that operating module temperature is less for simple PV strings compared to the operating temperature of unglazed PV-CPC system. This drop in voltage under concentration gives rise to need of cooling the module to reduce the operating temperature.

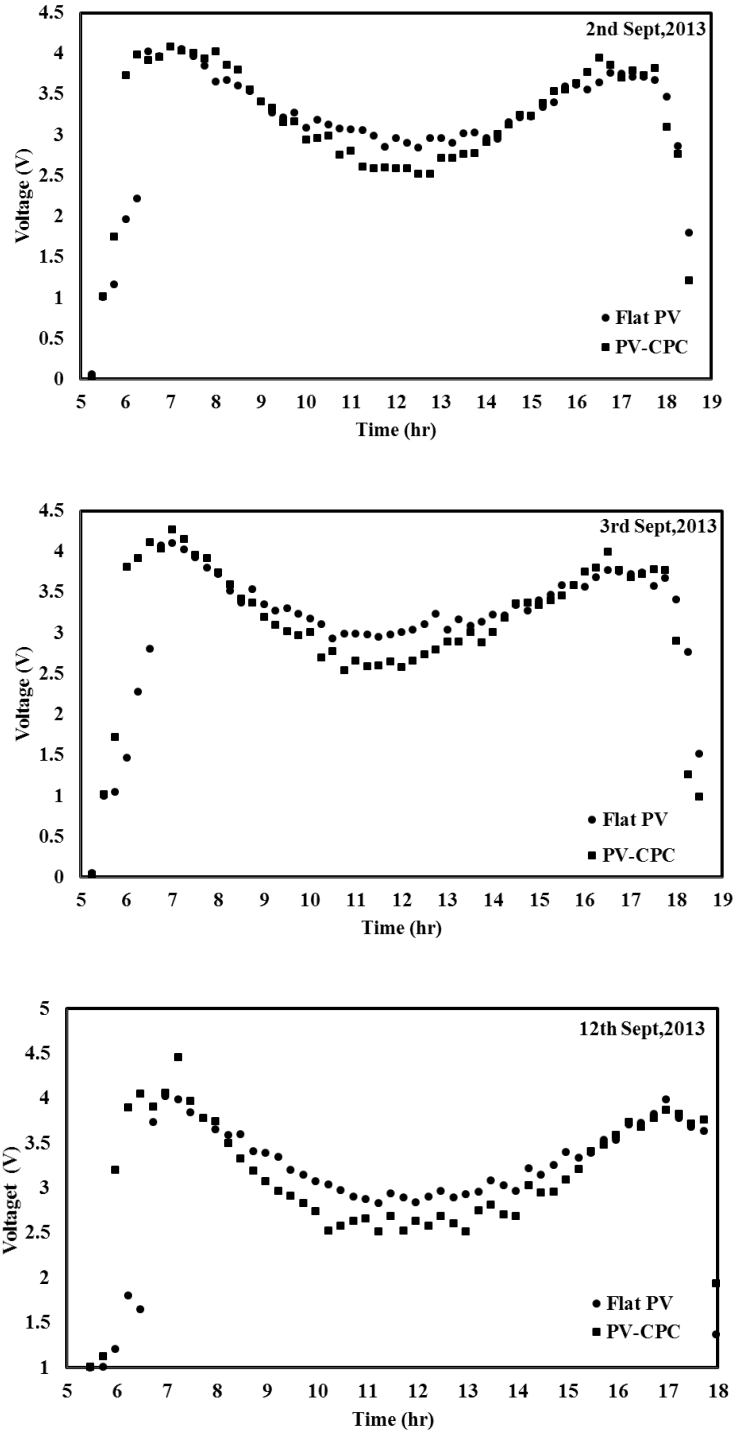

.

Figure 5.17: Variation of maximum power point voltage over time on 2nd, 3rd and 12th Sept, 2013

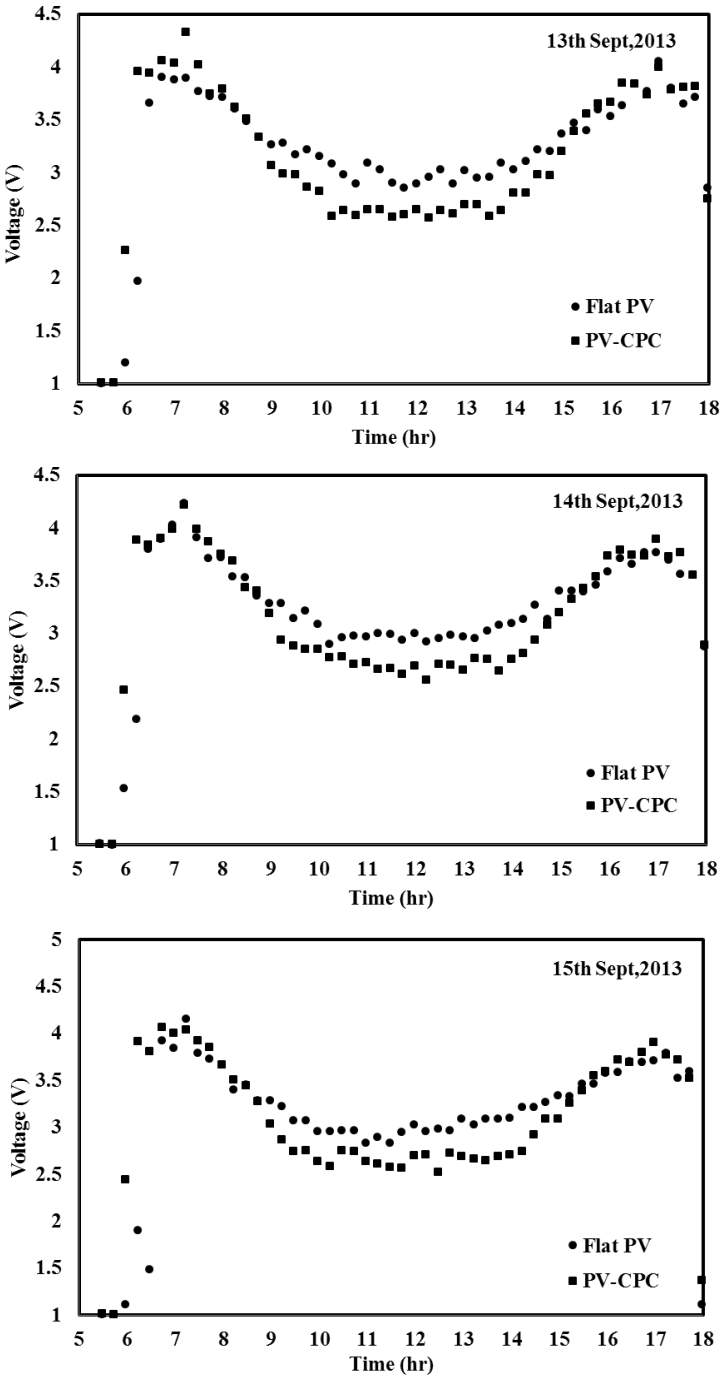

Figure 5.18: Variation of maximum power point voltage over time on 13,14 and 15 Sept,2013

Figure 5.19 and Figure 5.20 shows the variation of maximum output power over time for unglazed PV-CPC and simple PV strings. Maximum Power output increases from 14.4 to 18.2 W when CPC is integrated with simple PV strings. This result indicates that there is an addition of 26.4 % in the maximum power output when CPC reflectors are integrated with flat PV strings. It is important to use a PV system at its maximum power point (MPP). The change of maximum power point leads to a change in the efficiency of the system. The unglazed PV-CPC system with a theoretical concentration of 2.3 effectively increases the solar radiation at the PV surface and thus the short circuit current and open circuit voltage. However the increase in open circuit voltage and short circuit current are not of the same magnitude. The increase in the solar cell temperature due to concentration decreases the open circuit voltage and thus the output power from the PV panel.

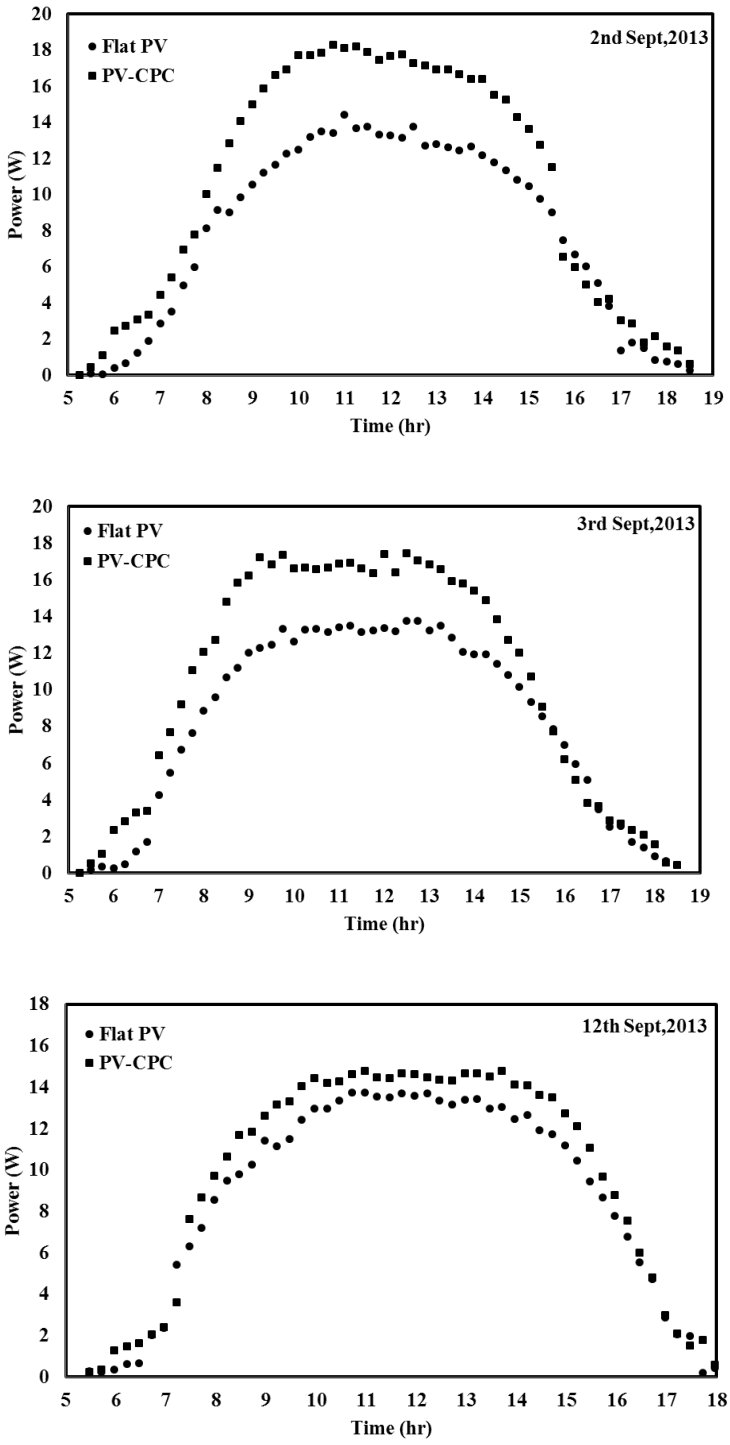

Figure 5.19: Variation of power over time on 2nd, 3rd and 12th Sept, 2013

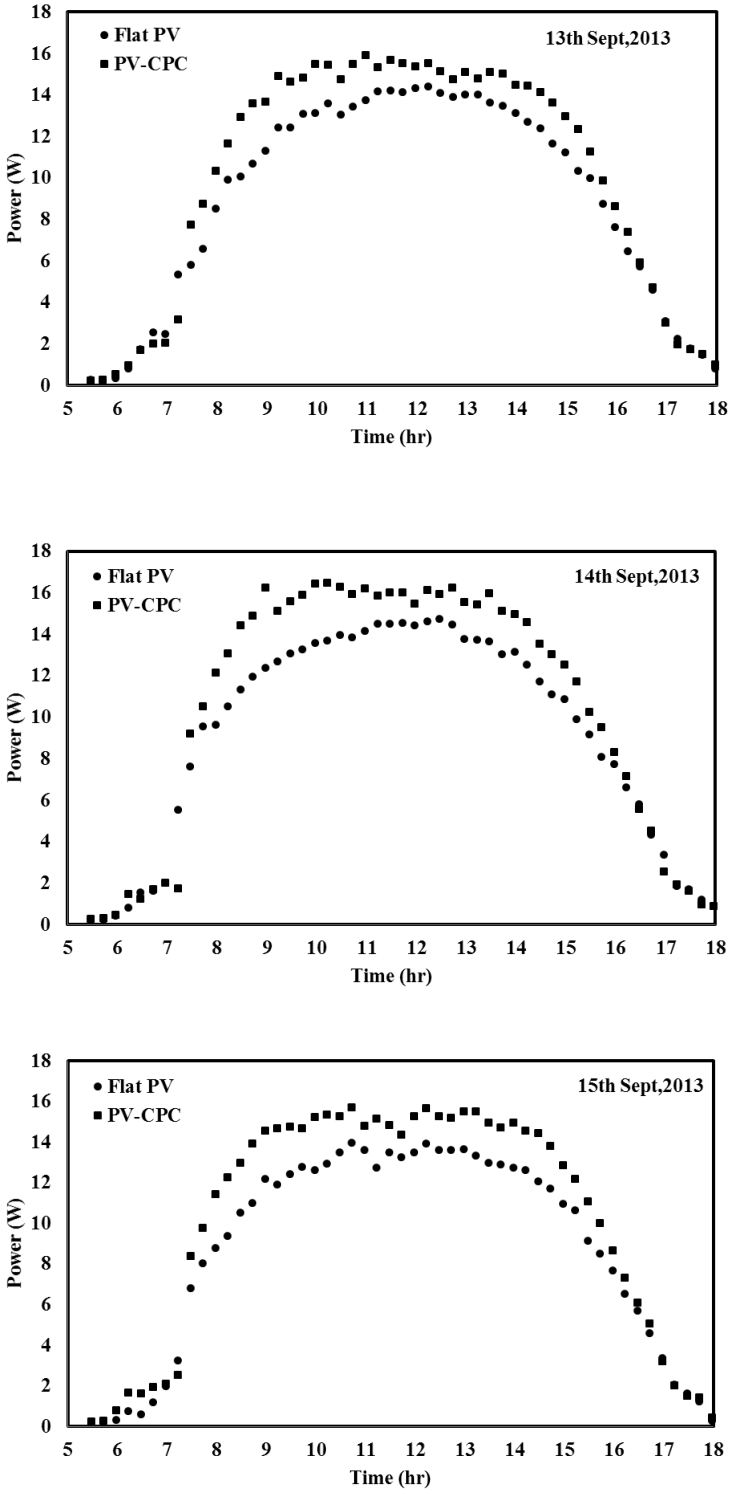

Figure 5.20: Variation of power over time on 13,14 and 15 Sept,2013

Phase II

In the 2nd phase of the experimental analysis all the six configurations were simultaneously tested. This phase of experimental investigation was conducted for 14 days. The measurements were recorded for 7 hours from 9:00 to 16:00 with 60 minutes of interval between successive data points. The electrical performance of the glazed PV-CPC system, unglazed PV-CPC system and flat PV string without cooling is presented in Figure 5.21. Variation of electric power output for all the three cases is presented for the test days. Unglazed PV-CPC system produces the maximum power output compared to glazed PV-CPC system and flat PV string. As discussed earlier, the higher value of operating cell temperatures in the case of glazed PV-CPC system causes a significant reduction in electrical output of the system. Maximum power output from the flat PV string on 4th February is 12.42 W and for glazed PV-CPC system it is 13.86 W. Removing the glazing from PV-CPC system considerably increases the maximum value of power output to 21.23 W. The reason for increase in the electrical power output is the reduction in the operating module temperature by removing the glazing. This result indicates that there is an addition of 70.9% in the maximum power output when CPC reflectors are integrated with flat PV strings. Similarly for the rest of the days unglazed PV-CPC system exhibits maximum power output compared with the other configurations.

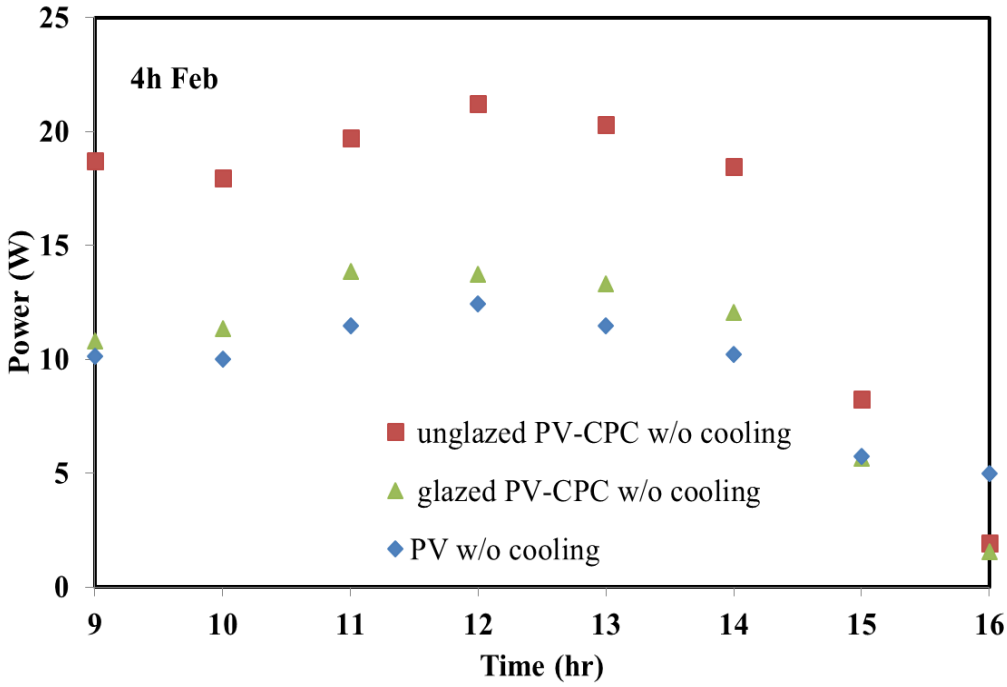
4h Feb
Power (W)
Time (hr)
unglazed PV-CPC w/o cooling
glazed PV-CPC w/o cooling
PV w/o cooling
0
5
10
15
20
25
9
10
11
12
13
14
15
16

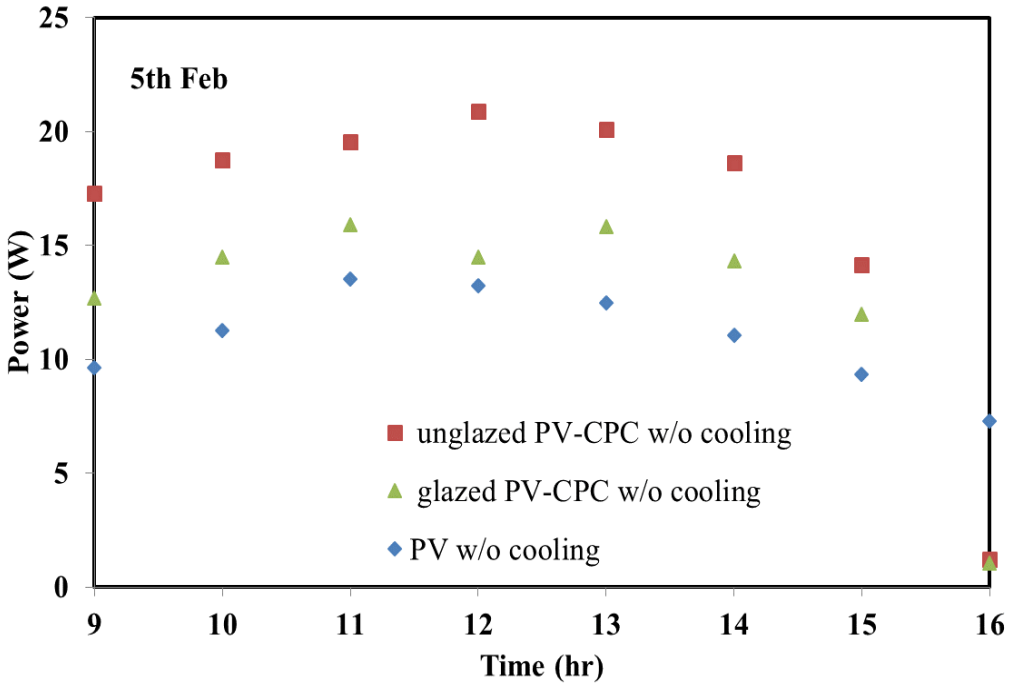
5th Feb
Power (W)
Time (hr)
unglazed PV-CPC w/o cooling
glazed PV-CPC w/o cooling
PV w/o cooling
0
5
10
15
20
25
9
10
11
12
13
14
15
16

Fig. 5.21 (a)

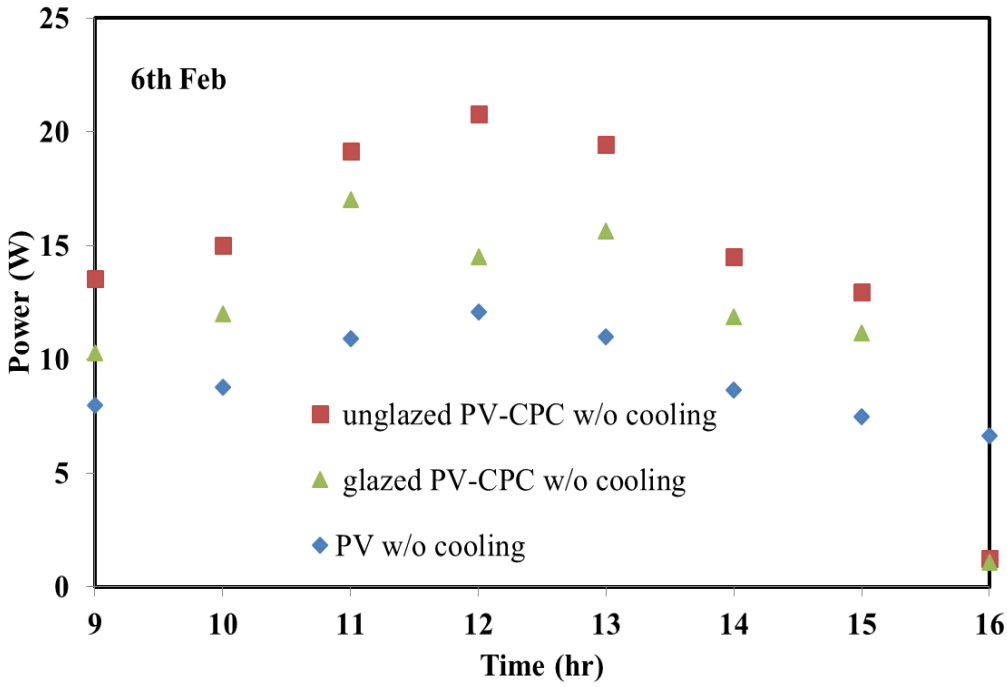
6th Feb
Power (W)
Time (hr)
unglazed PV-CPC w/o cooling
glazed PV-CPC w/o cooling
PV w/o cooling
0
5
10
15
20
25
9
10
11
12
13
14
15
16

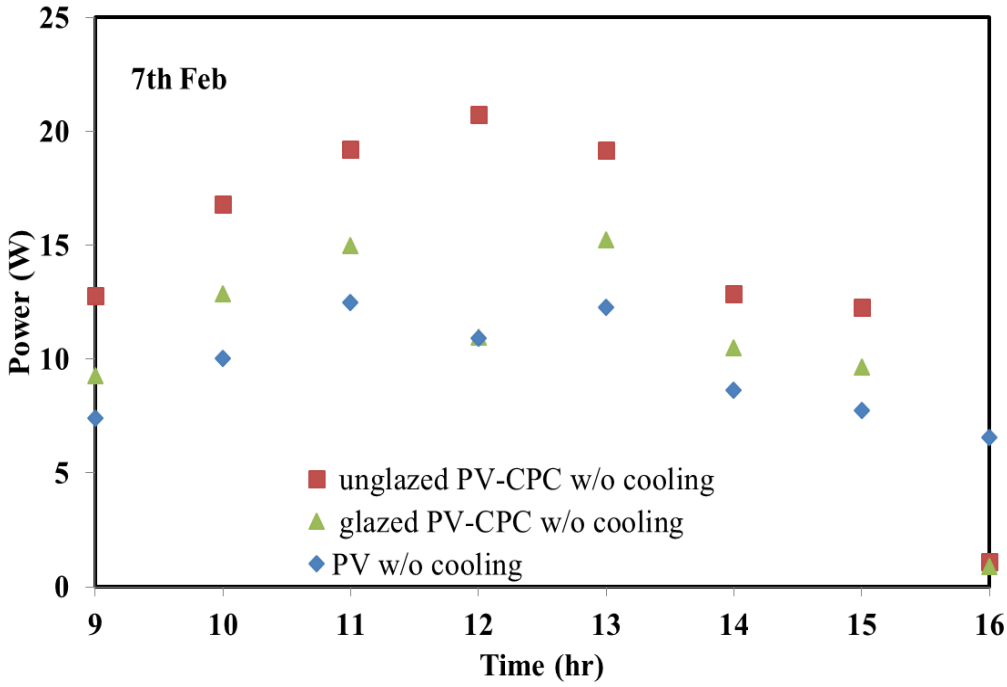
7th Feb
Power (W)
Time (hr)
unglazed PV-CPC w/o cooling
glazed PV-CPC w/o cooling
PV w/o cooling
0
5
10
15
20
25
9
10
11
12
13
14
15
16

Fig. 5.21 (b)

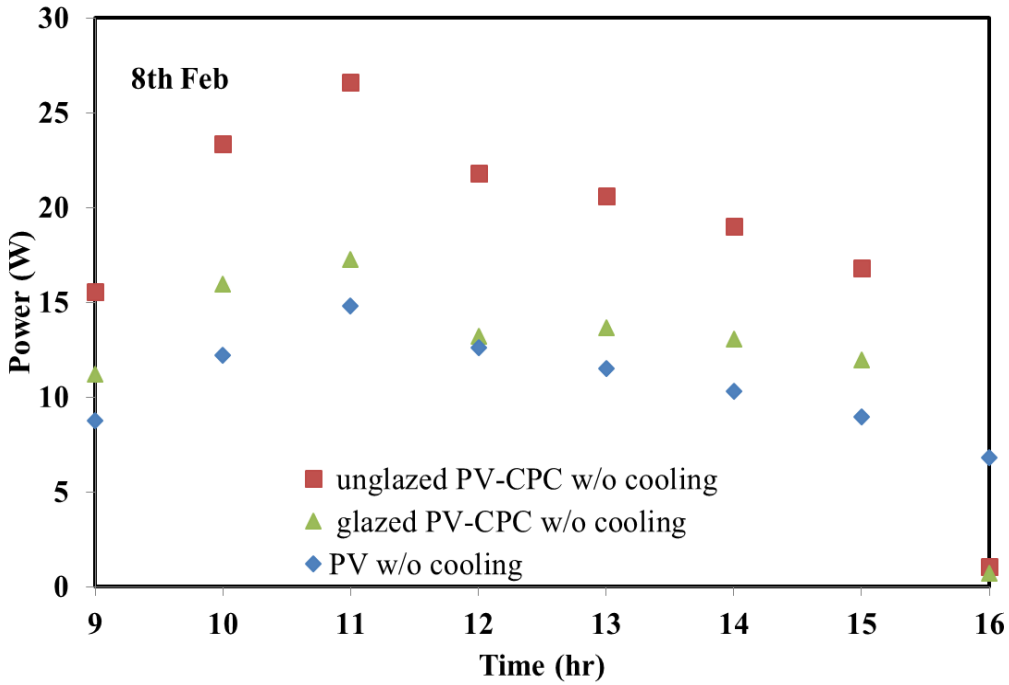
8th Feb
Power (W)
Time (hr)
unglazed PV-CPC w/o cooling
glazed PV-CPC w/o cooling
PV w/o cooling
0
5
10
15
20
25
30
9
10
11
12
13
14
15
16

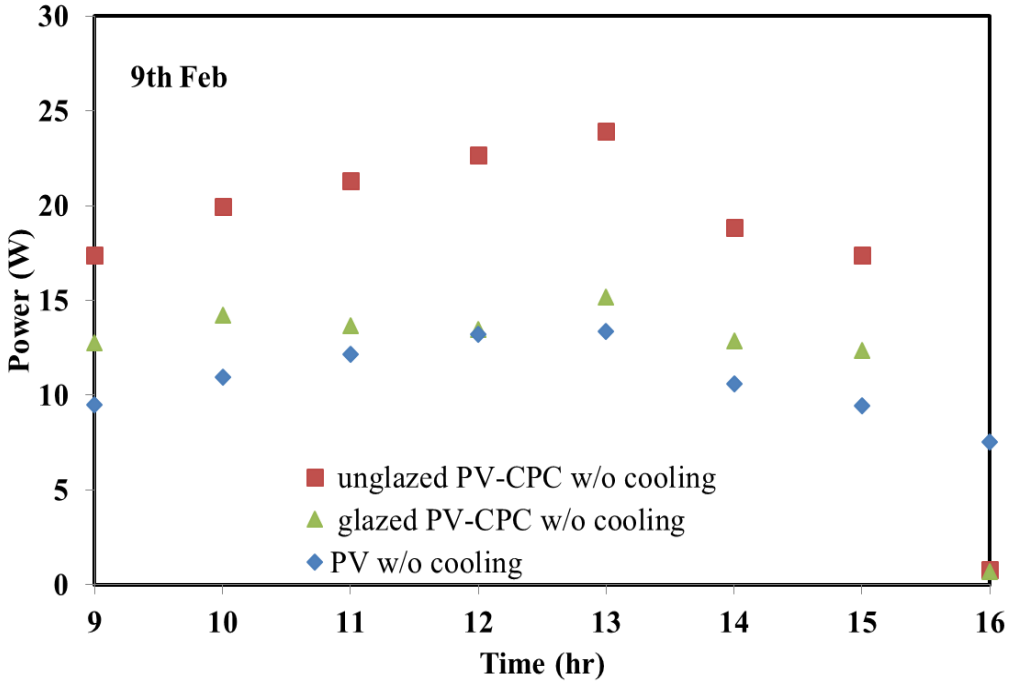
9th Feb
Power (W)
Time (hr)
unglazed PV-CPC w/o cooling
glazed PV-CPC w/o cooling
PV w/o cooling
0
5
10
15
20
25
30
9
10
11
12
13
14
15
16

Fig. 5.21 (c)

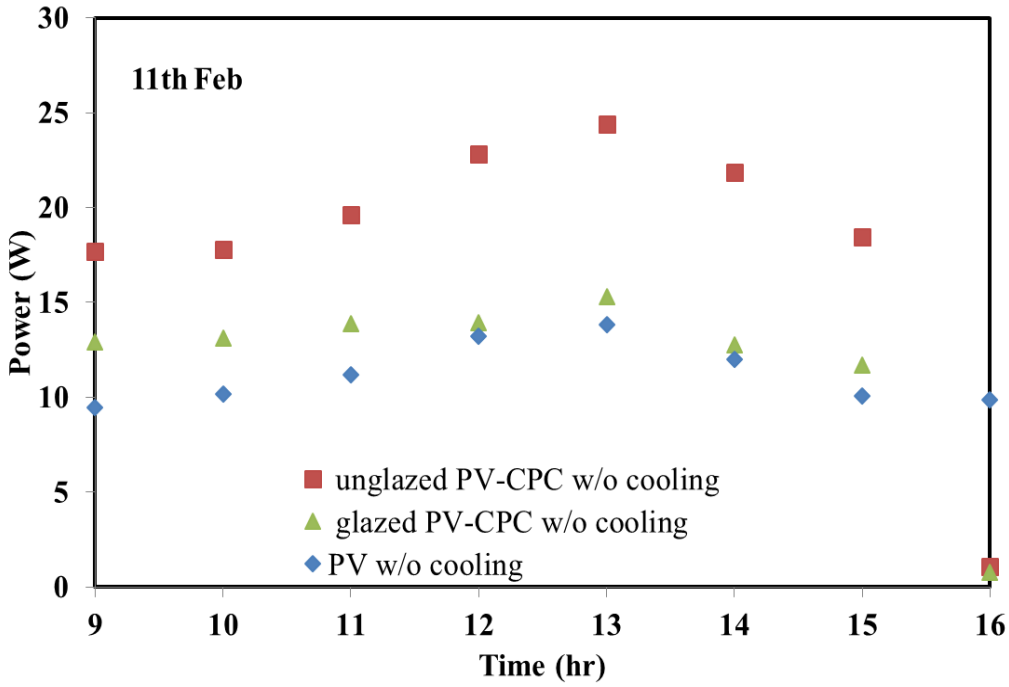
11th Feb
Power (W)
Time (hr)
unglazed PV-CPC w/o cooling
glazed PV-CPC w/o cooling
PV w/o cooling
0
5
10
15
20
25
30
9
10
11
12
13
14
15
16

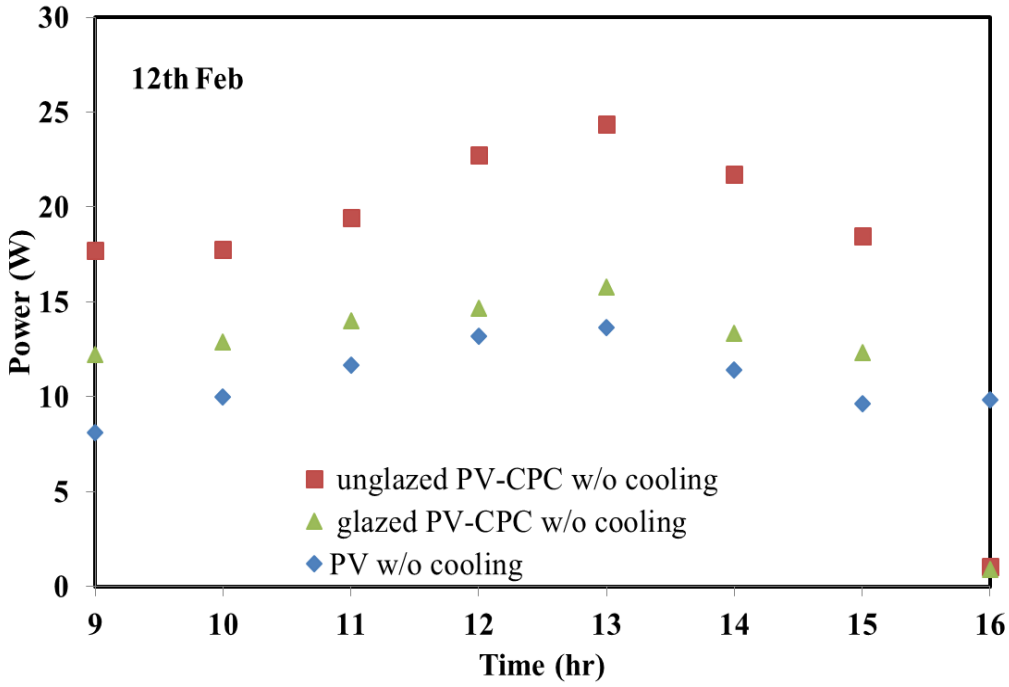
12th Feb
Power (W)
Time (hr)
unglazed PV-CPC w/o cooling
glazed PV-CPC w/o cooling
PV w/o cooling
0
5
10
15
20
25
30
9
10
11
12
13
14
15
16

Fig. 5.21 (d)

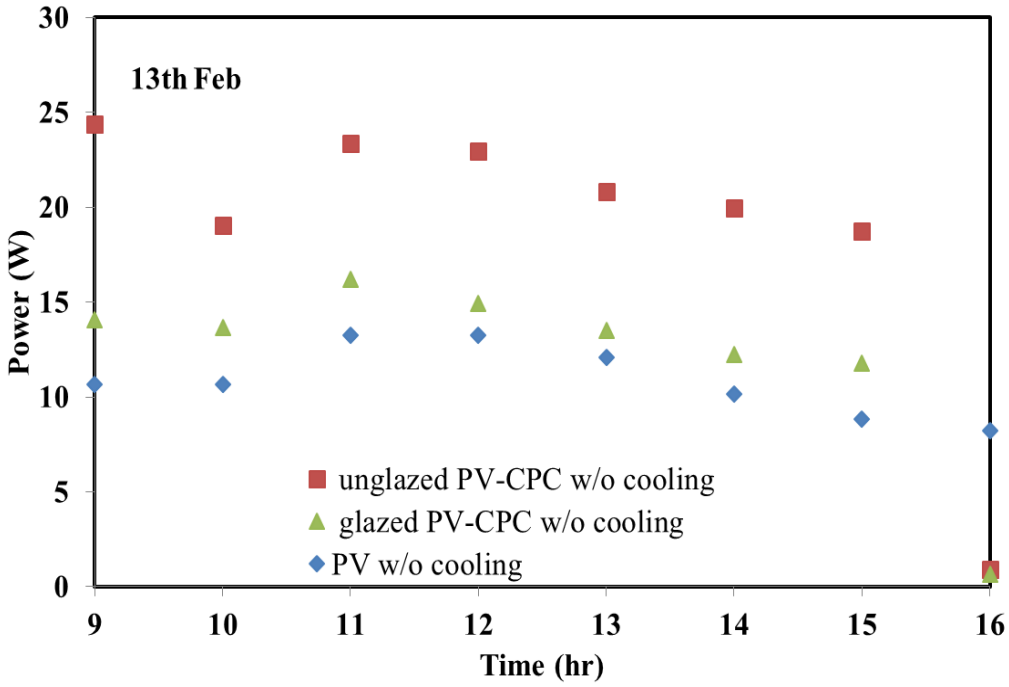

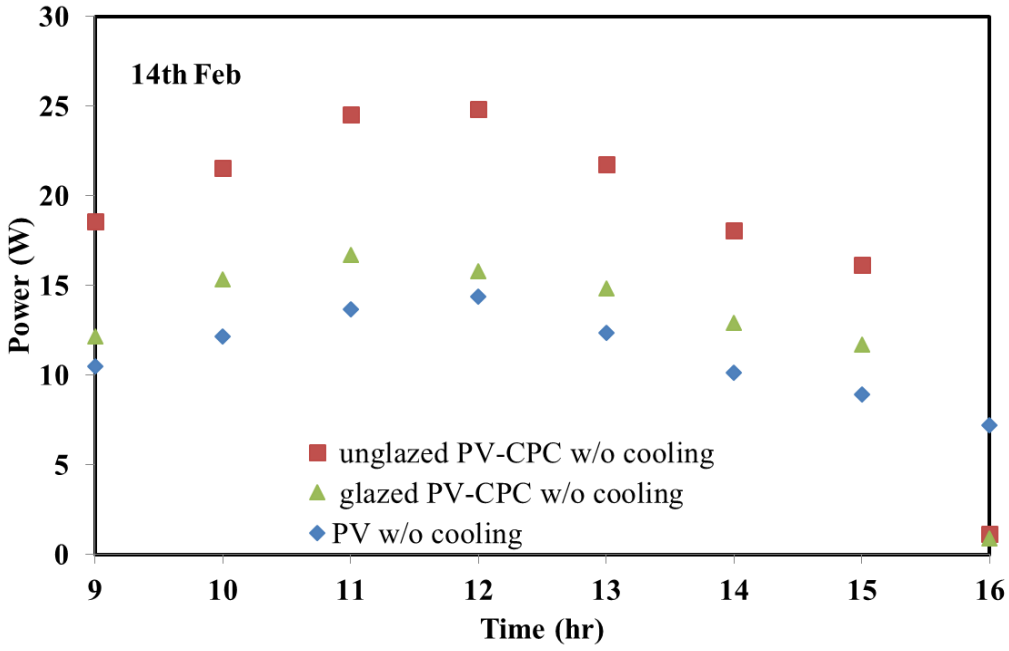

Figure 5.21 Variation of power over time for uncooled flat PV, unglazed PV-CPC and glazed PV-CPC on different test days

Figure 5.22 shows the results when active cooling is incorporated in all the three configurations. There is a substantial increase in the maximum value of the power output once active cooling is incorporated along with the existing system. The mass flow rate for the cooling water was kept at 1 LPM (litre per min). After applying active cooling the maximum power output from the unglazed PV-CPC system reached 36.75 W. This result indicates that there is an addition of 73.1% in the value of maximum power output delivered from the unglazed PV-CPC system after applying cooling. When cooling is integrated, unglazed PV-CPC produces 195% more power than simple uncooled flat PV panel and 65.1% more power than simple cooled flat PV panel. In the case of glazed PV-CPC system the amount of power increase is 16.85 W, which shows that there is 147% increase in power as compared to uncooled simple flat PV panel.

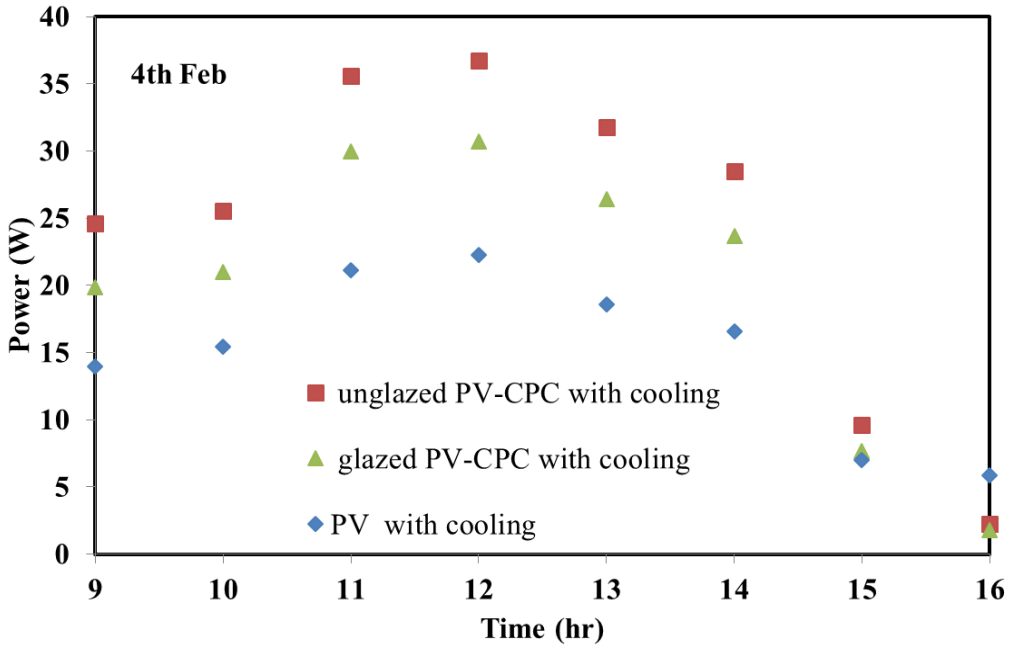
4th Feb
Power (W)
Time (hr)
unglazed PV-CPC with cooling
glazed PV-CPC with cooling
PV with cooling
0
5
10
15
20
25
30
35
40
9
10
11
12
13
14
15
16

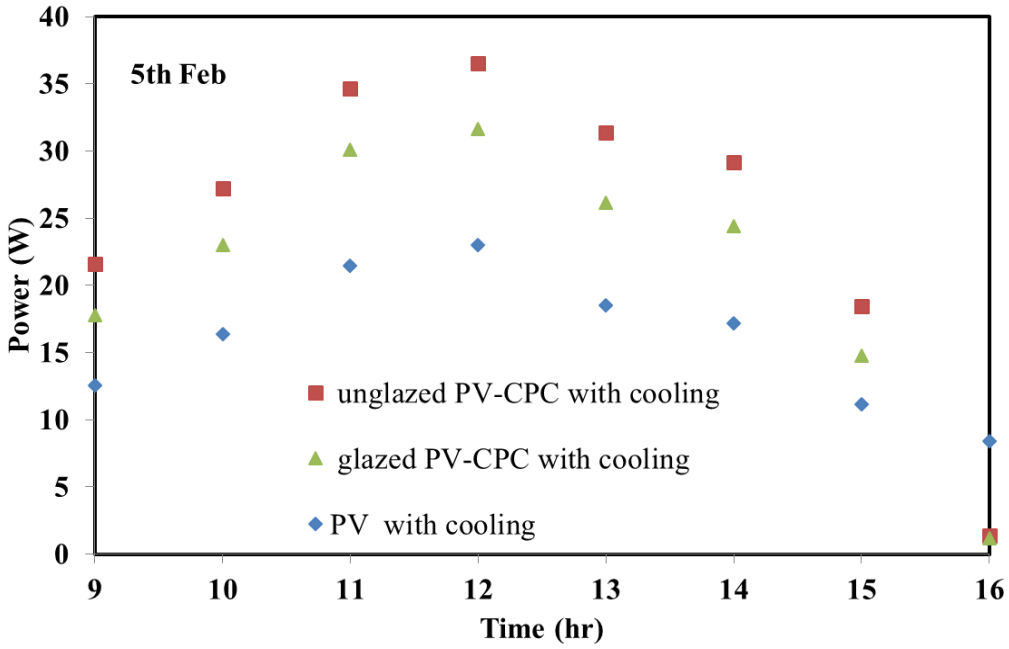
5th Feb
Power (W)
Time (hr)
unglazed PV-CPC with cooling
glazed PV-CPC with cooling
PV with cooling
0
5
10
15
20
25
30
35
40
9
10
11
12
13
14
15
16

Fig. 5.22(a)

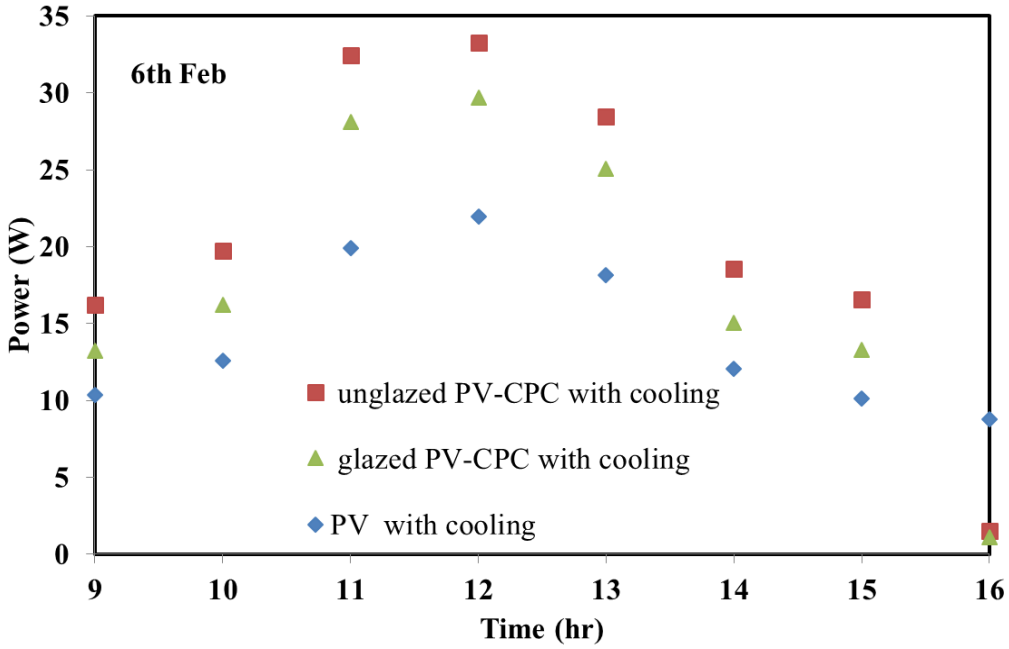
6th Feb
Power (W)
Time (hr)
unglazed PV-CPC with cooling
glazed PV-CPC with cooling
PV with cooling
0
5
10
15
20
25
30
35
9
10
11
12
13
14
15
16

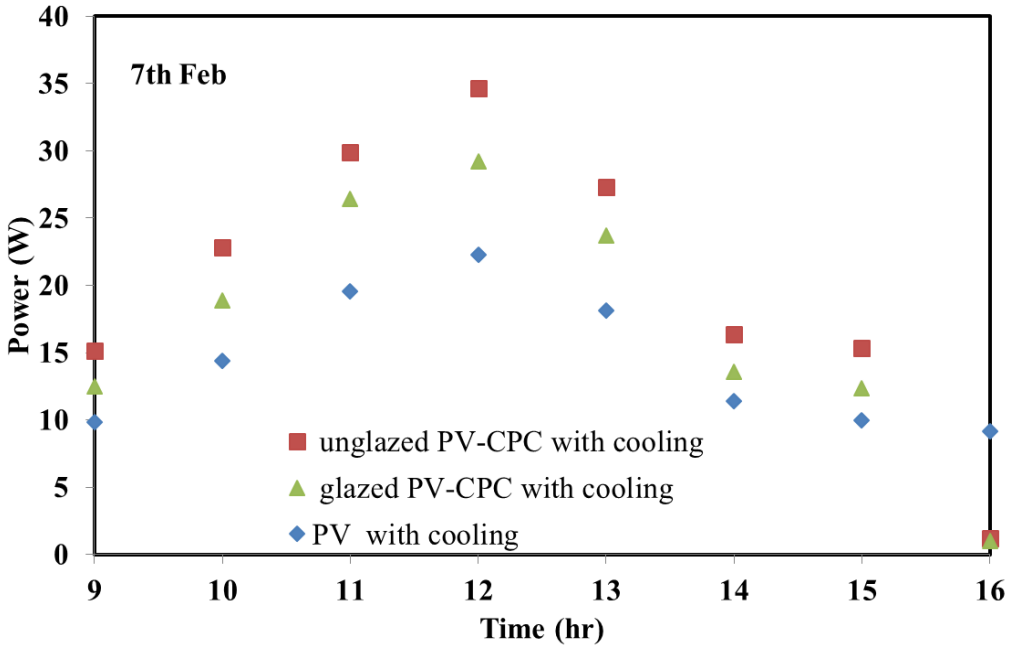
7th Feb
Power (W)
Time (hr)
unglazed PV-CPC with cooling
glazed PV-CPC with cooling
PV with cooling
0
5
10
15
20
25
30
35
40
9
10
11
12
13
14
15
16

Fig. 5.22(b)

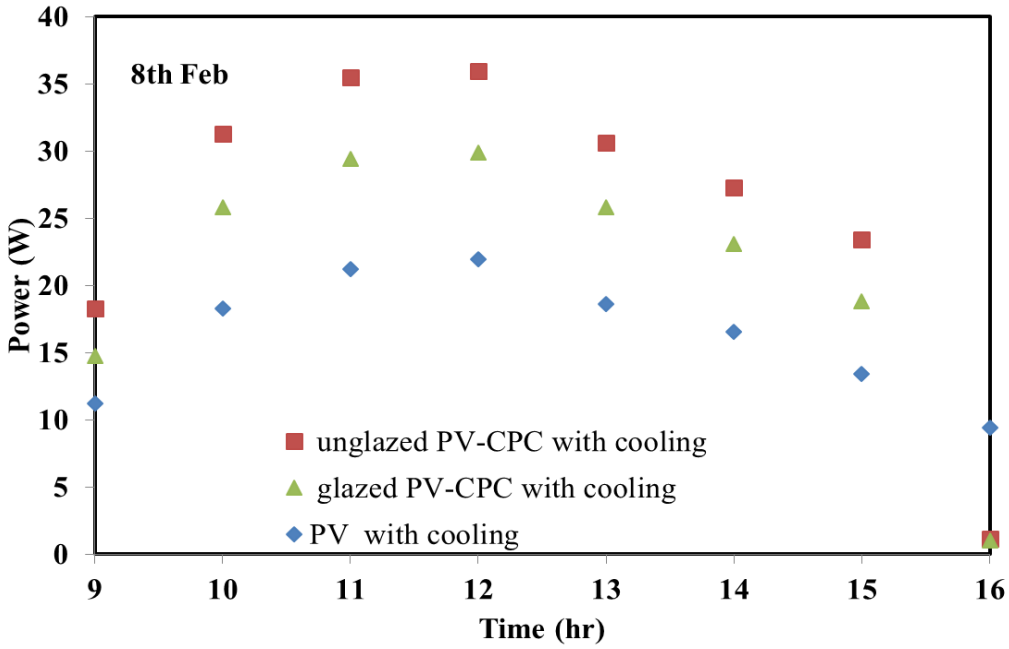
8th Feb
Power (W)
Time (hr)
unglazed PV-CPC with cooling
glazed PV-CPC with cooling
PV with cooling
0
5
10
15
20
25
30
35
40
9
10
11
12
13
14
15
16

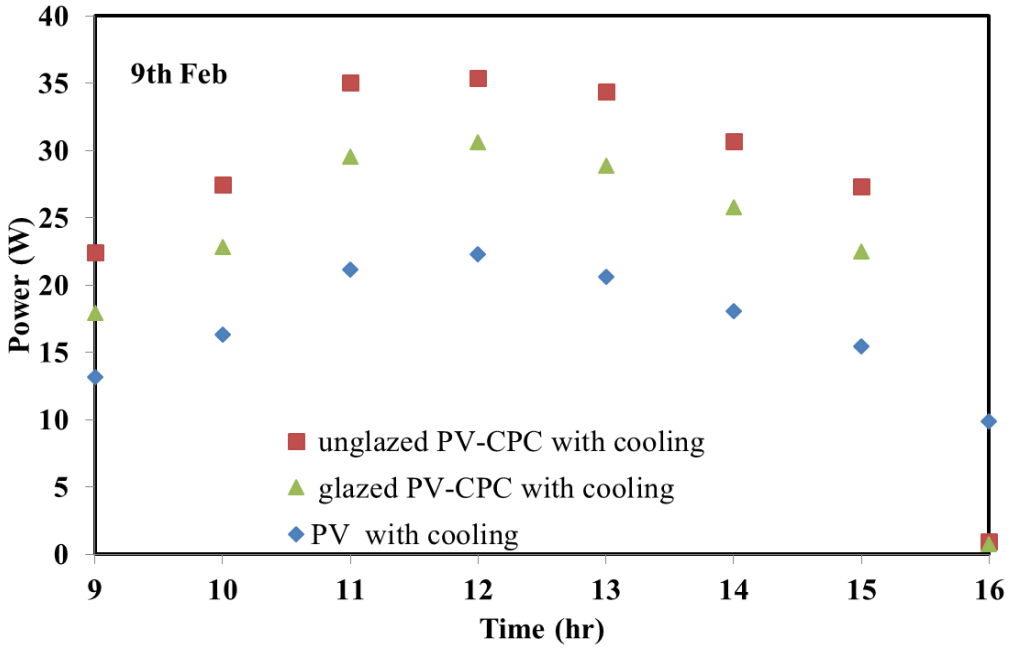
9th Feb
Power (W)
Time (hr)
unglazed PV-CPC with cooling
glazed PV-CPC with cooling
PV with cooling
0
5
10
15
20
25
30
35
40
9
10
11
12
13
14
15
16

Fig. 5.22(c)

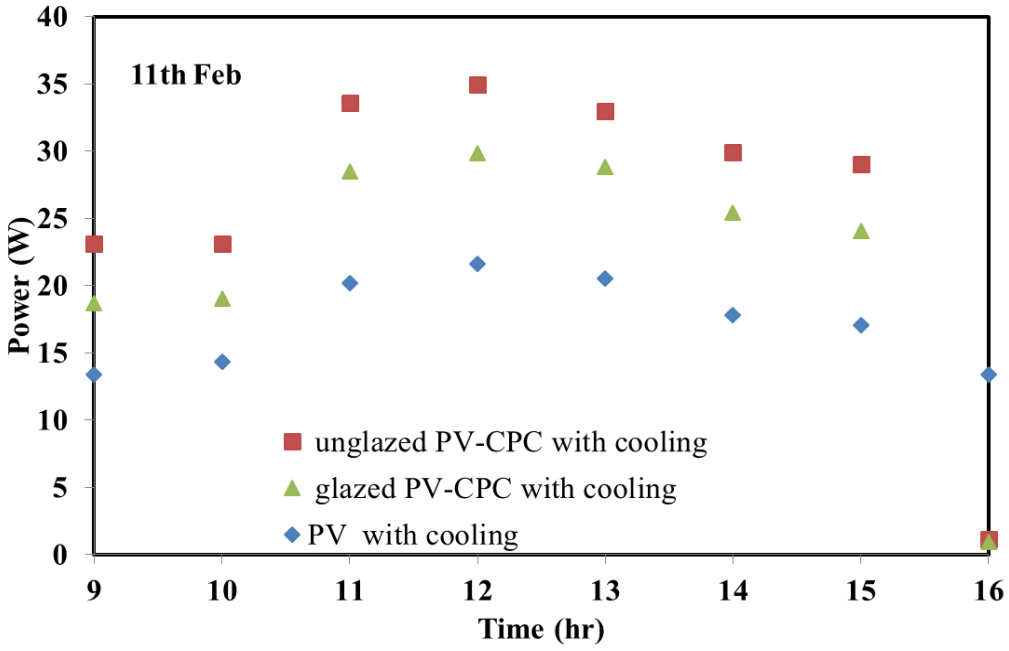
11th Feb
Power (W)
Time (hr)
unglazed PV-CPC with cooling
glazed PV-CPC with cooling
PV with cooling
0
5
10
15
20
25
30
35
40
9
10
11
12
13
14
15
16

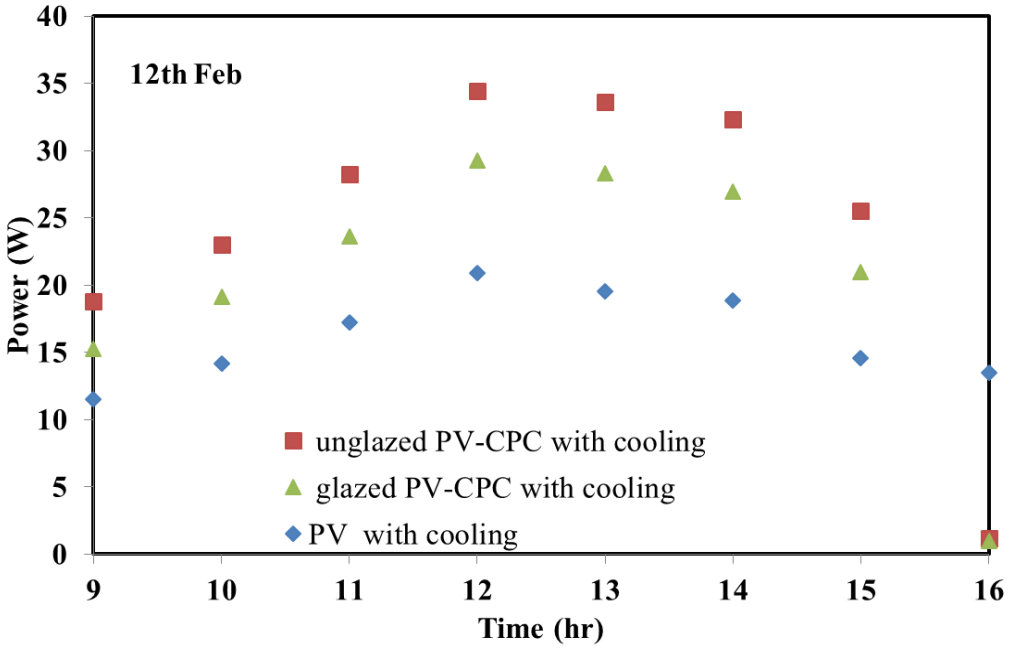
12th Feb
Power (W)
Time (hr)
unglazed PV-CPC with cooling
glazed PV-CPC with cooling
PV with cooling
0
5
10
15
20
25
30
35
40
9
10
11
12
13
14
15
16

Fig. 5.22(d)

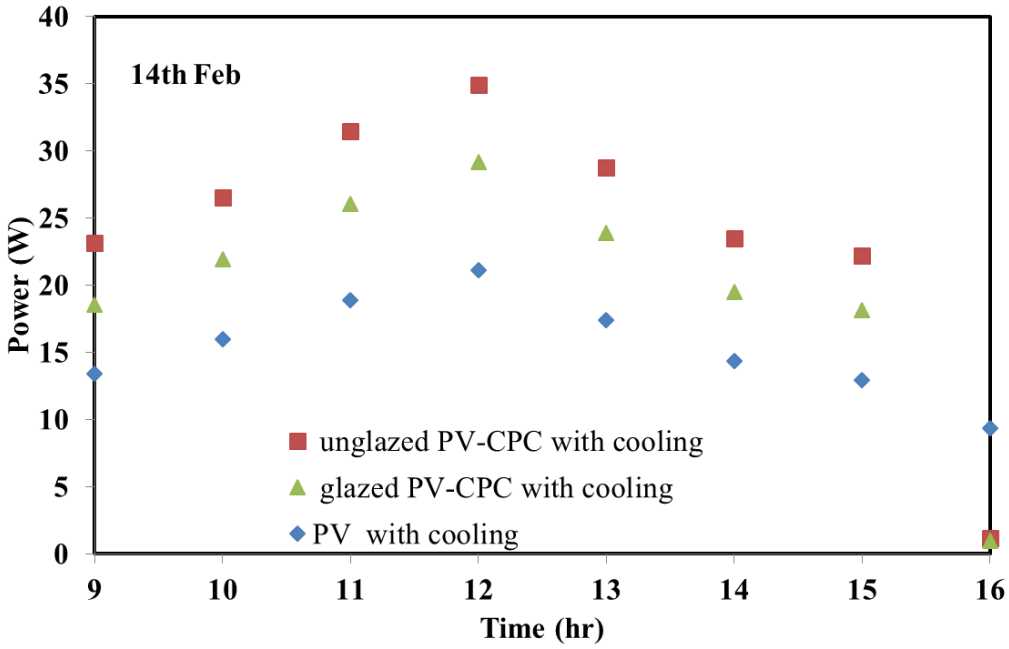

Figure 5.22 Variation of power over time for flat PV, unglazed PV-CPC and glazed PV-CPC with cooling

5.1.5 Comparison of Experimental and Numerical Results for PV-CPC system

In this section the validity of the numerical modeling technique is verified by the experimental results. The numerical results obtained are validated with the experimental data from the tests conducted at KFUPM in the month of Feb. 2013. In order to investigate how well the predicted power output obtained by the analytical model fits the experimental measured power, the two cases are compared. Further, in order to compare the computed results with the experimental measurements, root mean square per cent deviation (e) has been evaluated by the equation presented in chapter 4.

The results reported here are recorded in the month of Feb, 2014 which were consistently clear days. Figure 5.23 shows the diurnal variation of solar radiation intensity throughout the day from 9:00 to 16:00 for Dhahran. The effective radiation reaching the module is the function of intensity of direct and diffuse short wave radiation inputs, and the absorptivity of the cell. The intensity of solar radiation also depends on the time of the day, season and latitude of the location. The maximum values of solar radiation intensity and ambient temperature can be noted along noon since the sun's rays have smallest angle of incidence to the earth's surface are spread over the smallest area. They also have to pass through the least amount of atmosphere, so there is less reflection. Variation of wind speed and ambient temperature for the test day is shown in Figure 5.24.

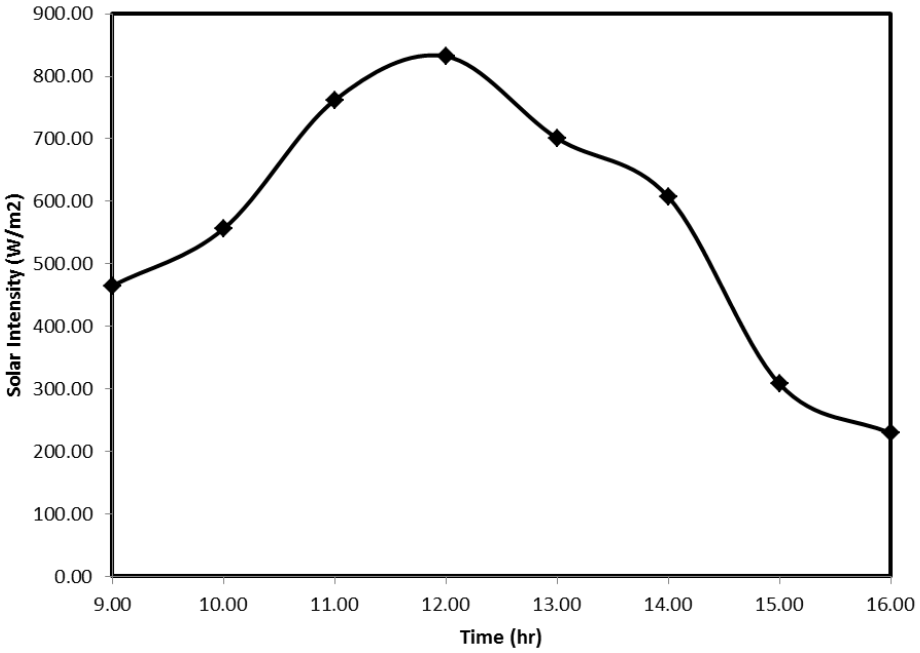

Figure 5.23 Hourly variation of solar intensity

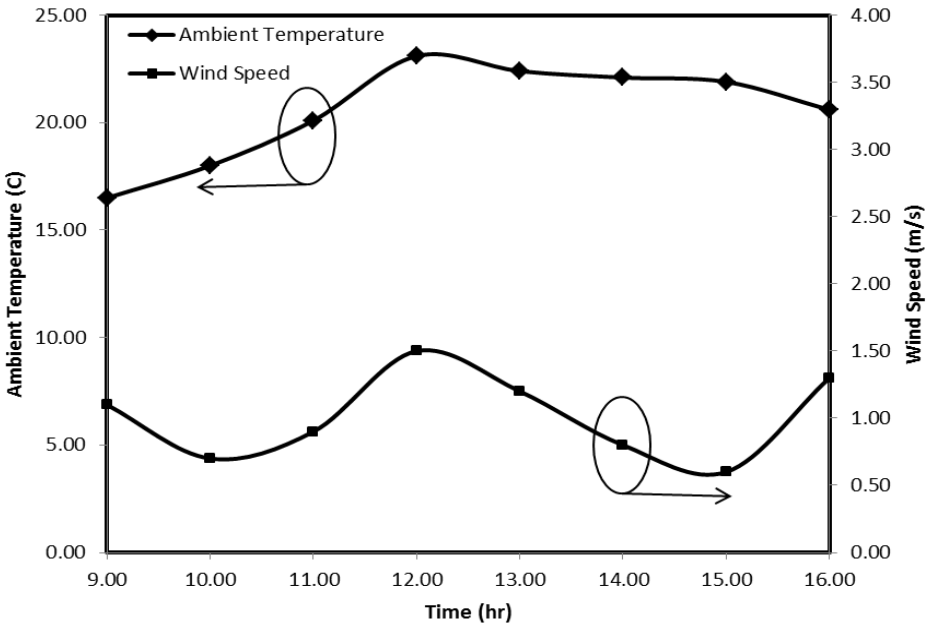

Figure 5.24 Ambient temperature and wind speed on test day

Figure 5.25 to Figure 5.27 show the comparison of numerical and experimental results of maximum power for simple PV strings, unglazed PV-CPC and glazed PV-CPC system. The range of root mean square percent deviation (e) for the experimental and numerical values lie between 3.04-6.64 %. The numerical model predicts reasonable results in order to perform the performance analysis of PV-CPC and simple flat PV system. Numerical modeling is very effective tool in order to predict the performance of the system under different operating conditions. This enables us to make the decision about the selection of proper system suitable for the current location.

Numerical modeling of PV-CPC system involves the estimation of amount of energy absorbed by using compound parabolic collectors. The model used in the current case assumes constant flux distribution from the CPC reflectors onto the panels. In actual case the flux distribution profile for the CPC is not constant as in the case of V-trough PV system which utilizes the simple planar mirrors for concentration.

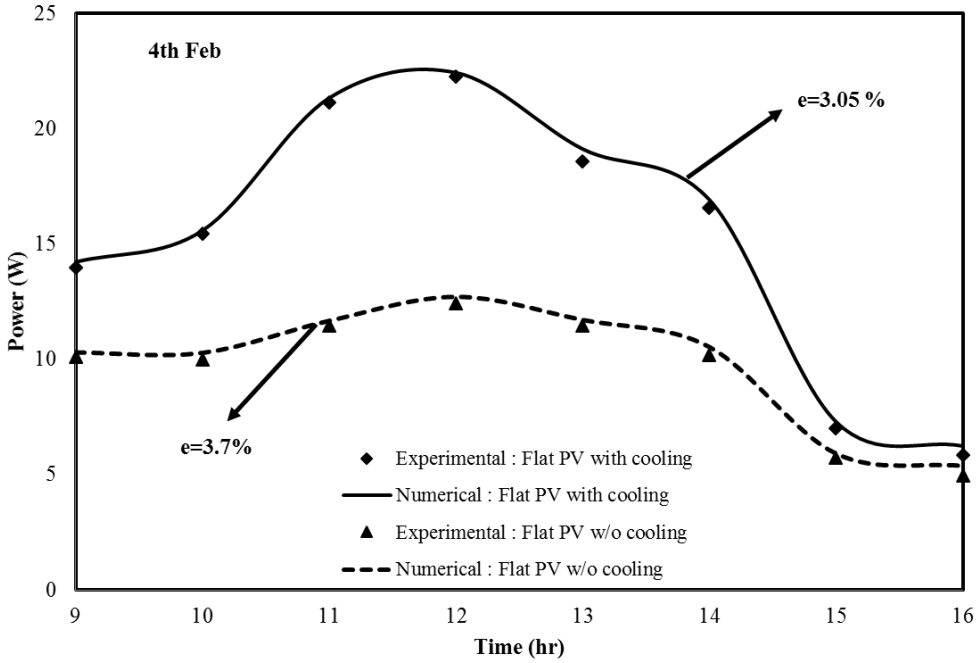

Figure 5.25: Comparison of experimental and numerical results for flat PV system with and without cooling

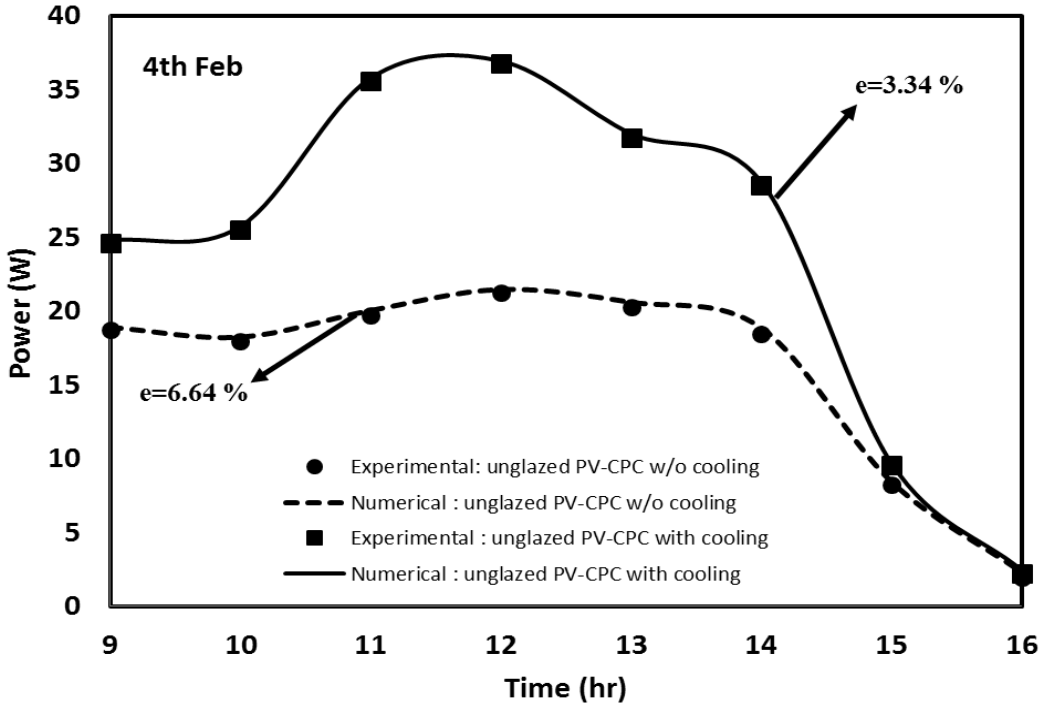

Figure 5.26 Comparison of experimental and numerical results for unglazed PV-CPC system with and without cooling

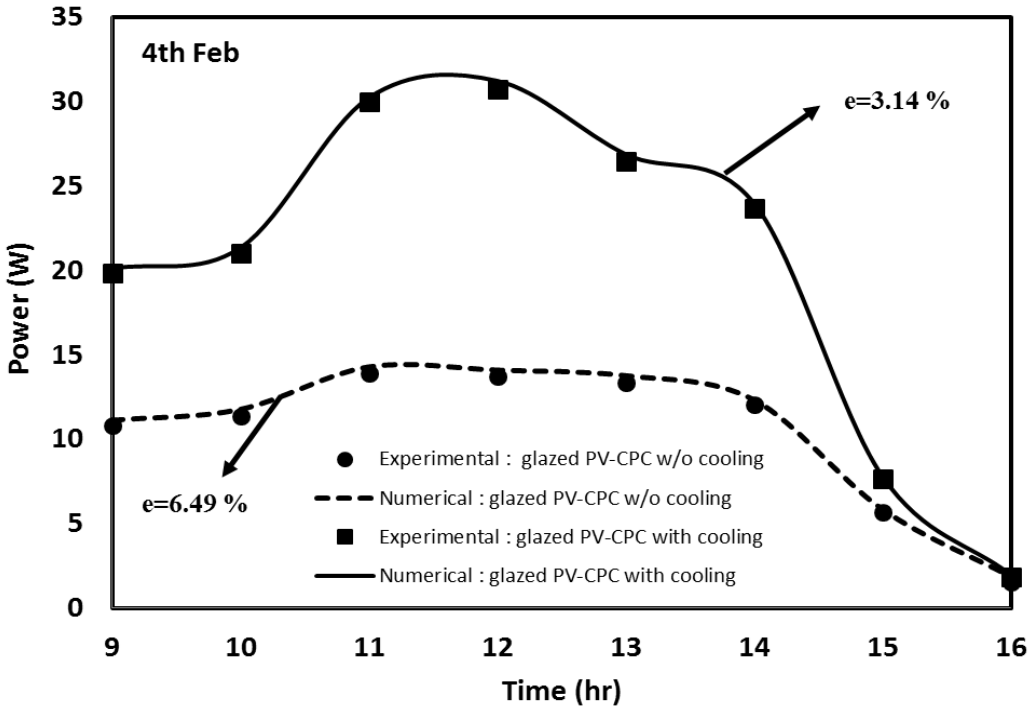

Figure 5.27 Comparison of experimental and numerical results for glazed PV-CPC system with and without cooling

5.2 V-TROUGH PV SYSTEM

5.2.1 Optical Modeling

As discussed earlier, the solar flux need to be enhanced on the given cell area for improving the performance of PV system and reducing the cost of electric power produced per unit area. In this section a different low concentration photovoltaic configuration known as V-trough is used. In this case there are two planar reflectors attached with the PV panel that make a V-trough shape.

V-trough performance analysis was made for the location of Dhahran with latitude of 26.5°. The slope of the collector was kept at 45°. Incident solar radiation over a geographic location varies with different months in a year. Figure 5.28 shows the solar irradiance absorbed in V-trough PV system and simple PV panel. Simulations were carried out for the ambient conditions of representative days of March and September. In March the maximum amount of absorbed radiation absorbed by flat PV string is about 963 W/m^2. When V-trough is integrated with it, the amount of absorbed radiation increases up to 1416 W/m^2.This shows that absorbed radiation is increased up to 47.04%. Similarly on 16th September the amount of enhancement in the absorbed radiation by the help of planar reflectors is 53%. The amount of solar energy absorbed is needed to calculate the thermal and electrical performance of the PV system, as part of the absorbed energy is used to generate electric current and the rest of it increases the temperature of the cell. This amount of absorbed energy is then given as the input parameter to the thermal and electrical model.

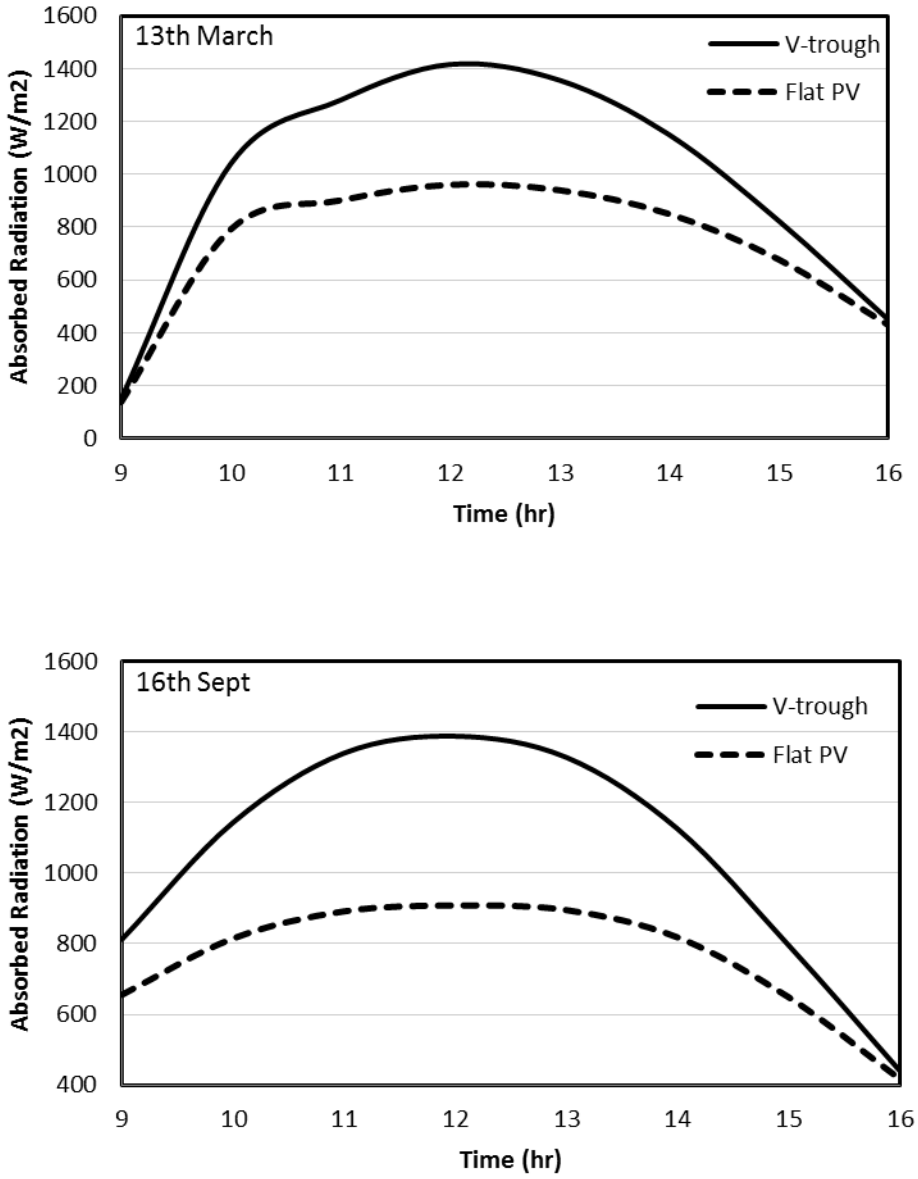

Figure 5.28: Comparison of absorbed radiation for V-trough PV system and simple PV panel

5.2.2 Thermal Modeling

Photovoltaic cells are able to utilize the part of the absorbed solar radiation and generate electric power, while the rest of the absorbed radiation increases the temperature of the cells. The operating temperature of the module depends on the equilibrium maintained between the heat generated by the module and the heat lost to surrounding environment. By applying the energy balance equations the thermal network of the PV system is solved and the module temperature is estimated. Figure 5.29 shows the maximum cell temperatures for V-trough PV system and simple PV panel under operating conditions. Maximum Cell temperature for V-trough PV system is 47.1°C on the day of March, whereas for simple PV panel the temperature remains under the range of 40.3°C. Increase in cell temperature for V-trough PV system is due to increased amount of absorbed radiation compared to simple PV panels. This unwanted heat lowers the electrical efficiency of the system.

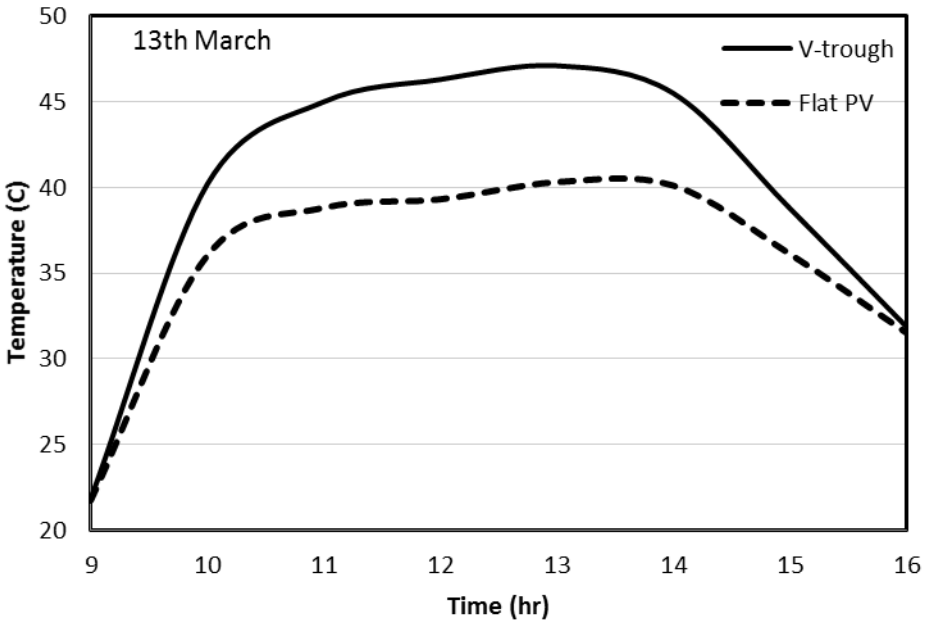

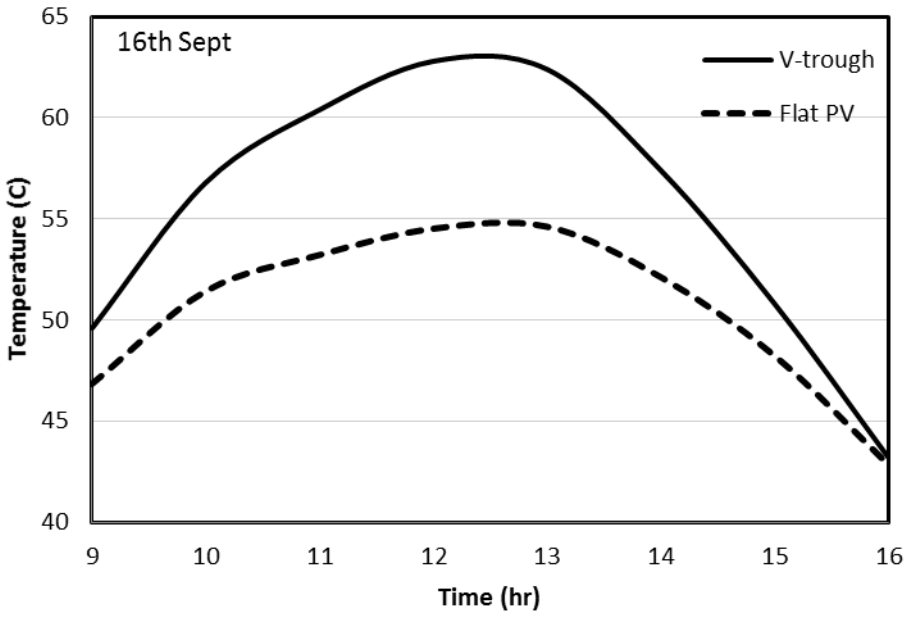

Figure 5.29: Cell temperature without cooling

In order to lower the operating range of cell temperatures and increase the electrical efficiency of the PV system, active cooling is incorporated in the system. Results show that by circulating water at the mass flow rate of 1 LPM, the module temperature is effectively reduced. Figure 5.30 shows the values of operating cell temperatures after the integration of cooling system with the simple PV panel and V-trough PV system. The maximum value of cell temperature in the case of V-trough PV system reduces to 39.2°C which is 16.8% less than compared to V-trough PV system without cooling. Similarly, for flat PV panel the operating temperature of the panel remains at the maximum value of 33.4°C which is also 16.9% reduced as compared to uncooled panel. In September when the ambient temperature is on the higher side, the maximum value of the module temperature increases to 62.8°C, which is lowered by 14.5% to the value of 53.7°C by applying active cooling. Therefore in order to utilize the maximum benefit from the available concentrated panel, cooling is necessary.

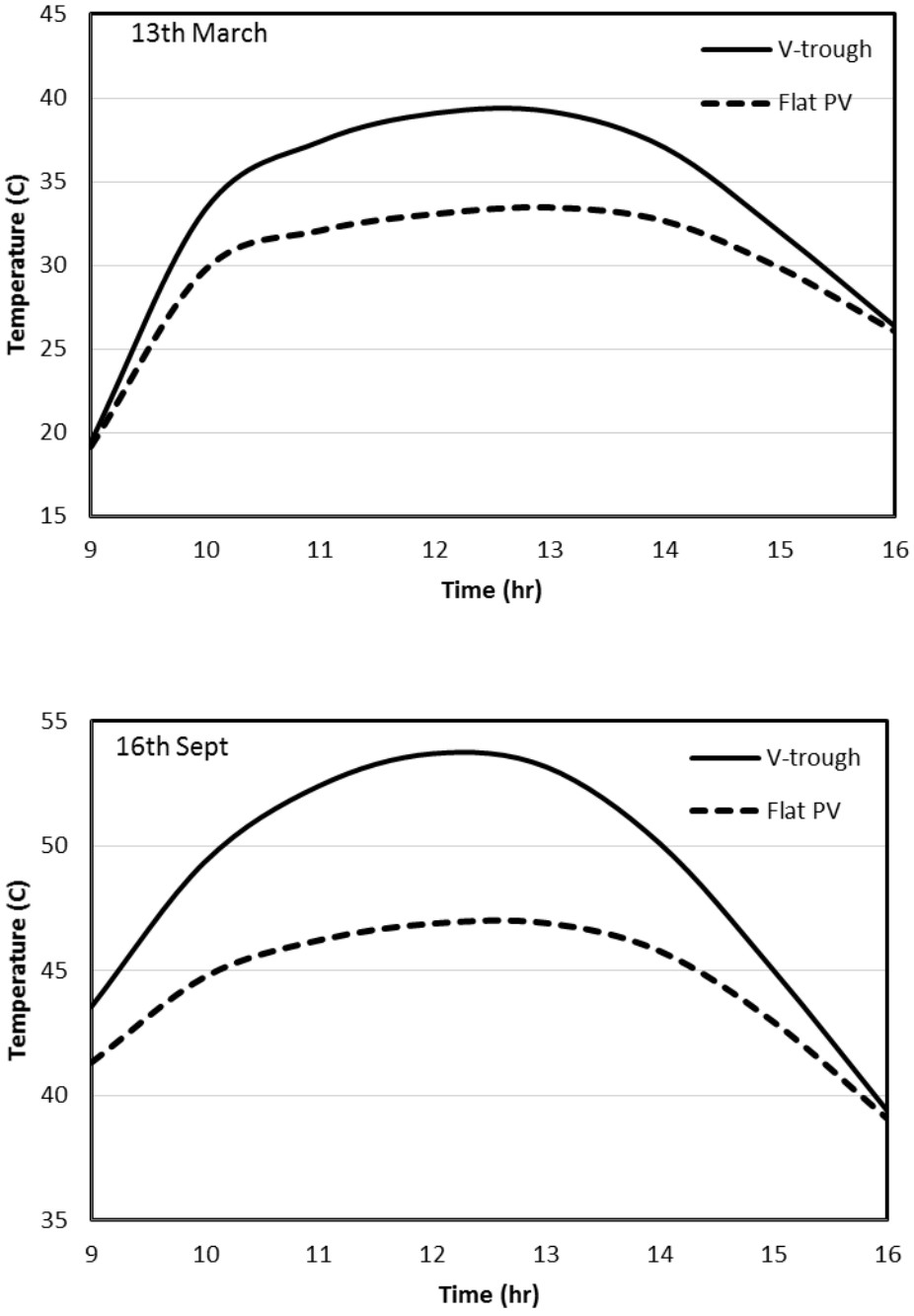

Figure 5.30: Cell temperature with cooling

5.2.3 Electrical Modeling

In order to analyze the electrical performance of the photovoltaic cells, five parameter model is used in the current study as discussed in chapter 3. The estimation of five reference parameters is carried out by solving highly non-linear equations in EES software. After the estimation of five parameters the electrical performance of the PV system can be analyzed by giving absorbed radiation and cell temperature as the input parameters. The solar panel used for present case is SunPower 230W monocrystalline. The reference parameters are estimated by the data given in the data sheet provided by the manufacturer. The electrical performance of the V-trough PV system and simple PV panel is shown in Figure 5.31. Variation of electric power output for both the cases is predicted for different ambient conditions. The maximum power output from the flat PV panel on 13th March reaches 168.9W and when the V-trough reflectors are integrated along with the same panel the maximum power output increases up to 227.3W. By utilizing the two planar reflectors the power output is enhanced by 34.6%. Similarly on 16th September the power output from the flat PV is 142.7 W and with V-trough PV system the maximum power output reaches up to 195.6 W. On 16th September, the power is increased by 37% with the integration of V-trough to simple PV panel.

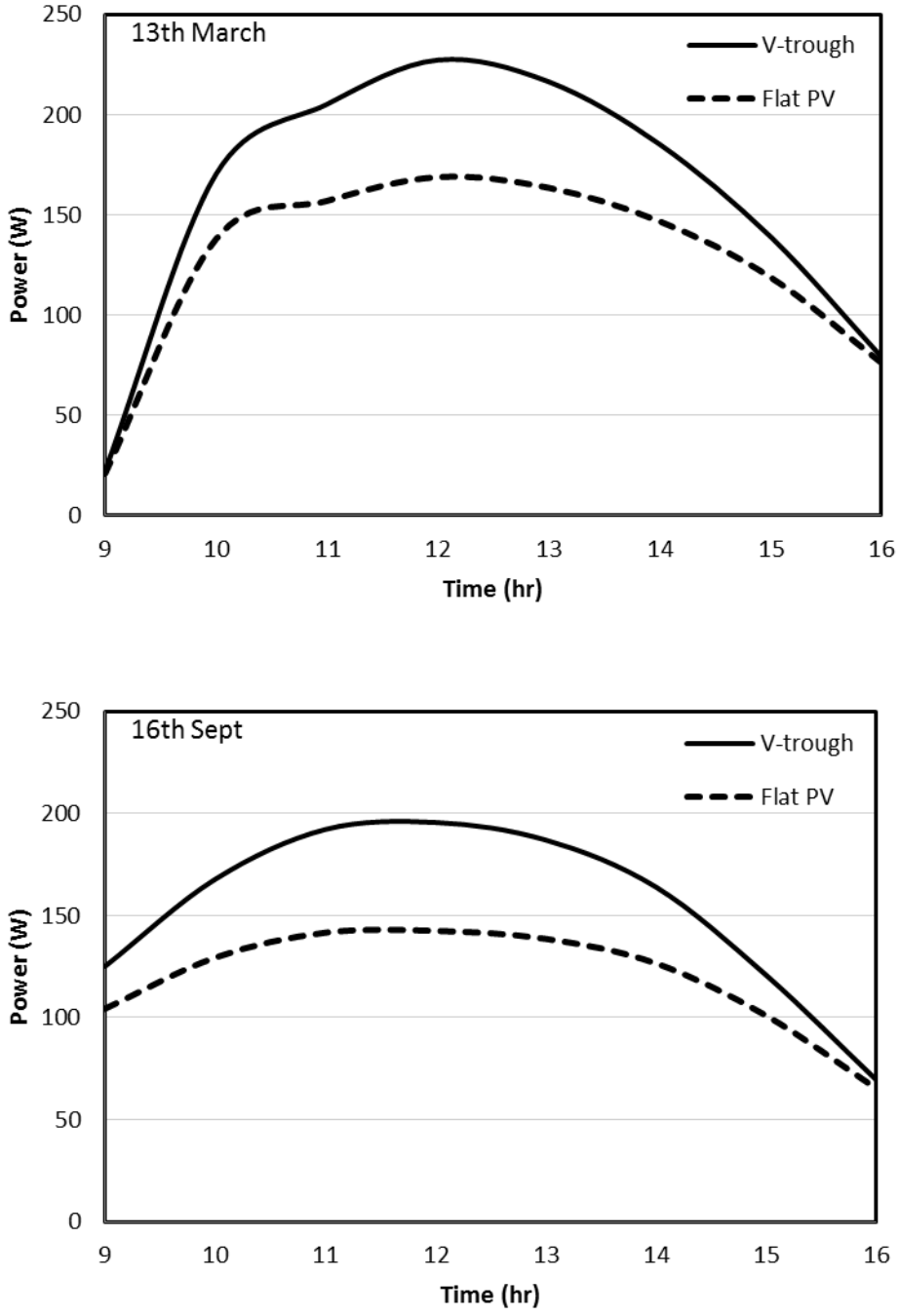

Figure 5.31: Maximum power output (uncooled)

When the solar intensity is enhanced by the reflectors, the module of the temperature rises up as discussed earlier. This increase in the cell temperature causes certain reduction in the electrical performance of the system. In order to estimate the effect of cell temperature on the electrical performance, active cooling is applied as discussed earlier. There is a significant increase in the maximum value of the power output once active cooling is incorporated along with the existing system as shown in Figure 5.32. After applying active cooling, the maximum power output for the simple PV panel reached 207.4W for the ambient conditions on the day of March. This shows that there is increase of 22.8% in the value of maximum power output delivered from the flat PV system. In the case of V-trough PV system, there is an increase of 71.6 W which results in the percentage increase of 31.5%. Amount of power increase in each case by applying cooling is shown in Figure 5.33 and Figure 5.34. As shown in these figures there is a significant amount of increase in the power output by applying cooling in these configurations.

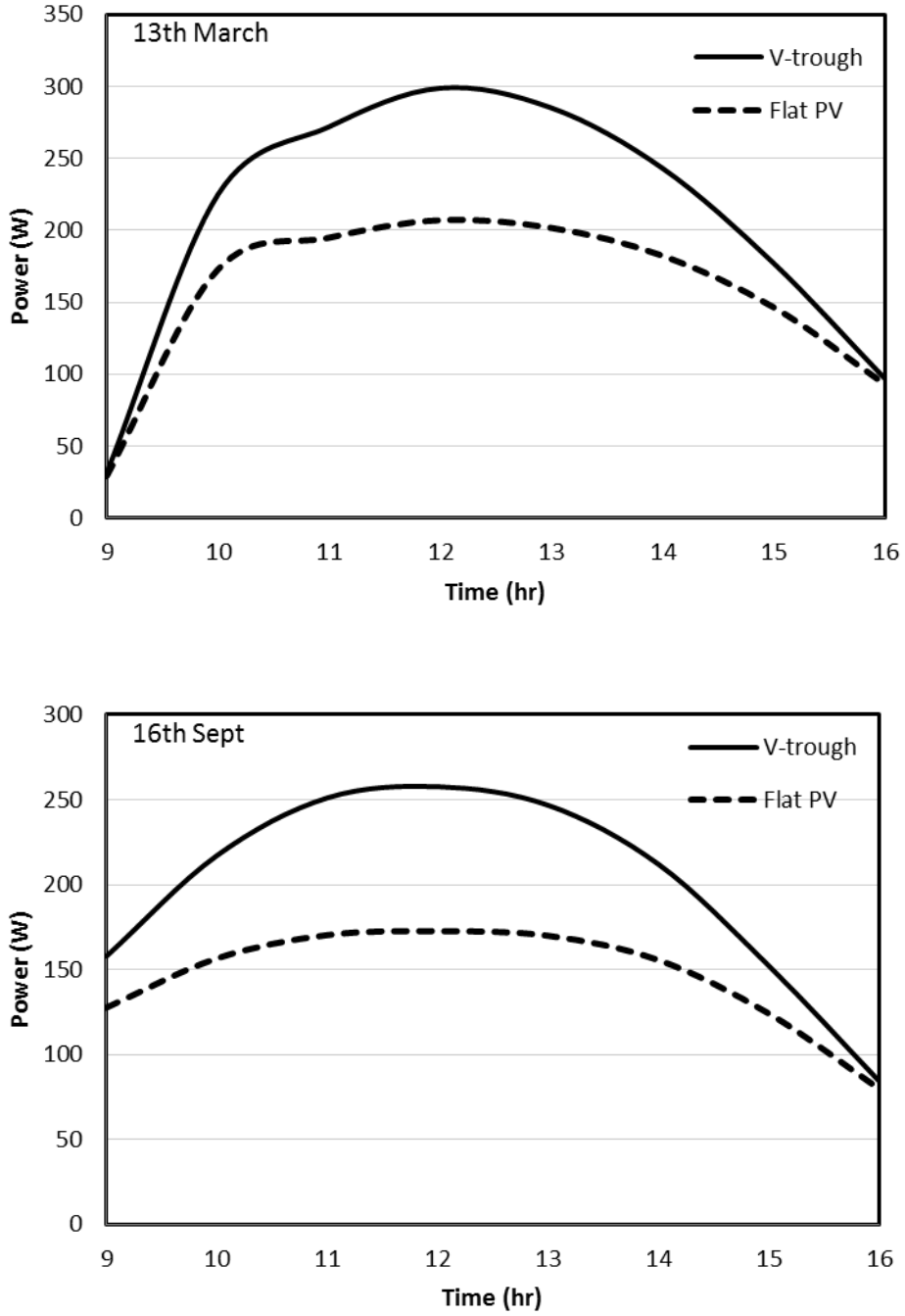

Figure 5.32: Maximum power output (cooled)

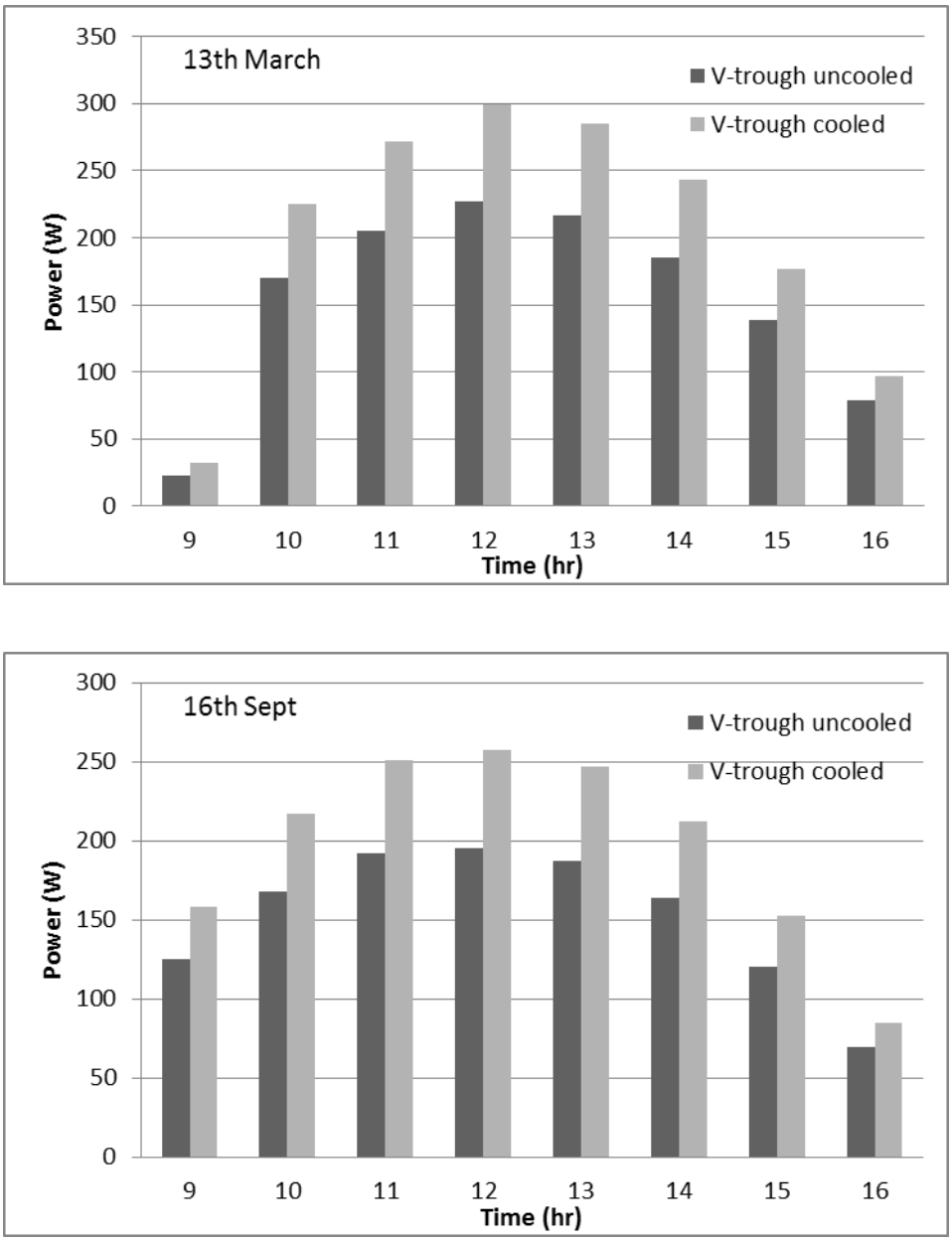

Figure 5.33: Comparison of power output for V-trough PV system with and without cooling

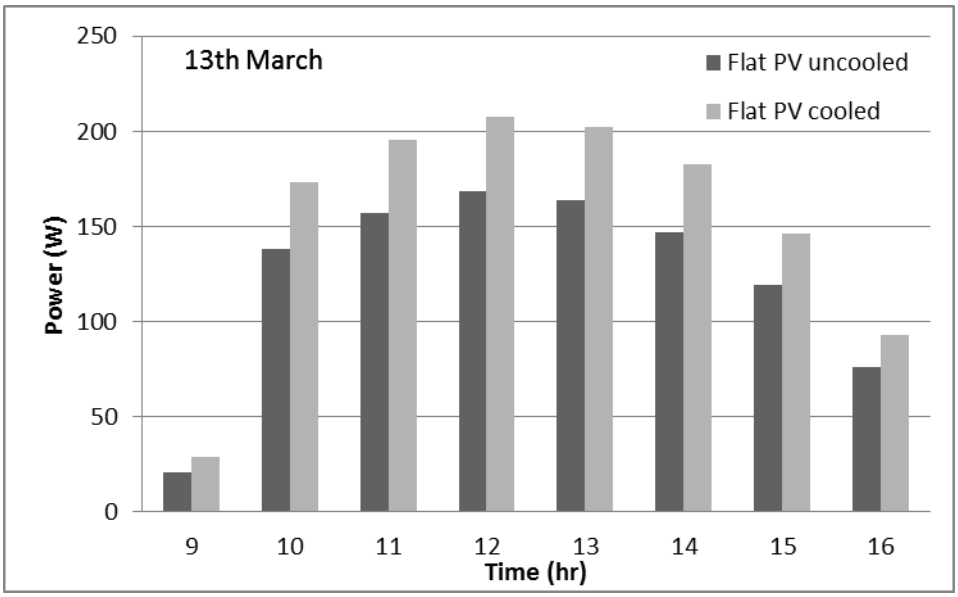

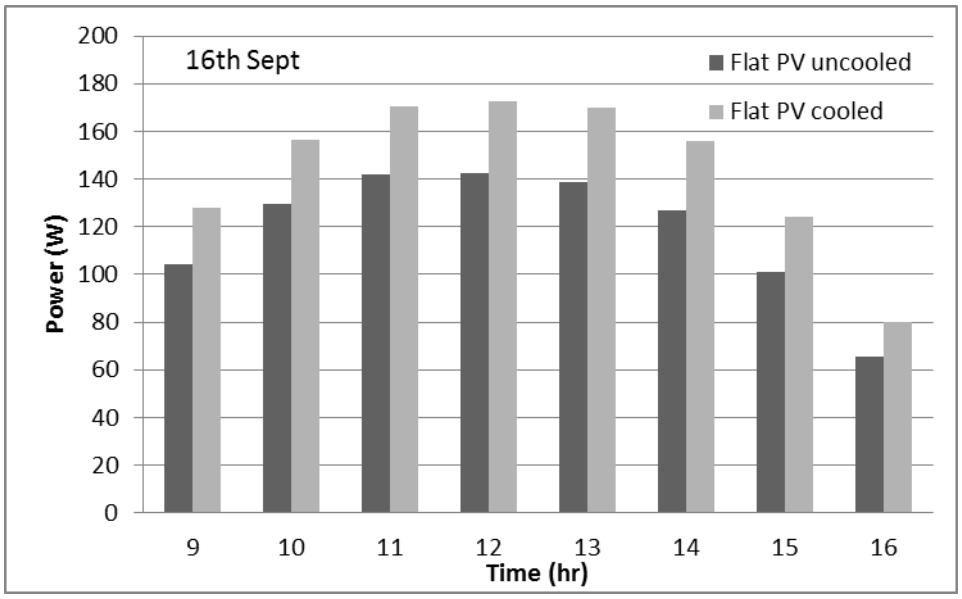

Figure 5.34: Comparison of power output for flat PV system with and without cooling

The I-V and P-I curves of the V-trough PV system and flat PV system are described in Figure 5.35. The monocrystalline panel has a good I-V characteristics curve for both configurations with and without concentrators. This indicates that the panel has good output characteristics even in low concentration. As shown in the Figure 5.35, it can be

seen that maximum output power of the actively cooled module changes sharply under concentration and non-concentration conditions. The maximum power increases from 207.4(non-concentration) to 298.8 W (concentration) with a percentage increase of 44%.

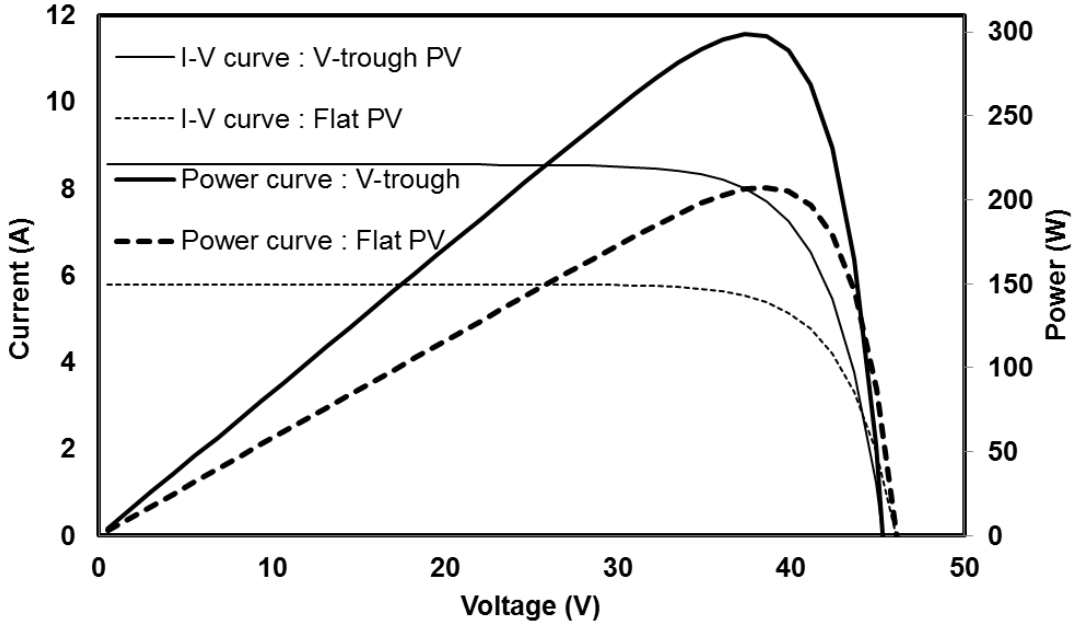

Figure 5.35: *I-V* and *P-V* curves for flat PV and V-trough PV system (cooled)

5.2.4 Experimental Results of V-trough PV system

In this section the results obtained by the experimentation performed on V-trough PV experimental setup. Experimentation was carried out for different days in March and June 2012. Effect of mass flow rate on fluid outlet temperature, top surface temperature and maximum power was studied. Mass flow rate was varied from 0.6-1 LPM. Results obtained from 0.6 LPM showed that with this flow rate the maximum value of outlet fluid temperature was obtained. Figure 5.36 shows the front panel temperature for three different flow rates. It can be seen that the front surface temperature is maximum in the case of 0.6 LPM. As the flow rate is increased the outlet fluid temperature decreases as the time for the fluid to extract more heat is reduced. As shown in Figure 5.37, the maximum outlet fluid temperature is observed at the mass flow rate of 0.6 LPM, whereas the minimum outlet temperature is observed at maximum flow rate, which in the present case is 1 LPM.

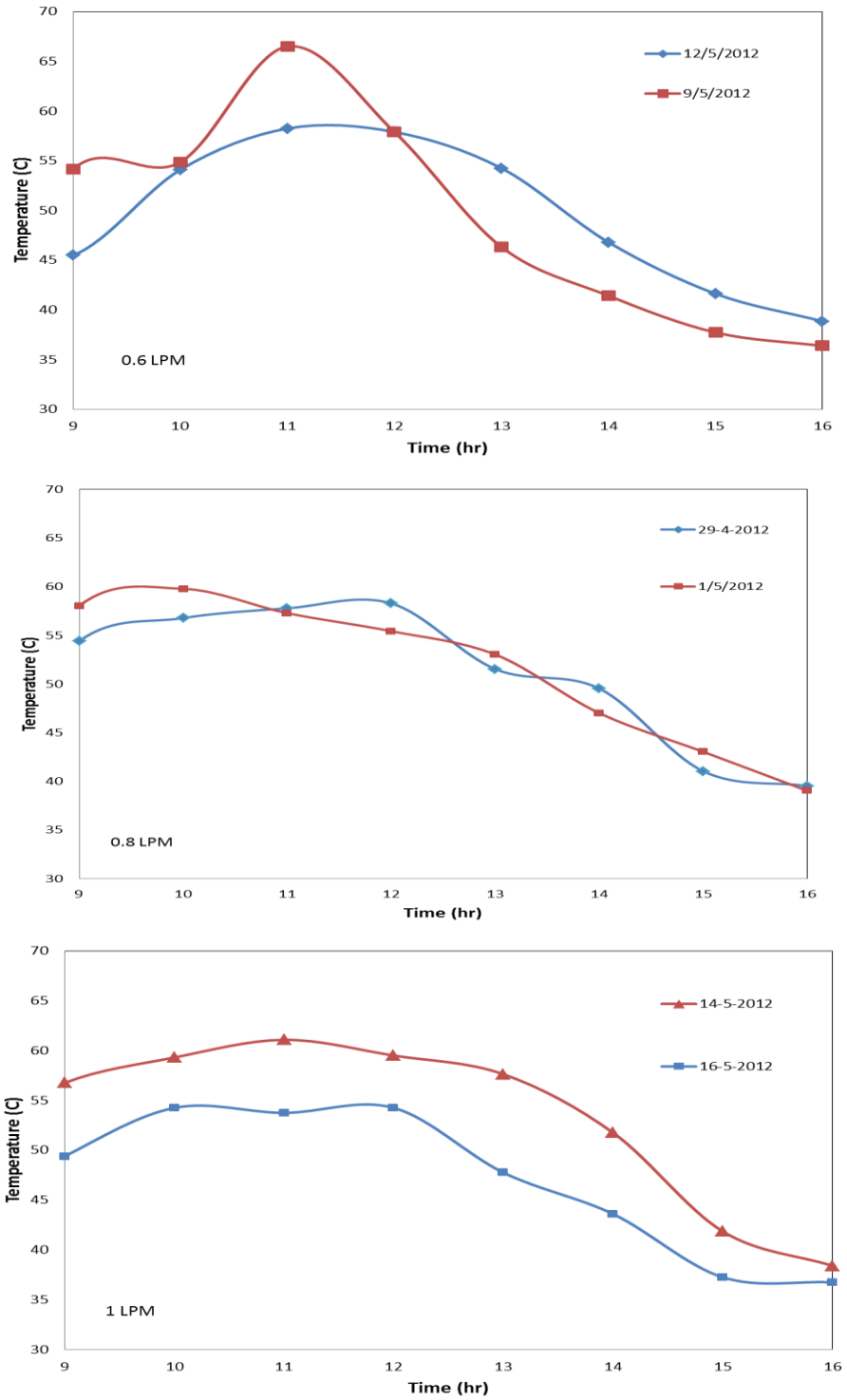

Figure 5.36: Front panel temperature

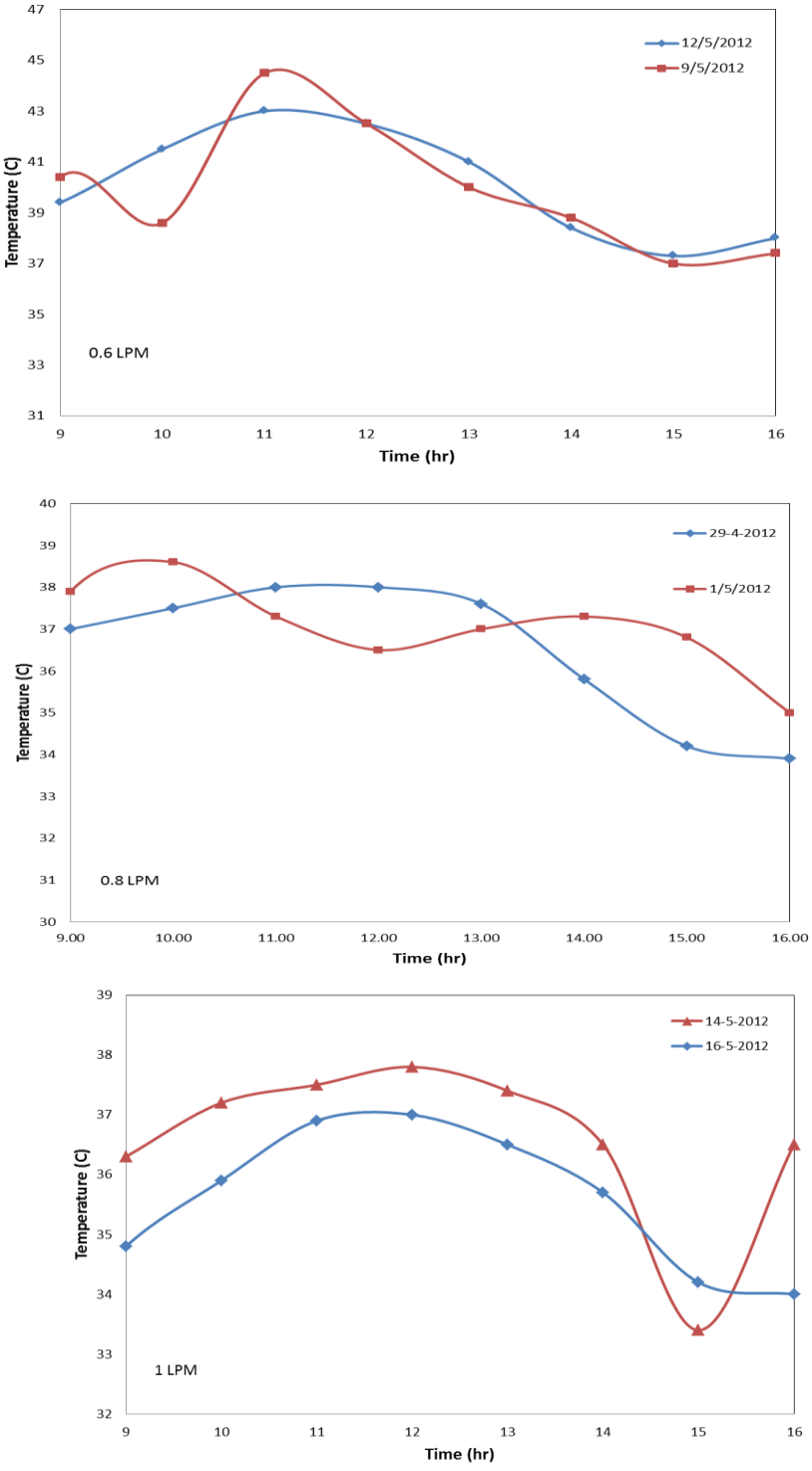

Figure 5.37: Outlet fluid temperature

In order to find the optimum mass flow rate, the maximum power output from the panel was recorded on different test days. The main purpose of applying active cooling is to keep the temperature of the module at the minimum range so that the maximum power can be extracted from the module. Figure 5.38 shows the variation of power output with time at different flow rates. It is observed that the maximum power output is achieved at the mass flow rate of 0.8 LPM. At 0.6 LPM and 1 LPM almost similar trend is observed. Therefore it is concluded from the results that optimum flow rate for achieving the maximum power is 0.8 LPM.

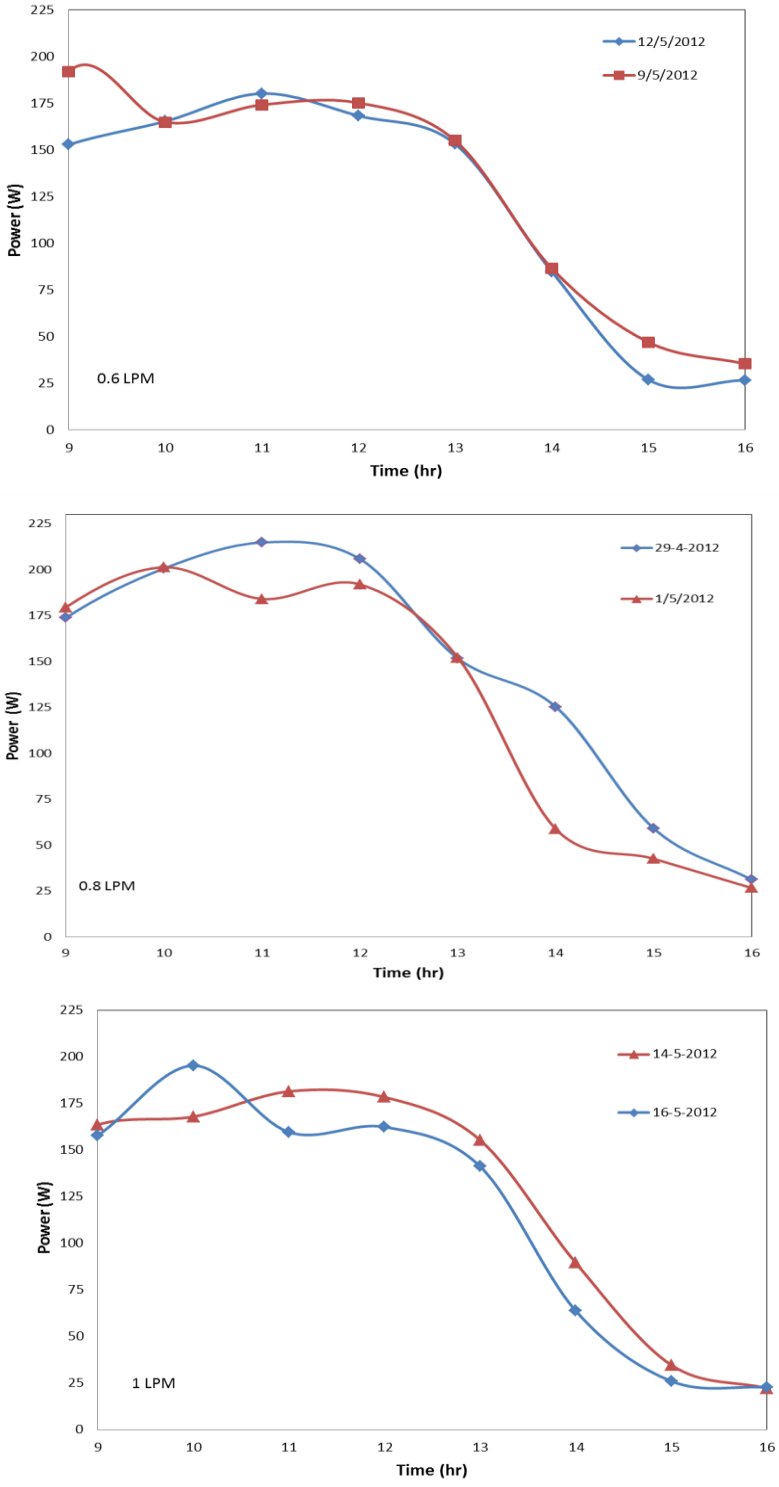

Figure 5.38: Power output from V-trough PV system

The effect of each reflector in the V-trough PV system was also studied with the help of this experimental setup. Figure 5.39 shows the contribution of each reflector on the performance of V-trough PV system. It is observed that south facing reflector has more contribution as compared to north facing reflector. The angle of the reflectors is very important parameter in deciding the amount of concentration. The angle for the south facing reflector was 50° which could not be increased to 60° due to limitation of the experimental setup. The results show that limiting angle for the north facing reflector was 60°. If the angle of the north facing reflector is decreased from 60°, all the reflected beams of the solar radiation strike the south facing reflector and are reflected out of the system. Therefore from this analysis it is concluded that the angle of both the reflectors are very important in determining the amount of increase in the concentration. It was found that when the south facing reflector was applied alone, there was shading in the later part of the day. In the case of north facing reflector, there was no shading throughout the day. Therefore north facing reflector alone can be used as compared to south facing reflector.

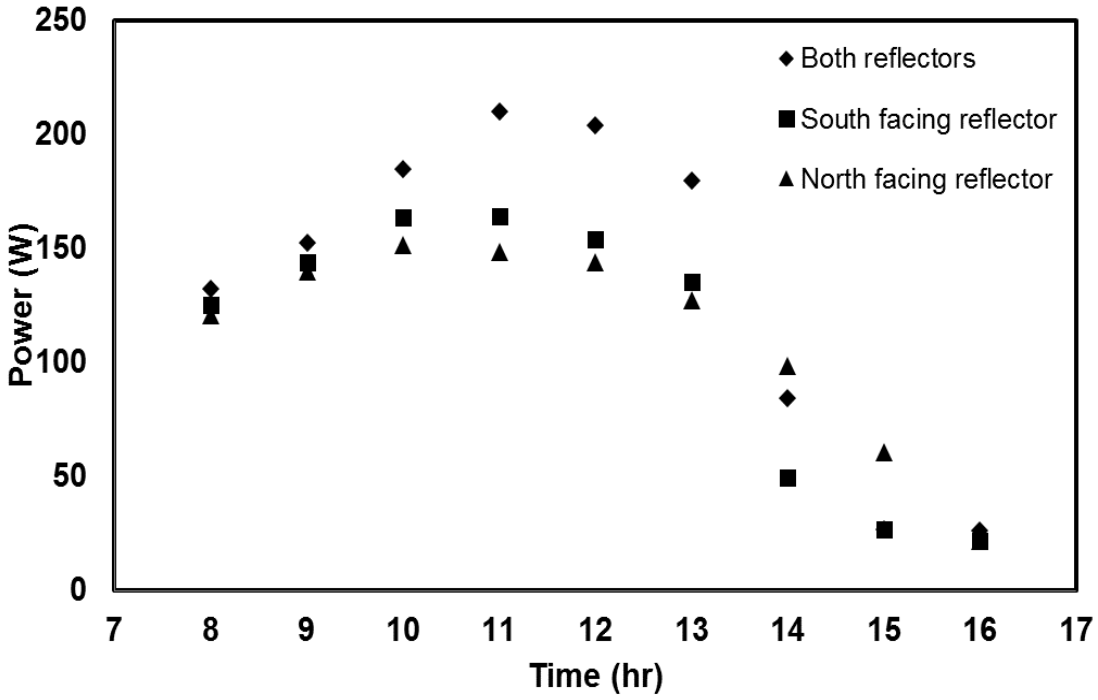

Figure 5.39: Comparison of both reflectors power output

5.2.5 Comparison of Experimental and Numerical Results for V-trough PV system

In this section the validity of the numerical modeling technique is verified by the experimental results. The numerical results obtained are validated with the experimental data from the tests conducted at KFUPM in the month of June, 2012.

Figure 5.40 shows the comparison of numerical and experimental results of maximum power for V-trough PV system. The measured power output fairly matches with the numerical result in the first half of the day i.e. from 8am to 1 pm as shown in Figure 5.40. After 2 pm the south facing reflector causes shading due to which the power suddenly drops. In the experimental setup the slope of the V-trough PV system and the reflectors was not much flexible. There were some constraints due to which the slope of the

reflectors and the panel could not be much varied. It was found that this sudden drop in power can be avoided by changing the orientation and the slope of the panel and the reflectors.

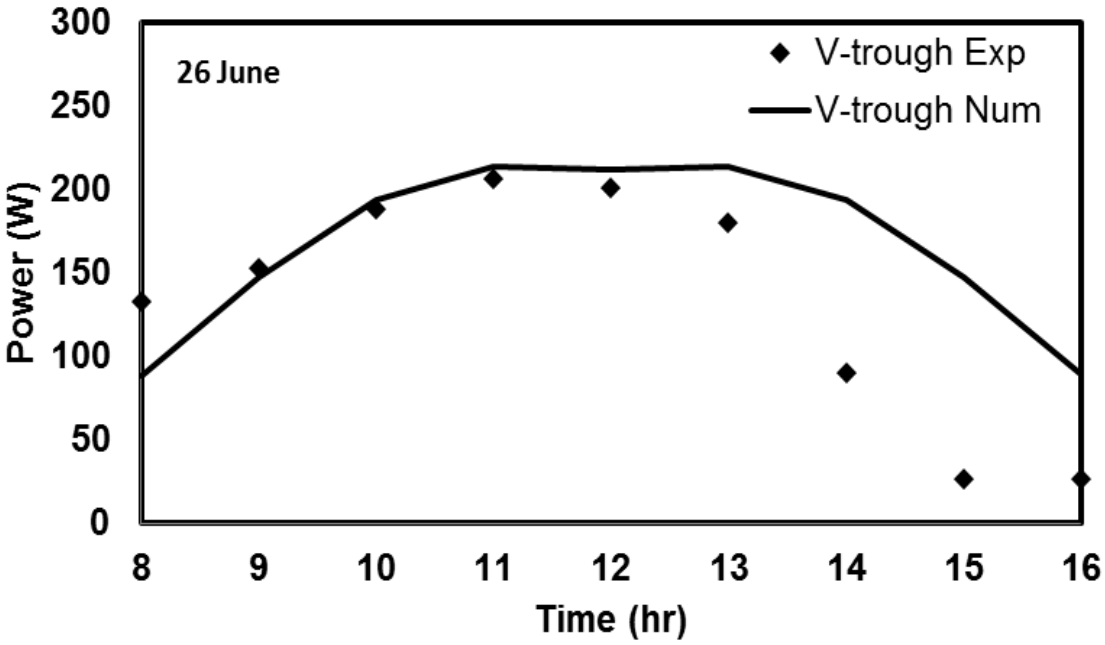

Figure 5.40: Comparison of power by numerical and experimental values

Numerical modeling of V-trough PV system involves the estimation of amount of energy absorbed by using simple planar reflectors. The model used in the current case assumes constant flux distribution from the planar reflectors onto the panels. Figure 5.41 shows the comparison of cell temperature between numerically predicted values and experimentally measured values. Results from the numerical model follow the same trend

as measured experimentally. This shows that there is a fair agreement between the numerical and experimental results.

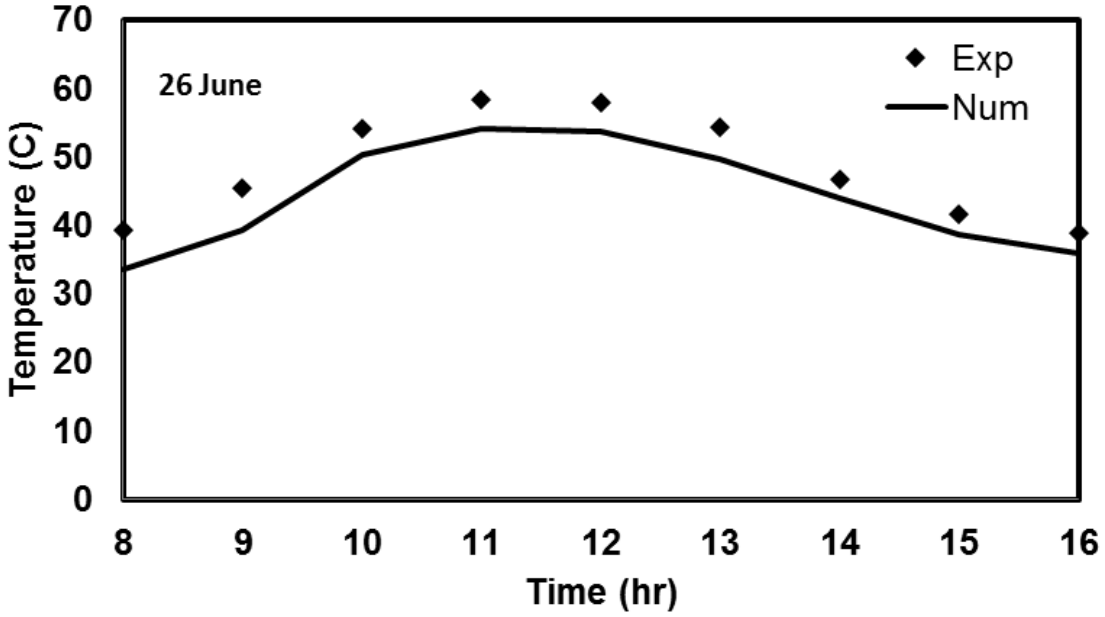

Figure 5.41: Comparison of cell temperature by numerical and experimental values

CONCLUSIONS AND FUTURE WORK

The aim of this research was to analyse the different low concentration photovoltaic systems used to generate the cost effective PV electricity. This thesis was focussed on the performance of two low concentration photovlotaics (LCPV) systems, namely V-trough PV system and PV-CPC system. Their performances were predicted through detail numerical modelling which included optical, thermal and electrical models. Experimental setup was designed, fabricated and tested to investigate and evaluate the performance of V-trough PV system and PV-CPC system. Experimental results were used to validate the results predicted from detail numerical modelling. Following are the conclusions drawn from the present study:

6.1 CONCLUSIONS

6.1.1 PV-CPC system

This study dealt with the use of non-imaging type Compound Parabolic Concentrator (CPC) with standard PV modules. In this study a detailed optical modeling was presented by which the amount of absorbed radiation with the PV-CPC system was estimated. Absorbed radiation was estimated for glazed PV-CPC system and unglazed PV-CPC system. It was found that the maximum solar radiation was absorbed by the unglazed PV-

CPC system. Since the efficiency of concentrating PV cell drops as the cell temperature increases, the thermal energy was extracted in the present study by circulating water through a rectangular channel placed at the bottom surface of the PV cells. Energy balance equations have been developed to perform the thermal analysis for the various configurations of the system with and without cooling. In the thermal analysis the presence of electrical efficiency makes the thermal analysis dependent on electrical model. Therefore, in order to estimate the PV module electrical efficiency and its electrical parameters, five parameters electrical model was used and solved in EES software. Finally, the absorbed radiation and the module temperature were given as input parameters from the optical and thermal modeling into the electrical model to find the power output from a simple PV string and the PV string integrated with CPC .Based on the climatic conditions of Dhahran, the numerical results showed that by integrating uncooled PV string with unglazed CPC, the amount of power was enhanced by 45.2%. If water cooling was provided along with the unglazed CPC reflectors and compared with uncooled simple flat PV string, the increase in the electrical power was about 73.6%. Water cooling reduced the operating temperature of unglazed PV-CPC system from 69.2°C to 46°C. In order to validate the numerical results, a laboratory scale bench-top PV-CPC system was designed and fabricated to achieve the concentration of 2.3X.A fair agreement between the numerical and experimental results was found. Effect of glazing was also studied in PV-CPC system. Glazing protects the reflectors and PV-panel from dust and moisture, but on the other hand it also raises the temperature of the PV panel. From electrical point of view glazing reduces the power output and from thermal

point of view it is beneficial as it increases the thermal gain of the PV-CPC system. Therefore, unglazed PV-CPC is recommended for greater electric power output but with a little compensation to the advantages of glazing.

6.1.2 V-trough PV system

In this study the technical and photovoltaic-cells quantity comparisons were made between common PV panel and V-trough PV system. The purpose of this study was to determine the suitability of V-trough PV concentrating technology over simple PV panels.A combined optical, thermal and electrical model was developed which predicts the characteristic curves of V-trough PV system. PV integrated with V-trough can serve as a good mean of enhancing the electrical efficiency of PV system and reducing the cost of electricity generated by the use of low cost reflectors. Applying cooling enhances the power output considerably and also the thermal gain of the V-trough PV system.The established steady state model predicts the thermal performance of V-trough PV system with and without cooling. Both thermal and electrical performance of the collector are presented and discussed. Applying water cooling enhances the power output considerably and also the thermal gain of the PV/T system. Results show that by applying cooling the power of the simple PV panel increased by 22.8% and for V-trough there was an increase of 31.5%. Experimental Setup was designed and built for V-trough PV system. The experimental results showed a good agreement with the numerical results. It is concluded from the results that V-trough PV system has more benefits than the normal flat PV system, such as the electrical efficiency is enhanced and consequently cost of PV electric power per unit area is reduced. Therefore, V-trough PV is recommended for

greater electric power output and an efficient way to reduce the cost of PV electricity generated.

6.2 FUTURE WORK

The extension of the current work can be focused on the cooling techniques used to lower the operating cell temperature. The main design considerations for the cooling systems are low and uniform cell temperatures as solar flux distribution is uneven and is not addressed through conventional cooling mechanisms. For gaining uniformity, jet impingement or converged channel configuration may be used to eliminate non-uniform heat transfer across the surface of PV panel. The effect can be validated through modelling and experimentation.

The current work incorporates a five parameter electrical model. A better and a more reliable version of the same model is the seven parameter electrical model which includes the effect of modified ideality factor and light intensity factor within the five translation equations of the original five parameter model.

.

APPENDICES

APPENDIX-A: SUNPOWER 230 SOLAR PANEL DATASHEETS

SUNPOWER

230 SOLAR PANEL

EXCEPTIONAL EFFICIENCY AND PERFORMANCE

BENEFITS

Highest Efficiency
SunPower™ Solar Panels are the most efficient photovoltaic panels on the market today.

More Power
Our panels produce more power in the same amount of space—up to 50% more than conventional designs and 100% more than thin film solar panels.

Reduced Installation Cost
More power per panel means fewer panels per install. This saves both time and money.

Reliable and Robust Design
Proven materials, tempered front glass, and a sturdy anodized frame allow panel to operate reliably in multiple mounting configurations.

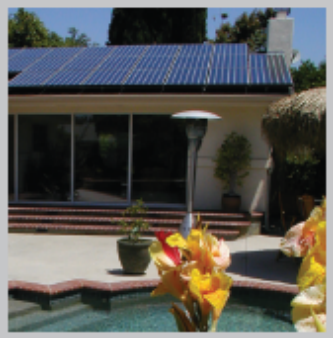

SPR-230-WHT-U

The SunPower™ 230 Solar Panel provides today's highest efficiency and performance. Utilizing 72 all back-contact solar cells, the SunPower 230 delivers a total panel conversion efficiency of 18.5%. The panel's reduced voltage-temperature coefficient and exceptional low-light performance attributes provide outstanding energy delivery per peak power watt.

SunPower's High Efficiency Advantage - Up to Twice the Power

	Thin Film	Conventional	SunPower
Peak Watts / Panel	65	170	230
Efficiency	9.0%	13.0%	18.5%
Peak Watts / ft²(m²)	8 (90)	12 (130)	17 (185)

About SunPower

SunPower designs, manufactures and delivers high-performance solar electric technology worldwide. Our high-efficiency solar cells generate up to 50% more power than conventional solar cells. Our high-performance solar panels, roof tiles and trackers deliver significantly more energy than competing systems.

c UL us

SUNPOWER

230 SOLAR PANEL

EXCEPTIONAL EFFICIENCY AND PERFORMANCE

Electrical Data

Peak Power (+/-5%)	P_{max}	230 W
Rated Voltage	V_{mpp}	41.0 V
Rated Current	I_{mpp}	5.61 A
Open Circuit Voltage	V_{oc}	48.7 V
Short Circuit Current	I_{sc}	5.99 A
Maximum System Voltage	UL	600 V
Temperature Coefficients		
	Power	-0.38% / K
	Voltage (V_{oc})	-132.5mV / K
	Current (I_{sc})	3.5mA / K
NOCT		45° C +/-2° C
Series Fuse Rating		20 A

I-V Curve

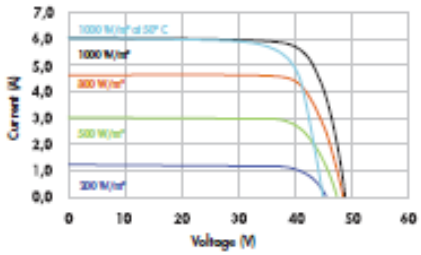

Current/voltage characteristics with dependence on irradiance and module temperature.

Tested Operating Conditions

Temperature	-40° F to +185° F (-40° C to + 85° C)
Max load	113 psf 550kg/m² (5,400 Pa) front – e.g. snow; 50 psf 245kg/m² (2,400 Pa) front and back – e.g. wind
Impact Resistance	Hail 1 in (25 mm) at 52mph (23 m/s)

Mechanical Data

Solar Cells	72 SunPower all-back contact monocrystalline
Front Glass	High transmission tempered glass
Junction Box	IP-65 rated with 3 bypass diodes Dimensions: 32 x 155 x 128 (mm)
Output Cables	1000mm length cables / MultiContact (MC4) connectors
Frame	Anodized aluminum alloy type 6063 (black)
Weight	33.1 lbs. (15.0 kg)

Warranties and Certifications

Warranties	25 year limited power warranty
	10 year limited product warranty
Certifications	Tested to UL 1703. Class C Fire Rating

Dimensions

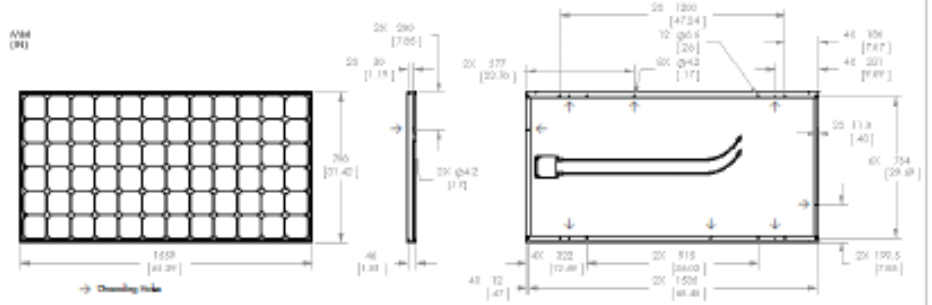

CAUTION: READ SAFETY AND INSTALLATION INSTRUCTIONS BEFORE USING THE PRODUCT.

Visit sunpowercorp.com for details

sunpowercorp.com

APPENDIX-B: C60 SOLAR PANEL DATASHEETS

SUNPOWER

C60 SOLAR CELL
MONO CRYSTALLINE SILICON

Physical Characteristics

Construction:	All-back contact
Dimensions:	125mm x 125mm - nominal
Thickness:	165 µm ±40 µm

ELECTRICAL CHARACTERISTICS OF TYPICAL CELL AT STANDARD TEST CONDITIONS (STC)

STC is defined as irradiance of 1000W/m², spectrum AM 1.5g and cell temperature of 25°C

Open Circuit Voltage:	0.680 V
Short Circuit Current:	6.28 A
Maximum Power Voltage:	0.575 V
Maximum Power Current:	5.92 A
Rated Power:	3.40 W
Efficiency:	Up to 22.6%

Un-laminated Cell Temperature Coefficients

Voltage:	-1.8 mV / °C
Power:	-0.32% / °C

ATTRIBUTES

- High efficiency reduces module assembly and system installation costs
- Uniform front appearance - no contact grid
- Back contact design simplifies circuit assembly
- Lower temperature coefficient improves energy delivery

PACKAGING

- Cells are packed in boxes of 1000 each, grouped in shrink-wrapped stacks of 100 with interleaving
- Twelve boxes are packed in a water-resistant "Master Carton" containing 12,000 cells suitable for air transportation

C60 CELL PERFORMANCE – TYPICAL I-V CURVE

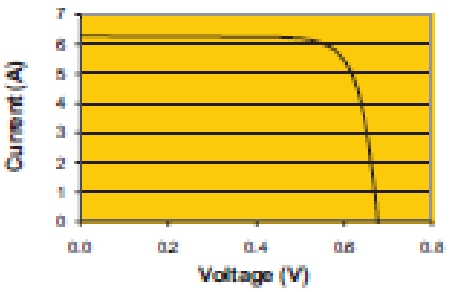

C60 CELL & BOND PAD DIMENSIONS

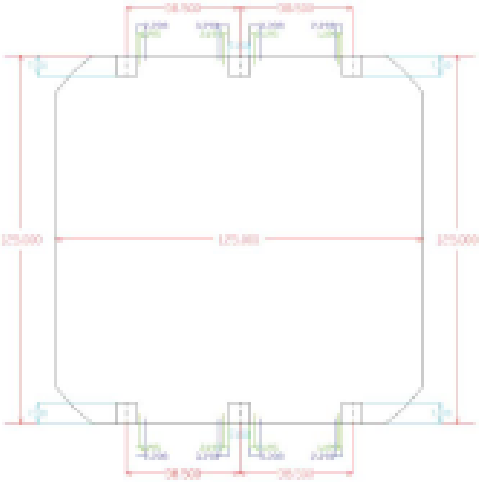

Bond pad area dimensions are 7.1mm x 7.1mm

NOMENCLATURE

a	ideality factor
C	concentration ratio
C_p	specific heat capacity (kJ/kg K)
F	control function
g	gravitational constant (m/s^2)
G	solar radiation intensity (W/m^2)
h	height(m), heat transfer coefficient (W/m^2K)
h_r	radiation heat transfer coefficient (W/m^2K)
h_T	conductive heat transfer coefficient (W/m^2K)
h_w	wind related heat transfer coefficient (W/m^2K)
I	irradiance, current (A)
I_L	light generated current (A)
I_o	extraterrestrial Radiation (W/m^2), diode reverse current (A)
I_T	total incident solar radiation (W/m2)
k	Boltzman's constant (J/K), thermal conductivity (W/m K)
K	extinction coefficient, incident angle modifier
$K_{\tau\alpha}$	incidence angle modifier
L	thickness of glass(m), plate spacing (m)
M	air mass modifier
$\dot{m}$	mass flow rate (kg/s)
N	number of cell
Nu	nusselt number
q	electronic charge
Q_u	rate of heat transfer (W/m^2)
R	resistance (ohm)
R_b	geometric factor
S	absorbed Radiation (W/m^2)
s	width of the PV string (m)
t	hour from midnight (hr)
T	temperature (K)
ΔT	temperature difference between plates
U	Heat transfer coefficient (W/m^2K)

V	voltage (V)
V_w	wind speed (m/s)
$\bar{h}$	truncated height (m)
$\bar{e}$	truncated opening aperture (m)
$\bar{T}$	mean temperature (K)

Subscript

a	ambient
b	beam
bs	backsheet
bsf	back sheet to fluid
c	cell
cbs	cell to backsheet
cg	cell to glass
CPC	compound parabolic collector
cpc	glazing cover
cpca	glazing cover to ambient
d	diffuse
dp	dew point
f	fluid
fa	fluid to ambient
fi	fluid inlet
fo	fluid outlet
g	ground reflected, glass
ga	glass to ambient
gcpc	glass to glazing cover
i	insulation
i-a	insulation to ambient
mp	maximum power
n	normal
oc	open circuit
p	plate
r	refraction, radiation

ref	reference
ref,r1	reflector 1
ref,r2	reflector 2
s	sky, series
sc	short circuit
sh	shunt
t	top loss coefficient
tot	Total

Greek Symbols

α	solar altitude angle, absorptance, thermal diffusivity (m^2/s)
β	slope (deg.)
β'	volumetric coefficient of expansion
$\tau\alpha$	transmissivity absorptance product
ρ_{Al}	reflectivity of aluminum
α_1	angle of reflector 1 (deg.)
α_2	angle of reflector 2 (deg.)
φ	latitude (deg.)
δ	solar declination angle (deg.)
ω	hour angle (deg.)
η_{mp}	maximum power point efficiency
μ_{Isc}	temperature coefficient of short circuit current
ρ_g	ground reflectivity
ϵ	emissivity
τ	transmittance
γ_s	solar azimuth angle
ν	kinematic viscosity (m^2/s)
Θ	half acceptance angle (deg.)
Θi	incidence angle (deg.)
Θ_r	angle of refraction (deg.)
Θ_z	zenith angle
ϵ	emissivity
σ	Stefan-Boltzmann constant ($W/m^2\ K^4$), standard deviation

REFERENCES

[1] E. I. A. (US), *International Energy Outlook 2013*. OECD Publishing, 2013.

[2] S. Arabia and R. Ernst, "Renewable Energy Country Attractiveness Indices Overview Of Indices," 2012.

[3] R. Winston, J. C. Minano, and P. Benitez, "Nonimaging Optics," *Elsevier Acad. Press*, pp. 1–217, 2005.

[4] Q. Liu, G. Yu, and J. J. Liu, "Solar Radiation as Large-Scale Resource for Energy-Short World," *Energy Environ.*, vol. 20, no. 3, pp. 319–329, Jul. 2009.

[5] N. S. Lewis, "Toward Cost-Effective Solar Energy Use," *Science*, vol. 315, no. 5813, pp. 798–801, Feb. 2007.

[6] G. Sala, D. Pachon, and I. Anton, *"Book 1: Classification of PV Concentrators", Test, Rating, and Specification of PV Concentrator Components and Systems, C-Rating Project*. 2000.

[7] "SolarEmpower Ltd.," 2010. [Online]. Available: http://www.solarempower.com/.

[8] A. Mahoney, J. Cannon, and J. Woodworth, "Accelerated UV-Aging of Acrylic Materials used in PV Concentrator Systems," in *Conference Record of the Twenty Third IEEE Photovoltaic Specialists Conference*, 1993, pp. 1216–1221.

[9] A. Terao, W. P. Mulligan, S. G. Daroczi, O. C. Pujol, P. J. Verlinden, R. M. Swanson, J. C. Minano, P. Benitz, and J. L. Alvarez, "A Mirror-Less Design for Micro-Concentrator Modules," in *Conference Record of the Twenty-Eighth IEEE Photovoltaic Specialists Conference*, 2000, pp. 1416–1419.

[10] A. J. Chatten, K. W. J. Barnham, B. F. Buxton, N. J. Ekins-Daukes, and M. A. Malik, "Quantum Dot Solar Concentrators," *Semiconductors*, vol. 38, no. 8, pp. 909–917, Aug. 2004.

[11] J. A. Manrique, "A Compound Parabolic Concentrator," *Int. Commun. Heat Mass Transf.*, vol. 11, no. 3, pp. 267–273, May 1984.

[12] V. B. Omubo-Pepple, C. Israel-Cookey, and G. I. Alaminokuma, "Effects of Temperature, Solar Flux and Relative Humidity on the Efficient Conversion of Solar Energy to Electricity," *Eur. J. Sceintific Res.*, vol. 35, no. 2, pp. 173–180, 2009.

[13] G. M. Kaplan, “Volunteers in Technical Assistance (VITA),” 1985.

[14] Y. Tripanagnostopoulos, “The Fresnel Lens Concept for Solar Control of Buildings,” *Sol. Energy*, vol. 81, pp. 661–675, 2007.

[15] K. Yoshioka, S. Goma, S. Hayakawa, and T. Saitoh, “Preparation and Properties of an Experimental Static Concentrator with a new Three-Dimensional Lens,” *Prog. Photovoltaics Res. Appl.*, vol. 5, no. 2, pp. 139–145, Mar. 1997.

[16] T. T. and C. W. Wheldon A., R. Bentley, G. Whitfield, “Payback Times for Energy and Carbon Dioxide: Comparison of Concentrating and Non-Concentrating PV Systems,” in *16th European Photovoltaic Solar Energy Conference*, 2000, pp. 2622–2625.

[17] M. I. Irshid and M. O. Othman, “V-Troughs with high Concentration Ratios for Photovoltaic Concentrator Cells,” *Sol. Cells*, vol. 23, pp. 159–172, 1988.

[18] H. F. Chiam, “Bi-yearly adjusted V-trough concentrators,” *Sol. Energy*, vol. 28, no. 5, pp. 407–412, Jan. 1982.

[19] F. Reis, M. C. Brito, V. Corregidor, J. Wemans, and G. Sorasio, “Modeling the Performance of Low concentration Photovoltaic Systems,” *Sol. Energy Mater. Sol. Cells*, vol. 94, no. 7, pp. 1222–1226, Jul. 2010.

[20] M. A. M. Shaltout, A. Ghettas, and M. Sabry, “V-trough Concentrator on a Photovoltaic Full Tracking System in a hot desert climate,” *Renew. Energy*, vol. 6, no. 5–6, pp. 527–532, Jul. 1995.

[21] N. Martín and J. M. Ruiz, “Optical Performance Analysis of V-trough PV concentrators,” *Prog. Photovoltaics Res. Appl.*, vol. 16, no. 4, pp. 339–348, Jun. 2008.

[22] R. Tang and X. Liu, “Optical Performance and Design Optimization of V-trough Concentrators for Photovoltaic Applications,” *Sol. Energy*, vol. 85, no. 9, pp. 2154–2166, Sep. 2011.

[23] C. Q. Yan, “Output Characteristics Study of V-trough PV Concentration System,” *Appl. Mech. Mater.*, vol. 71–78, pp. 2077–2080, Jul. 2011.

[24] F. Reis, M. C. Brito, V. Corregidor, J. Wemans, and G. Sorasio, “Ageing of Standard PV Module when Integrated in a V-trough Concentration System,” *MRS Proc.*, vol. 1210, pp. 1–6, Jan. 2011.

[25] S. Maiti, S. Banerjee, K. Vyas, P. Patel, and P. K. Ghosh, "Self regulation of photovoltaic module temperature in V-trough using a metal–wax composite phase change matrix," *Sol. Energy*, vol. 85, no. 9, pp. 1805–1816, Sep. 2011.

[26] C. Solanki, C. Sangani, D. Gunashekar, and G. Antony, "Enhanced heat dissipation of V-trough PV modules for better performance," *Sol. Energy Mater. Sol. Cells*, vol. 92, no. 12, pp. 1634–1638, Dec. 2008.

[27] T. N. Anderson, R. R Künnemeyer, M. Duke, and J. K. Carson, "A Combined Optical , Thermal and Electrical Performance Model of a Building Integrated Photovoltaic / Thermal Concentrator (BIPVTC)," in *Proceedings of the 18th Electronics New Zealand Conference*, 2011, pp. 107–112.

[28] L. T. Kostic, T. M. Pavlovic, and Z. T. Pavlovic, "Influence of reflectance from flat aluminum concentrators on energy efficiency of PV/Thermal collector," *Appl. Energy*, vol. 87, no. 2, pp. 410–416, Feb. 2010.

[29] O. C. Vilela, J. Bione, and N. Fraidenraich, "Simulation of grape culture irrigation with photovoltaic V-trough pumping systems," *Renew. Energy*, vol. 29, no. 10, pp. 1697–1705, Aug. 2004.

[30] C. SANGANI and C. SOLANKI, "Experimental evaluation of V-trough (2 suns) PV concentrator system using commercial PV modules," *Sol. Energy Mater. Sol. Cells*, vol. 91, no. 6, pp. 453–459, Mar. 2007.

[31] I. S. Hermenean and D. V Diaconescu, "On the Geometric Modelling of a Concentrating PV-Mirror System," *Bull. Transilv. Univ. Brasov*, vol. 2, no. 51, p. 73, 2009.

[32] A. Rabl, "Optical and Thermal Properties of Compound Parabolic Concentrators," *Sol. Energy*, vol. 18, pp. 497–511, 1976.

[33] H. P. Garg and R. S. Adhikari, "Optical Design Calculations for CPC's," *Energy*, vol. 23, no. 10, pp. 907–909, 1998.

[34] H. P. Garg and R. S. Adhikari, "Performance Analysis of a Hybrid Photovoltaic/Thermal (PV/T) Collector with Integrated CPC Troughs," *Int. J. Energy Res.*, vol. 23, no. 15, pp. 1295–1304, Dec. 1999.

[35] J. Li, G. Pei, Y. Li, and J. Ji, "Design and Performance Analysis of Low Temperature Solar Thermal Electric Generation Integrated PV Cells," in *2010 Asia-Pacific Power and Energy Engineering Conference*, 2010, pp. 1–4.

[36] Y. Su, S. B. Riffat, and G. Pei, "Comparative Study on Annual Solar Energy Collection of a Novel Lens-Walled Compound Parabolic Concentrator (Lens-walled CPC)," *Sustain. Cities Soc.*, vol. 4, pp. 35–40, Oct. 2012.

[37] L. Guiqiang, P. Gang, Y. Su, Z. Xi, and J. Jie, "Preface," *Energy Procedia*, vol. 14, Jan. 2012.

[38] M. Y. Othman, B. Yatim, K. Sopian, and M. N. Abu Bakar, "Performance Analysis of a Double-Pass Photovoltaic/Thermal (PV/T) Solar Collector with CPC and Fins," *Renew. Energy*, vol. 30, no. 13, pp. 2005–2017, Oct. 2005.

[39] M. Brogren, P. E. R. Nostell, and B. Karlsson, "Optical Efficiency of a PV – Thermal Hybrid CPC Module for High Latitudes," *Sol. Energy*, vol. 69, pp. 173–185, 2001.

[40] S. Hatwaambo, H. Hakansson, J. Nilsson, and B. Karlsson, "Angular characterization of Low Concentrating PV–CPC using Low-Cost Reflectors," *Sol. Energy Mater. Sol. Cells*, vol. 92, no. 11, pp. 1347–1351, Nov. 2008.

[41] R. Tang, M. Wu, Y. Yu, and M. Li, "Optical Performance of Fixed East–West aligned CPC's used in China," *Renew. Energy*, vol. 35, no. 8, pp. 1837–1841, Aug. 2010.

[42] M. E. A. Alfegi, K. Sopian, M. Y. H. Othman, and B. Bin Yatim, "Experimental Investigation of Single Pass Double Duct Photovoltaic Thermal (PV/T) Air Collector with CPC and Fins," *Am. J. Appl. Sceinces*, pp. 866–871, 2008.

[43] H. a. Zondag, D. W. de Vries, W. G. J. van Helden, R. J. C. van Zolingen, and a. a. van Steenhoven, "The Thermal and Electrical Yield of a PV-Thermal Collector," *Sol. Energy*, vol. 72, no. 2, pp. 113–128, Feb. 2002.

[44] T. T. Chow, "A Review on Photovoltaic/Thermal Hybrid Solar Technology," *Appl. Energy*, vol. 87, no. 2, pp. 365–379, Feb. 2010.

[45] H. Singh and P. C. Eames, "A Review of Natural Convective Heat Transfer Correlations in rectangular cross-section Cavities and their Potential Applications to Compound Parabolic Concentrating (CPC) Solar Collector Cavities," *Appl. Therm. Eng.*, vol. 31, no. 14–15, pp. 2186–2196, Oct. 2011.

[46] R. Zakharchenko, "Photovoltaic Solar Panel for a Hybrid PV/Thermal System," *Sol. Energy Mater. Sol. Cells*, vol. 82, no. 1–2, pp. 253–261, May 2004.

[47] J. Ji, J.-P. Lu, T.-T. Chow, W. He, and G. Pei, "A Sensitivity Study of a Hybrid Photovoltaic/Thermal Water-Heating System with Natural Circulation," *Appl. Energy*, vol. 84, no. 2, pp. 222–237, Feb. 2007.

[48] B. J. Huang, T. H. Lin, W. C. Hung, and F. S. Sun, "Performance Evaluation of Solar Photovoltaic/Thermal Systems," *Sol. Energy*, vol. 70, no. 5, pp. 443–448, Jan. 2001.

[49] T. Bergene and O. M. Løvvik, "Model Calculations on s Flat-Plate Solar Heat Collector with Integrated Solar Cells," *Sol. Energy*, vol. 55, no. 6, pp. 453–462, Dec. 1995.

[50] B. Sandnes and J. Rekstad, "A Photovoltaic/Thermal (PV/T) Collector with a Polymer Absorber Plate. Experimental Study and Analytical Model," *Sol. Energy*, vol. 72, no. 1, pp. 63–73, Jan. 2002.

[51] W. He, T.-T. Chow, J. Ji, J. Lu, G. Pei, and L. Chan, "Hybrid Photovoltaic and Thermal Solar-Collector designed for Natural circulation of Water," *Appl. Energy*, vol. 83, no. 3, pp. 199–210, Mar. 2006.

[52] S. A. Kalogirou, "Use of TRNSYS for Modelling and Simulation of a Hybrid PV–Thermal Solar System for Cyprus," *Renew. Energy*, vol. 23, no. 2, pp. 247–260, Jun. 2001.

[53] T. Fujisawa and T. Tani, "Annual exergy evaluation on photovoltaic-thermal hybrid collector," *Sol. Energy Mater. Sol. Cells*, vol. 47, no. 1–4, pp. 135–148, Oct. 1997.

[54] H. P. Garg and R. K. Agarwal, "Some aspects of a PV/T Collector/Forced Circulation flat plate Solar Water Heater with Solar Cells," *Energy Convers. Manag.*, vol. 36, no. 2, pp. 87–99, Feb. 1995.

[55] D. F. Menicucci and J. P. Fernandez, "User's Manual for PVFORM : A Photovoltaic System Shulation Program For Stand-Alone and Grid-interactive Applications," *SANDIA REPORT*, 1989. [Online]. Available: http://prod.sandia.gov/techlib/access-control.cgi/1985/850376.pdf.

[56] Y. Hishikawa, Y. Imura, and T. Oshiro, "Irradiance-dependence and translation of the I-V Characteristics of Crystalline Silicon Solar Cells," in *Conference Record of the Twenty-Eighth IEEE Photovoltaic Specialists Conference*, 2000, pp. 1464–1467.

[57] B. Marion, S. Rummel, and A. Anderberg, “Current-Voltage curve Translation by bilinear Interpolation,” *Prog. Photovoltaics Res. Appl.*, vol. 12, no. 8, pp. 593–607, Dec. 2004.

[58] D. King, J. Kratochvil, and W. Boyson, “Photovoltaic Array Performance Model,” 2004. [Online]. Available: http://prod.sandia.gov/techlib/access-control.cgi/2004/043535.pdf.

[59] Sandia National Laboratories, “Database of Photovoltaic Module Performance Parameters.” [Online]. Available: http://www.sandia.gov/pv/docs/Database.htm>.

[60] Q. Kou, S. A. Klein, and W. A. Beckman, “A Method for estimating the Long-Term Performance of Direct-coupled PV Pumping Systems,” *Sol. Energy*, vol. 64, no. 1–3, pp. 33–40, Sep. 1998.

[61] N. D. Benavides and P. L. Chapman, “Modeling the Effect of Voltage Ripple on the Power Output of Photovoltaic Modules,” *IEEE Trans. Ind. Electron.*, vol. 55, no. 7, pp. 2638–2643, Jul. 2008.

[62] Y. T. Tan, D. S. Kirschen, and N. Jenkins, “A Model of PV Generation Suitable for Stability Analysis,” *IEEE Trans. Energy Convers.*, vol. 19, no. 4, pp. 748–755, Dec. 2004.

[63] M. C. Glass, “Improved Solar Array Power Point Model with SPICE Realization,” in *IECEC 96. Proceedings of the 31st Intersociety Energy Conversion Engineering Conference*, 1996, vol. 1, pp. 286–291.

[64] Y. Kuo, T. Liang, and J. Chen, “Novel Maximum-Power-Point-Tracking Controller for Photovoltaic Energy Conversion System,” *IEEE Trans. Ind. Electron.*, vol. 48, no. 3, pp. 594–601, Jun. 2001.

[65] W. G. Dunford and A. Capel, “A Novel Modeling method for Photovoltaic Cells,” in *2004 IEEE 35th Annual Power Electronics Specialists Conference*, 2004, pp. 1950–1956.

[66] A. N. Celik and N. Acikgoz, “Modelling and experimental verification of the operating current of mono-crystalline photovoltaic modules using four- and five-parameter models,” *Appl. Energy*, vol. 84, no. 1, pp. 1–15, Jan. 2007.

[67] F. González-Longatt, “Model of Photovoltaic Module In Matlab,” in *II CIBELEC*, 2005, pp. 1–5.

[68] R. Chenni, M. Makhlouf, T. Kerbache, and a. Bouzid, "A detailed Modeling method for Photovoltaic Cells," *Energy*, vol. 32, no. 9, pp. 1724–1730, Sep. 2007.

[69] K. Ishaque, Z. Salam, and H. Taheri, "Modeling and Simulation of Photovoltaic (PV) System during partial shading based on a Two-Diode Model," *Simul. Model. Pract. Theory*, vol. 19, no. 7, pp. 1613–1626, Aug. 2011.

[70] W. De Soto, S. A. Klein, and W. A. Beckman, "Improvement and Validation of a Model for Photovoltaic array Performance," *Sol. Energy*, vol. 80, no. 1, pp. 78–88, Jan. 2006.

[71] C. Carrero, J. Amador, and S. Arnaltes, "A Single Procedure for Helping PV designers to select Silicon PV Modules and Evaluate the Loss Resistances," *Renew. Energy*, vol. 32, no. 15, pp. 2579–2589, Dec. 2007.

[72] R. A. Dougal, "Dynamic Multiphysics Model For Solar Array," *IEEE Trans. Energy Convers.*, vol. 17, no. 2, pp. 285–294, Jun. 2002.

[73] M. G. Villalva, J. R. Gazoli, and E. R. Filho, "Comprehensive Approach to Modeling and Simulation of Photovoltaic Arrays," *IEEE Trans. Power Electron.*, vol. 24, no. 5, pp. 1198–1208, May 2009.

[74] J. a. Gow and C. D. Manning, "Development of a Photovoltaic Array Model for use in Power-Electronics Simulation Studies," *IEE Proc. - Electr. Power Appl.*, vol. 146, no. 2, p. 193, 1999.

[75] N. Pongratananukul and T. Kaspafis, "Tool for Automated Simulation of Solar Arrays using general-purpose Simulators," in *2004 IEEE Workshop on Computers in Power Electronics, 2004. Proceedings.*, 2004, vol. 00, pp. 10–14.

[76] S. Chowdhury, G. a. Taylor, S. P. Chowdhury, a. K. Saha, and Y. H. Song, "Modelling, Simulation and Performance Analysis of a PV Array in an Embedded Environment," in *2007 42nd International Universities Power Engineering Conference*, 2007, no. 1, pp. 781–785.

[77] W. Herrmann, W. Wiesner, and W. Vaassen, "Hot Spot Investigations on PV Modules-New Concepts for a Test Standard and consequences for Module Design with respect to Bypass Diodes," in *Conference Record of the Twenty Sixth IEEE Photovoltaic Specialists Conference - 1997*, 1997, pp. 1129–1132.

[78] H. Kawamura, K. Naka, N. Yonekura, S. Yamanaka, H. Kawamura, H. Ohno, and K. Naito, "Simulation of I–V characteristics of a PV module with shaded PV cells," *Sol. Energy Mater. Sol. Cells*, vol. 75, no. 3–4, pp. 613–621, Feb. 2003.

[79] H. Patel and V. Agarwal, “MATLAB-Based Modeling to Study the Effects of Partial Shading on PV Array Characteristics,” *IEEE Trans. Energy Convers.*, vol. 23, no. 1, pp. 302–310, Mar. 2008.

[80] H. Patel and V. Agarwal, “Maximum Power Point Tracking Scheme for PV Systems Operating Under Partially Shaded Conditions,” *IEEE Trans. Ind. Electron.*, vol. 55, no. 4, pp. 1689–1698, Apr. 2008.

[81] M. Zagrouba, A. Sellami, M. Bouaïcha, and M. Ksouri, “Identification of PV Solar Cells and Modules Parameters using the Genetic Algorithms: Application to Maximum Power Extraction,” *Sol. Energy*, vol. 84, no. 5, pp. 860–866, May 2010.

[82] J. P. Charles, M. Abdelkrim, Y. H. Muoy, and P. Mialhe, “A Practical Method of Analysis of the Current-Voltage Characteristics of Solar Cells,” *Sol. Cells*, vol. 4, no. 2, pp. 169–178, Sep. 1981.

[83] T. Ikegami, T. Maezono, F. Nakanishi, Y. Yamagata, and K. Ebihara, “Estimation of Equivalent Circuit parameters of PV Module and its Application to Optimal Operation of PV System,” *Sol. Energy Mater. Sol. Cells*, vol. 67, no. 1–4, pp. 389–395, Mar. 2001.

[84] J. a Jervase, H. Bourdoucen, and A. Al-Lawati, “Solar Cell Parameter Extraction using Genetic Algorithms,” *Meas. Sci. Technol.*, vol. 12, no. 11, pp. 1922–1925, Nov. 2001.

[85] W. Kim and W. Choi, “A Novel Parameter Extraction Method for the One-Diode Solar Cell Model,” *Sol. Energy*, vol. 84, no. 6, pp. 1008–1019, Jun. 2010.

[86] M. G. Villalva, J. R. Gazoli, and E. R. Filho, “Modeling and Circuit-Based Simulation of Photovoltaic Arrays,” in *2009 Brazilian Power Electronics Conference*, 2009, pp. 1244–1254.

[87] G. Walker, “Evaluating MPPT Converter Topologies using a MATLAB PV Model,” *J. Electr. Electron. Eng.*, vol. 21, no. 1, pp. 49–55, 2001.

[88] M. T. Boyd, S. A. Klein, D. T. Reindl, and B. P. Dougherty, “Evaluation and Validation of Equivalent Circuit Photovoltaic Solar Cell Performance Models,” *J. Sol. Energy Eng.*, vol. 133, no. 2, 2011.

[89] K. Ishaque and Z. Salam, “An improved Modeling Method to determine the Model Parameters of Photovoltaic (PV) Modules using Differential Evolution (DE),” *Sol. Energy*, vol. 85, no. 9, pp. 2349–2359, Sep. 2011.

[90] C. Carrero, D. Ramírez, J. Rodríguez, and C. a. Platero, "Accurate and Fast Convergence Method for Parameter Estimation of PV Generators based on three main points of the I–V Curve," *Renew. Energy*, vol. 36, no. 11, pp. 2972–2977, Nov. 2011.

[91] J. A. Duffie and W. A. Beckman, *Solar Engineering of Thermal Processes*, 4th ed. Hoboken, NJ, USA: John Wiley & Sons, Inc., 2013.

[92] L. T. Kostić, T. M. Pavlović, and Z. T. Pavlović, "Optimal Design of Orientation of PV/T Collector with Reflectors," *Appl. Energy*, vol. 87, no. 10, pp. 3023–3029, Oct. 2010.

[93] U. Stutenbaeumer and B. Mesfin, "Equivalent Model of Monocrystalline, Polycrystalline and Amorphous Silicon Solar Cells," *Renew. Energy*, vol. 18, no. 4, pp. 501–512, Dec. 1999.

VITAE

Name:	Bilal Tanweer
Date of birth:	2 April, 1987
Nationality:	Pakistani
Present Address:	KFUPM P.O. Box # 8606, King Fahd University of Petroleum and Mineral, Dhahran- 31261, Saudi Arabia
Permanent Address:	P.O. Box # 120389, Al-Jouf-21322, Saudi Arabia
Email Address:	uetian.81@gmail.com
Educational Qualification:	**M.S (Mechanical Engineering)** April, 2014 King Fahd University of Petroleum and Mineral, Dhahran, Saudi Arabia. **B.Sc. (Mechanical Engineering)** June, 2010 University of Engineering and Technology, Lahore, Pakistan.
Publications:	**1.** Haitham Bahaidarah, Bilal Tanweer, P. Gandhidasan, "Performance analysis of a low concentrating PV-CPC system," 39th IEEE Photovoltaic Specialists Conference, 2013.

2. Haitham Bahaidarah, Shafiqur Rehman, Bilal Tanweer, "Experimental Evaluation of the Performance of a Photovoltaic Panel with Water Cooling," 39th IEEE Photovoltaic Specialists Conference, 2013.

3. Haitham M. Bahidarah, Bilal Tanweer, P.Gandhidasan, Nasiru Ibrahim, Shafiqur Rehman, "Experimental and numerical study on non-concentrating and symmetric unglazed compound parabolic photovoltaic concentration systems." Applied Energy, 136(2014), pp. 527-536